Escola de Camins
Escola Tècnica Superior d'Enginyeria de Camins, Canals i Ports
UPC BARCELONATECH

TREBALL FINAL DE GRAU

Analysis of fluid-structure interaction on a bridge wash out phenomenon by the particle finite element method.

Treball realitzat per:
Adrià Estany Roura

Dirigit per:
Miguel Ángel Celigueta Jordana i
Eugenio Oñate Ibañez de Navarra

Grau en:
Enginyeria Civil

Barcelona, 27 de Setembre del 2019

Departament d'Enginyeria Civil i Ambiental

Acknowledgements

First and foremost, I would like to thank the supervisors of my project, Miguel Ángel Celigueta Jordana and Salva Latorre Sánchez, for their unconditional help throughout the realization of this project and helping me out with issues regarding the software.

Lastly, I would like to thank my family, friends and my partner for their help especially during my year abroad as an exchange student.

Abstract

In 2011, a huge tsunami stroke the north-eastern Japanese coast and caused numerous devastations, especially on public infrastructures such as highways, railways, bridges, etc. As bridges are essential for the recovery and prevention of a tsunami strike in terms of transporting goods and people, the prevention of the wash out phenomenon of the upper structure of the bridge is very important. With this motivation, a study of the wash out behaviour has been carried out using the Particle Finite Element Method (PFEM) for solving fluid-structure interaction problems. To validate the simulations carried out, a comparison between the simulations and some real-life experiments has been made. In the experiments, the motion of the girder (upper part of the bridge) has been tracked during the hit of the wave. Plus, a comparison between the simulations of the same problem with different mesh sizes has been done in order to compare and judge which mesh size best fits this specific problem. It is found that the rigid body motion of the girder of the bridge shows good agreement with the experimental results, and the optimal mesh size for this problem regarding the accuracy of results and computational time is the 10-mm mesh size.

Table of contents

List of tables

List of figures

1. Introduction.

Since humans stopped to be nomad and began to settle in a certain place on Earth and build houses and harvests around it, one of their biggest fears has been the danger to a natural disaster to happen. This hazard is present every day at every time and can strike without any previous warning. We understand a natural disaster by a major adverse event resulting from a natural source, not artificial or human-dependent. These hazards can be landslides, earthquakes, volcanic eruptions, floods, tsunamis, hurricanes and tornadoes, among others. All these natural disasters can cause loss of life and material damages in buildings and in the harvests.

Consequently, humans have tried to predict and to reduce the impact that these hazards might cause in villages, towns and cities, especially regarding the loss of life. Nowadays, there are several of the aforementioned natural disasters that can be predicted and, consequently, its effects on population can be mitigated before they happen in a certain place. These are storms, hurricanes, tornadoes and, in some cases, floods as well. Sadly, there are some other natural hazards, such as earthquakes, tsunamis and volcanic eruptions, which cannot be predicted with enough time before they happen, and catch people unprepared. These are the most hazardous natural disasters that are present nowadays in the Earth because they might cause massive material losses and normally they come with life losses as well.

In this project, one of these natural hazards is chosen and a study its behaviour when hitting an infrastructure is carried out. The chosen natural hazard for this project is the tsunami. The tsunamis are one of the most hazardous natural disasters that we find on Earth because they cause massive material losses (which is translated into big economical losses) and usually cause life losses. For local governments, it is crucial to recover from one of these disasters as quick as possible, especially in mobility infrastructures such as highways and bridges. If after a tsunami the highways of a certain place that was hit by the tsunami take too much time to rebuild and reset traffic, might cause traffic disorder throughout the recovery time. In order to mitigate the causes of a tsunami, disaster prevention and mitigation techniques are being developed in coastal infrastructures, as well as to establish a prediction method for tsunamis.

Although it would be an interesting topic to study, this project does not pretend to find ways to mitigate the consequences of a tsunami that hits a bridge and to propose methodologies for the faster recovery after the effects of a tsunami. Finding innovative ways to build bridges that erase the effects of a tsunami hit is out of the scope of this project. The aim of this project is to validate the Particle Finite Element Method (PFEM) for solving fluid-structure interaction problems by comparing some real-life experiments with the simulation of these same experiments with the PFEM method.

As it can be seen in further points of this project, the PFEM method requires de generation of a mesh in order to carry out the simulations. So, as the generation of the mesh and, hence, the choice of the mesh size is a key point of the PFEM, a comparison

with the experimental results and the simulation results is carried out, as well as a comparison of the simulation results with different mesh sizes. Then, in this project a simulation of a real experiment and its comparison is carried out and a comparison of the results between the mesh size choices for the simulation of this problem is carried out as well.

In the following sections, the bridge wash out phenomenon is selected and studied experimentally and numerically. Hence, in this project, a comparison between the experimental results and the numerical results solved with the PFEM is carried out. This will allow us to validate the PFEM method for solving fluid-structure interaction problems and to predict and preview the effects of a tsunami to a bridge and its consequences. A brief summary of the PFEM with its governing equations is presented along with the previous mathematical knowledge required to understand the functioning of the method, then some simple two-dimensional examples solved with the PFEM are described, then the experimental results of the bridge wash out phenomenon are presented and, finally, the simulations carried out imitating the experiments are shown. In the following subsection, the objectives of this project are presented.

1.1. Objectives.

Although it would be interesting to study the possible consequences and mitigation techniques of the effects caused by a tsunami to a bridge, in this project the only main objective is to validate the PFEM method for solving fluid-structure interaction problems, comparing the results of the simulations carried out with the experimental data that we will see in further sections, and to carry out a comparison between the mesh size choices for this problem. So, the objectives of this project are presented in the following points.

- To describe the basics of the functioning of the PFEM method for solving fluid-structure interaction problems along with the basic equations and boundary conditions.
- To simulate some basic two dimensional problems with the software in order to see the basic functioning of both the software and the PFEM method.
- To identify and describe properly the boundary conditions for the simulation of the bridge wash out phenomenon.
- To compare the results of the simulation with the real experimental data.
- To compare the meshes generated regarding number of nodes, elements, etc.
- To compare the results of the different simulations with the different mesh size choices between each other, especially regarding the computational time and accuracy of the results.

1.2. Limitations.

In this section, the limitations of this project are presented. We understand a limitation by the different shortcomings, conditions and influences that we cannot control over the realization of the project.

The main shortcoming I found when working on my project was that the PFLOW software was a bit left alone and was designed for older Windows versions. This software is developed by CIMNE[1] and it counts with a low number of habitual users, which means that the software is not fully-updated for newer versions of Windows. So my supervisor had to spend some time developing the software to make it compatible with my PC.

Another limitation I found was when running cases which required large meshes, like the case I am focusing on in this project. Obviously, this limitation was not present when running the simple two-dimensional cases, which did not require large meshes nor big computational time. This limitation was well present when running the main case of this project because it is a three dimensional problem and its mesh has millions of nodes. The computational time when running this case in my PC was of about 5 to 6 days with a mesh size of 10 millimetres. With a smaller mesh size, the computational time rises, so I had to ask my tutor for some help running this case because my PC could not hold the calculations due its low RAM capacity. When running this case, I usually found that the calculations crashed and had to reset them again.

So the major limitation is the amount of time I spent trying to run the main case of this project, which required a big computational time as well as a big storage space in my PC, so the results in this project might be slightly affected by this shortcoming.

1.3. Software used.

The softwares used for the realization of this project are:

- PFLOW software, which can be found in the GiD software. PFLOW is used in this project to simulate the examples and the main problem solved with the PFEM method.
- Microsoft office: Microsoft Word, PowerPoint and Excel for the writing of this document, its oral presentation and the calculation of the coordinates of the centroid of the girder.

[1] CIMNE stands for International Centre for Numerical Methods in Engineering, and it is a research centre linked to the UPC.

2. Mathematical background.

In this section, we will be focusing on the mathematical knowledge previous to explain the functioning of the PFEM, which are the Lagrangian description of motion, the Delaunay tessellation for creating the mesh at each time step and the Alpha Shape technique to identify the boundary of the problem. All these mathematical tools are used in the PFEM in order to make it a competitive and robust method for solving fluid-structure interaction problems. An extended explanation of the PFEM can be found in section 3.

2.1. Description of motion.

There are two main approaches of the description of motion. The first approach focuses on the particles and how are they moving and behaving through time and space. This first approach is known as material description of motion or Lagrangian description. The second of these approaches consists on focusing in a given point in space and analyse what is occurring at this point through time. This second approach is known as spatial description of motion or Eulerian description. In both descriptions, the arguments that appear in the mathematical functions are different: for the material description we will use the material coordinates (a particle) and for the spatial description we will use the spatial coordinates (a fixed point in space). In order to differentiate both coordinates, we will use the following notation.

$$X = (X_1, X_2, X_3) \stackrel{\text{def}}{=} material\ coordiantes \tag{1}$$

$$x = (x_1, x_2, x_3) \stackrel{\text{def}}{=} spatial\ coordiantes \tag{2}$$

In order to describe the different time derivatives of section 2.1.3., we need to define the equation of motion beforehand. This equation of motion allows to write the spatial coordinates as a function of the material coordinates and time (3).

$$x = x(X, t) \tag{3}$$

2.1.1. Lagrangian description of motion.

As mentioned previously, the material or Lagrangian description of motion is based upon the following of different particles and tracking their motion through space and time. It is a description typically used in solid mechanics.

Given a property, for instance the density ρ, described by a certain function

$$\bar{\rho}(\cdot, t)\colon R^3 \times R^+ \to R^+ \tag{4}$$

where the argument $(\cdot)$ in $\bar{\rho}(\cdot, t)$ represents the material coordinates. Therefore,

$$\rho = \bar{\rho}(X, t) = \bar{\rho}(X_1, X_2, X_3, t) \tag{5}$$

If these coordinates are fixed then the particle is being followed, which is the definition of the Lagrangian description of motion (see figure 2.1).

2.1.2. Eulerian description of motion.

The Eulerian or spatial description of motion is typically used in fluid mechanics as it focuses on just a point in space and analyses what is happening in this point as time progresses. Given the same property as in section 2.1.1., the density is described as a function

$$\rho(\cdot, t): R^3 \times R^+ \rightarrow R^+ \tag{6}$$

where

$$\rho = \rho(x, t) = \rho(x_1, x_2, x_3, t) \tag{7}$$

and x is a certain point in space.

If we fix a certain value of x, we can obtain the variation of the density for the different particles that pass by this point along time.

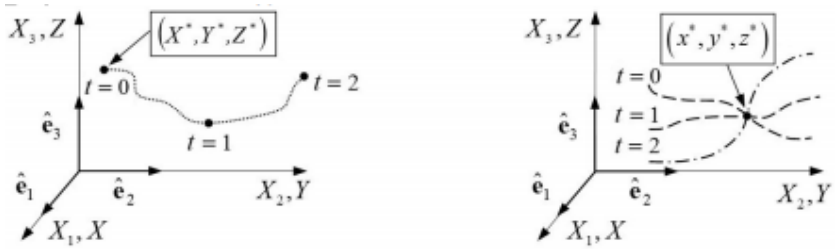

Figure 2.1. Lagrangian description (left) and Eulerian description (right) of a property. Source [5].

2.1.3. Local, material and convective derivatives.

The fact of considering different descriptions of motion results in different definitions of time derivatives. The definition of these different time derivatives is important because it sometimes allows the simplification the governing equations in any problem. Let us consider a certain property with the material and spatial descriptions

$$\Gamma(X, t) = \gamma(x, t) \tag{8}$$

Then, local and material derivatives are defined.

- The local derivative is defined as the variation of a certain property along time at a fixed point in space. Its expression is written as

$$\frac{\partial \gamma(x, t)}{\partial t} \tag{9}$$

- However, the material derivative of a given property is defined as the variation along time of a specific material point of the continuous medium. It means that the point is being followed. The expression for this derivative is given by

$$\frac{d}{dt}\Gamma = \frac{\partial \Gamma(X,t)}{\partial t} \tag{10}$$

Note that we can rewrite the material derivative using the equation of motion (3) as

$$\frac{d}{dt}\Gamma = \frac{d}{dt}\gamma(x(X,t),t) = \frac{\partial \gamma(x,t)}{\partial t} + \frac{\partial \gamma}{\partial x}\frac{\partial x}{\partial t} = \frac{\partial \gamma(x,t)}{\partial t} + \frac{\partial \gamma}{\partial x}\cdot v(x,t) \tag{11}$$

where $v(x,t)$ is the velocity. Therefore, for any property $\chi(x,t)$, the material derivative con be written as

$$\frac{d\chi(x,t)}{dt} = \frac{\partial \chi(x,t)}{\partial t} + v(x,t)\cdot \nabla \chi(x,t) \tag{12}$$

The expression (12) defines the convective derivative as the difference between the material and local derivatives. Note that if we consider the Lagrangian description of motion, the convective derivative is equal to zero and the local and material derivatives coincide, helping to simplify any problem with the Lagrangian description approach.

2.2. The Delaunay tessellation.

The Delaunay tessellation is a meshing methodology where each node of the set is the vertex of a polyhedron which define the mesh. The union of all these polyhedron is equal to the total volume of the problem analysed.

The problem we need to tackle is given a 3D random point set, to find an acceptable mesh and boundary surface in order to solve the differential equations that the problem needs with the appropriate boundary conditions. The definition of the boundary of the mesh will be seen in further points of this project.

In computational mechanics, several numerical methods need to subdivide the total domain of the problem tackled into some subdomains called elements. All these elements will form the mesh. In these kinds of problems, at each time step a new mesh is generated as the nodes move along the surface, therefore, the generation of the mesh must not have a big computational cost. The Delaunay tessellation requires a relatively low computational cost to generate the mesh, so this problem is avoided.

The problem that this project is focused on is based in a three-dimensional space. The Delaunay tessellation for three-dimensional problems consists in the linking of the nodes in the problem by means of tetrahedrons (in volumes) and triangles (in surfaces). In fact, the Delaunay tessellation can create polyhedrons with more than four sides but, for our case, the only polyhedrons created are tetrahedrons and triangles.

2.3. Alpha shapes.

Before presenting the definition of the alpha shapes, a few previous definitions must be presented. A convex hull of a random point set X is the smallest convex[2] set that contains X. Moreover, a definition of polytope is also needed to understand alpha shapes. A polytope is a geometric entity that represents the generalization into any number of dimensions of a polyhedron (a geometric entity with flat sides).

Now we can present the definition of the alpha shapes. Let X be a random finite set in $\mathbb{R}^3$ and α a real positive number. Then, the alpha shape of X is a polytope that is neither necessarily convex nor connected. Depending on the value of α, we can get different boundary surfaces (see figure 2.2). Alpha shapes are the generalization of a convex hull of a random point set X. Using the Delaunay tessellation, it is fairly easy to compute alpha shapes in the three dimensional space.

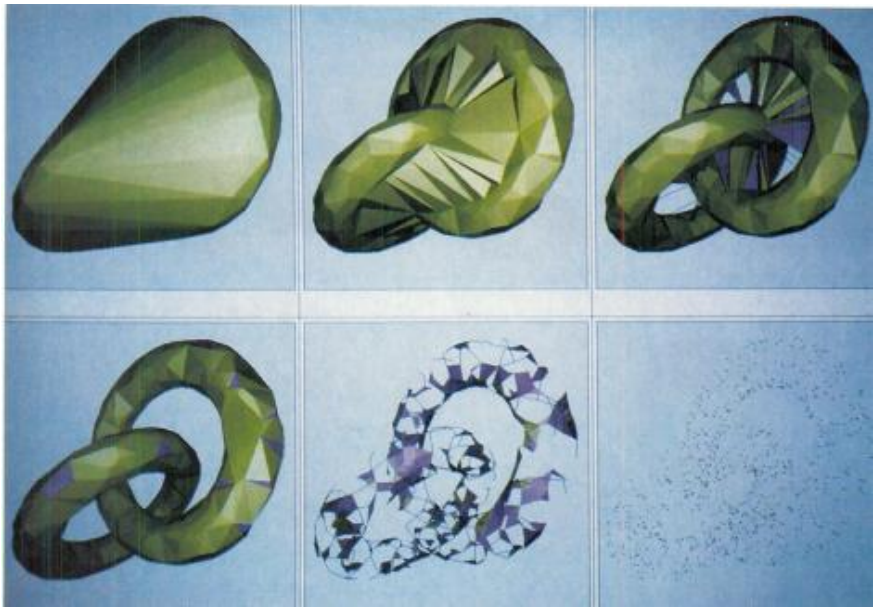

Figure 2.2. Different alpha shapes generated varying the value of α. For $\alpha = +\infty$ (top left) the alpha shape is equivalent to h¡the convex hull, however for $\alpha = 0$ (bottom right) the alpha shape is equal to the set of points itself. Source [7].

[2] In this context, we understand that a convex polygon is one that satisfies for any pair of points contained in the polygon, the straight line that joins these two points is also entirely contained in the polygon. Any triangle would be an example of a convex polygon, but a U-shaped polygon is not classified as a convex polygon.

3. The Particle Finite Element Method.

In this section of the project the Particle Finite Element Method (PFEM) is presented, with the basic ideas outlined alongside with the governing equations and their discretization. Some examples are as well presented using the PFEM in the PFLOW software.

3.1. Definition and basic ideas.

In recent years, the need to solve fluid-structure interaction problems has increased in many areas of engineering. For instance, one of the most devastating natural hazards in terms of life losses and material and structural damages is the flood risk via tsunamis which, sadly, seem to happen too often in south-eastern Asian countries. Hence, a robust method for solving fluid-solid interaction problems is needed in order to simulate the possible damages that these kind of floods can produce.

But the study of fluid-solid interaction problems is not only useful for the aforementioned case; ship hydrodynamics, off-shore structures, spillway dams, harbour engineering, geotechnical engineering problems among others would also beneficiate of a robust method for solving fluid-solid interaction problems, as water is nearly always present in these cases.

Traditionally, the finite element method (FEM) [9] has been used for analysing problems regarding the movement of solids in fluids using the Eulerian and the arbitrary Lagrangian-Eulerian (ALE) formulation. With this method, we encountered some difficulties which are the treatment of the convective terms (see section 2.1) and the incompressibility constraint in the fluid equations, the modelling of wave splashing, the different treatment of the solid and fluid domains, etc. The PFEM deals with these difficulties with innovative ways to generate the mesh, identifying the boundary and treating the nodes as “particles”, which will be explained shortly.

The PFEM is an innovative numerical method for solving fluid-solid interaction problems. It was the evolution of the works of Idelshon *et al.* (2003) [10] for solving these problems using Lagrangian finite element and meshless methods.

Using the Lagrangian description of motion to formulate the governing equations of solid and fluid domains, these problems disappear. As we know from section 2.1, the Lagrangian description of motion focuses on the movement of the nodes as they are followed along time. Hence, the nodes can be viewed as moving “particles”. Here is where the name of this numerical method comes from.

A finite element mesh connects the nodes defining the discretized domain where the governing equations, which we will see in further sections, are solved as the standard FEM. The PFEM treats the mesh nodes in fluid and solid domains as particles which can

freely move in the plane if it is a two-dimensional problem or in the space if the problem is in 3D.

With the Lagrangian formulation we avoid a lot of difficulties that we could encounter such as that the convective terms of the fluid equations disappear. However, we find a new difficulty regarding moving the mesh nodes adequately. To solve this problem, the Delaunay tessellation is used to generate de mesh at each time step. The Delaunay tessellation is characterized for being a low-computational method to generate the mesh of the solid and fluid domains. Furthermore, the shape functions used for the Delaunay tessellation are meshless finite element shape functions, which are well explained in Idelshon *et al.* (2003) [10].

As in the PFEM the Lagrangian description of motion is used, the information that the mesh gives us is typically nodal-based. This information given is usually the velocity or the pressure, among others, of each node of the discretized domain.

In terms of identification of the boundary of our initial set of nodes, the PFEM uses the so-called Alpha Shape technique (see section 2.3), which identifies the boundary nodes and links them, creating the general boundary for all nodes at each time step.

All in all, in the PFEM, the boundary is identified and generated by the Alpha Shape technique, then the mesh is created with the Delaunay tessellation and finally the equations are solved in the standard FEM fashion. All these steps are done for each time step so, for long-time analysis with the PFEM, the computational time is sometimes very large. In figure 3.1 we can see an overview of the steps explained above.

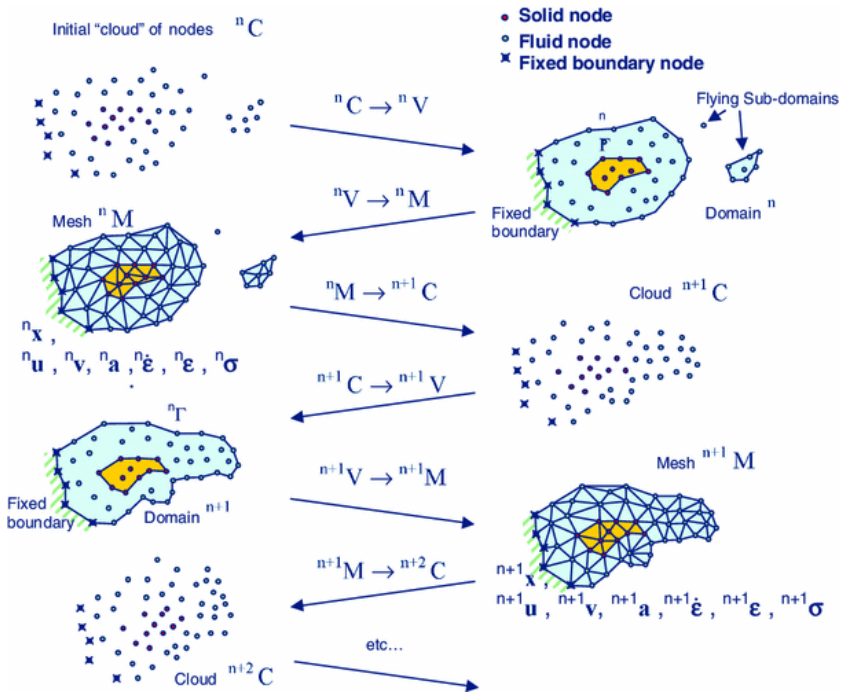

Figure 3.1. Sequence of steps to update the set of nodes representing a domain containing solid and fluid. Source [3].

Note that in figure 3.1, n represents a certain time step (t_n) and $n+1$ represents the next time step separated by the increment of time that we previously set ($t_n + \Delta t$).

Hence, the typical solution with the PFEM involves the following steps:

1. The starting point at each time step is a set of points in the fluid and solid domains.
2. Identify the boundaries for both the solid and fluid domains via the Alpha Shape method.
3. Discretize the fluid and solid domains with a finite element mesh generated by the Delaunay tessellation.
4. Solve the Lagrangian equations of motion for the fluid and solid domains.
5. Move the mesh nodes to the new position where they will be at the next time step.
6. Go back to step 2 and repeat the process for the next time step.

All in all, the PFEM is a promising numerical technique for solving fluid solid interaction problems which there involves large motions of fluid and solid particles.

3.2. PFEM formulation. Governing equations.

In this section, the governing equations used for the PFEM are presented. Further information and equations can be found in Oñate *et al.* (2014) [1]. Just the basic notions of the PFEM equations used will be presented.

We assume that water, which is the only fluid that we will work with, is a viscous incompressible fluid with constant density. The standard infinitesimal equations for this fluid can be written in the Lagrangian frame as

$$\rho \frac{\partial v_i}{\partial t} = \frac{\partial \sigma_{ij}}{\partial x_j} + b_i \tag{14}$$

$$\frac{1}{K}\frac{\partial p}{\partial t} - \frac{\partial v_i}{\partial x_i} = 0 \tag{15}$$

$$i, j = 1, \dots, n_d \tag{16}$$

where n_d is the number of dimensions of our problem, v_i is the velocity[3] along the *i*th global axis, ρ is the density of the fluid assumed to be constant, b_i are the body forces, p is the absolute pressure, σ_{ij} are the total stresses given by

$$\sigma_{ij} = s_{ij} - \delta_{ij} p \tag{17}$$

where s_{ij} are the viscous deviatoric stresses related to the viscosity of the fluid μ by

$$s_{ij} = 2\mu \left(\dot{\varepsilon}_{ij} - \delta_{ij} \frac{1}{3} \frac{\partial v_k}{\partial x_k} \right) \tag{18}$$

with δ_{ij} being the Kronecker delta and $\dot{\varepsilon}_{ij}$ the strain rates, given by the expression

[3] The velocity is understood as $v_i = \frac{\partial u_i}{\partial t}$, where u_i is the *i*th displacement.

$$\dot{\varepsilon}_{ij} = \frac{1}{2}\left(\frac{\partial v_i}{\partial x_j} + \frac{\partial v_j}{\partial x_i}\right) \quad (19)$$

Equations 14 and 15 are respectively the momentum equation and the mass balance equation.

As pointed above, water is assumed to be an incompressible fluid, so the bulk modulus (K) in equation 15 is equal to infinity. Hence, the first term disappears.

Equations 14-19 are completed with the standard boundary equations which are presented in Idelsohn *et al.* (2008) [11].

3.3. Examples.

In this section, some simple examples using the PFEM are presented. The software used to run these examples as well as the main problem of the project, which we will see in further sections, is called PFLOW which can be found in the software GiD. "*GiD is a universal, adaptative and user-friendly pre and post-processor for numerical simulations in science and engineering. It is designed to cover all common needs in the numerical simulations field*" [12]:

- Geometrical modelling (CAD).
- Mesh generation.
- Definition of analysis data.
- Data transfer to analysis software.
- Postprocessing operations.
- Visualization of results.

Three basic two-dimensional examples have been run: a collapse of a water column, a rigid cube falling into a water container and an inflow of water going in a container of water. All these examples are two-dimensional-based and, as we will see in further points, the main problem analysed is three-dimensional based. These examples are presented to show the potential of the PFEM for solving fluid-structure interaction problems.

3.3.1. Case 1: collapse of a water column.

The first of the three examples presented corresponds to a collapse of a water column. The initial conditions for this problem is that water is kept within a rectangle of dimensions of 40x50 square centimetres, and this water is retained via a board that holds it. The water is in a U-shaped container with two walls (vertical sides) of 50 cm each and a horizontal element which measures 100 cm (see figure 3.2). At $t = 0$, with an infinitesimal time step, the board is removed and water falls into the container describing a motion which we will see shortly.

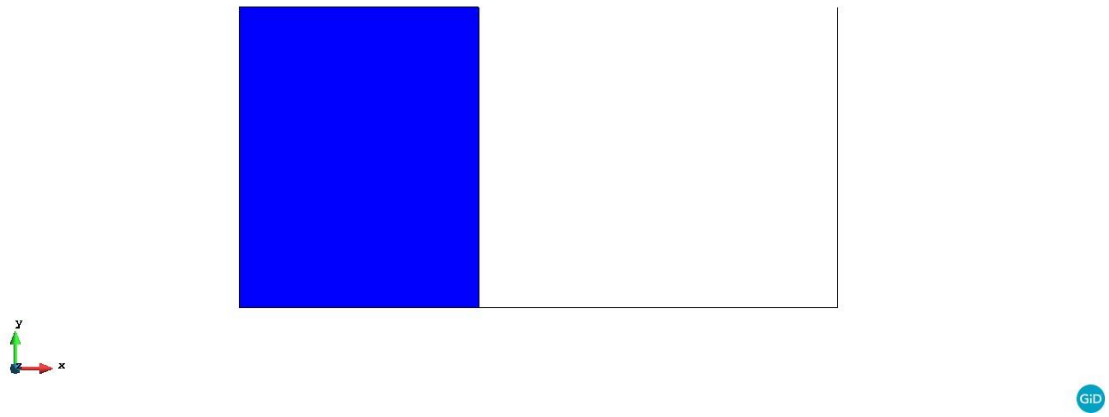

Figure 3.2. Case 1 at t = 0 seconds.

For this case, surface tension is neglected and we adopted a value of viscosity so small that we could consider that viscosity is as wall neglected. We set the container to be a solid with imposed motion, which is that it does not move throughout time. The total time of simulation is set to 5 seconds and the time steps to print results are 0.08 seconds, therefore we will have 63 files of results.

The parameter alpha for the generation of the mesh via the alpha shape method is set to 1.20. Regarding the generation of the mesh, the size is set to 0.2 which gives us a total of 660 nodes and 1263 elements. The smaller the mesh size we set, the bigger the number of nodes and elements and the bigger the total computational time. The resulting mesh can be seen in figure 3.3.

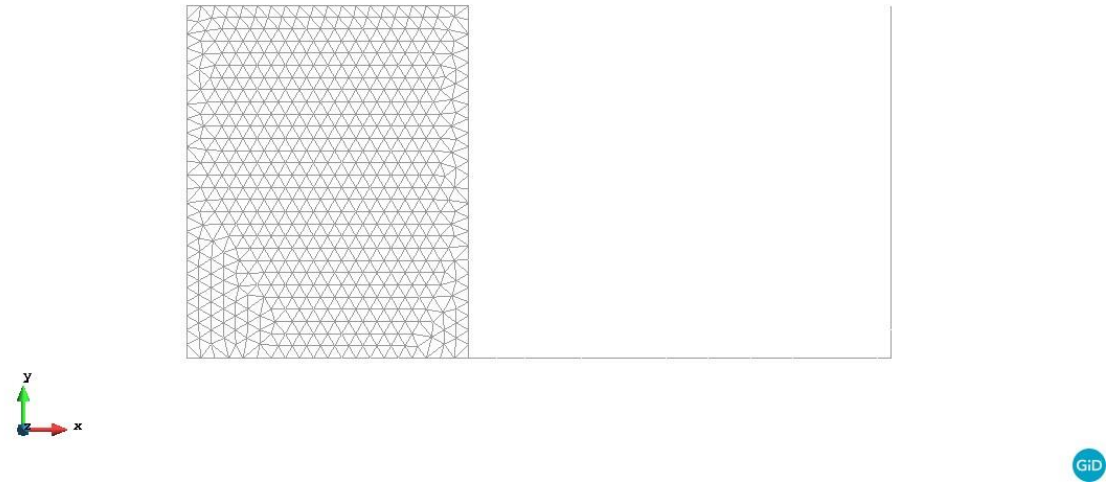

Figure 3.3. Resulting mesh of case 1.

Once the mesh is created, we can go ahead and calculate this first case. The results can be seen in figure 3.4, where the movement of water can be seen.

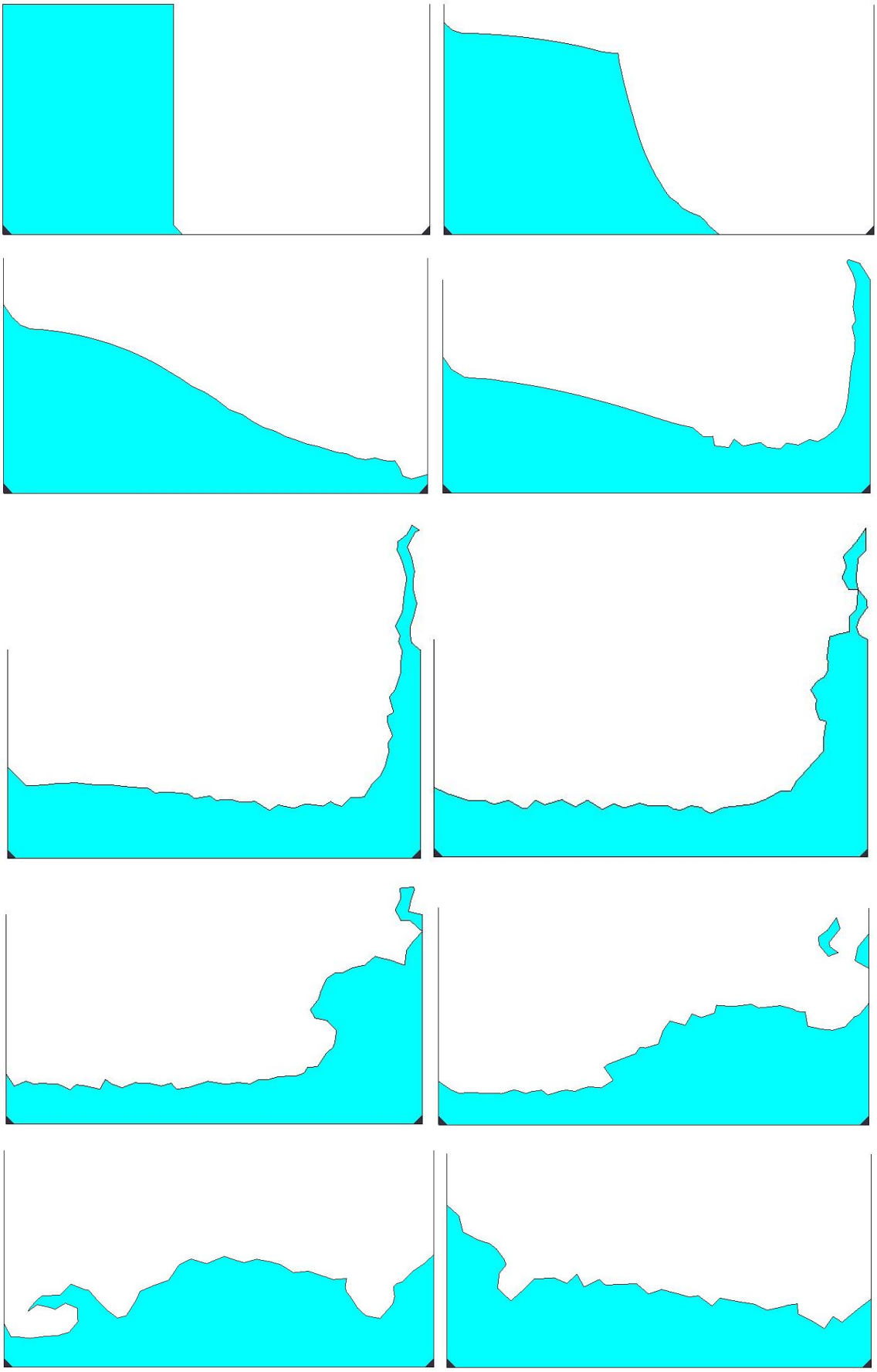

Figure 3.4. Results of the case 1 at different time steps.

Figure 3.4 shows us the motion of the collapse of the water column. The time steps represented by these ten images are respectively (from top left to bottom right) 0.08s, 0.56s, 0.96s, 1.36s, 1.92s, 2.40s, 2.96s, 3.52s, 4.00s and 4.56s. As we can see in this figure, the simulation is accurate enough to what would happen in reality so, regarding this example, we can say that PFEM is a robust method for solving fluid-structure interaction problems.

Next, the second of the simple cases analysed is presented.

3.3.2. Case 2: rigid cube falling into a water tank.

The second of the three simple cases analysed prior to the main problem is the case of a rigid cube falling into a water tank. In the first case analysed, as there was only water and an imposed-motion solid, we only had to "draw" two different layers. In this case we have to create three layers: one corresponding to the water tank (a solid with imposed motion), another corresponding to water and another corresponding to the rigid cube (a mobile solid).

So, the layers we created are:

- Boundary layer. This layer is a solid with imposed motion, which is that it does not move prom its position along time.
- Water layer. For this layer, as in the first case, the surface tension was neglected and we adopted a small value for the viscosity, which allows us to neglect the viscosity as well. The density is set to 1000 kg/m^3.
- Solid layer. This layer corresponds to the rigid moving cube. Its movement was set to begin at $t = 0$ seconds and to last the entirety of the time which the case is calculated and there are no constraints of centre of gravity set. The mass of the cube is 1 kilogram.

The water tank measures 10x5 square centimetres and the cube is a square with 10-centimetre sides. The cube is initially positioned as figure 3.5 shows.

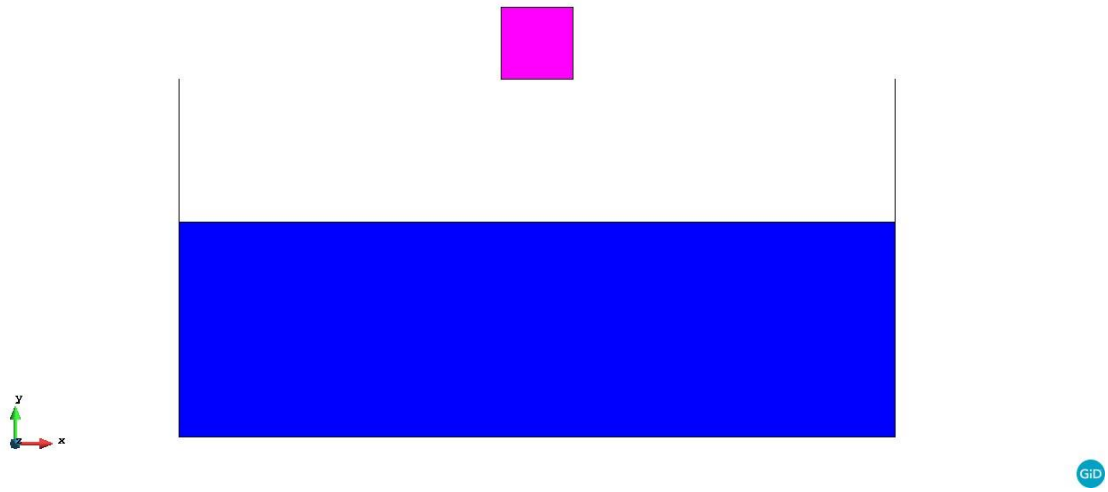

Figure 3.5. Case 2 at t = 0 seconds.

For the meshing process, the alpha parameter of the alpha shape method is set to 1.20. For this case, the mesh size is set to 0.1, which gives us a total of 3673 nodes and 7302 elements in the mesh. The mesh generated can be seen in figure 3.6. The total time of simulation is 5 seconds and the time step to print results is 0.1 seconds, so there will be 50 files of result data.

The results can be seen in figures 3.7 and 3.8.

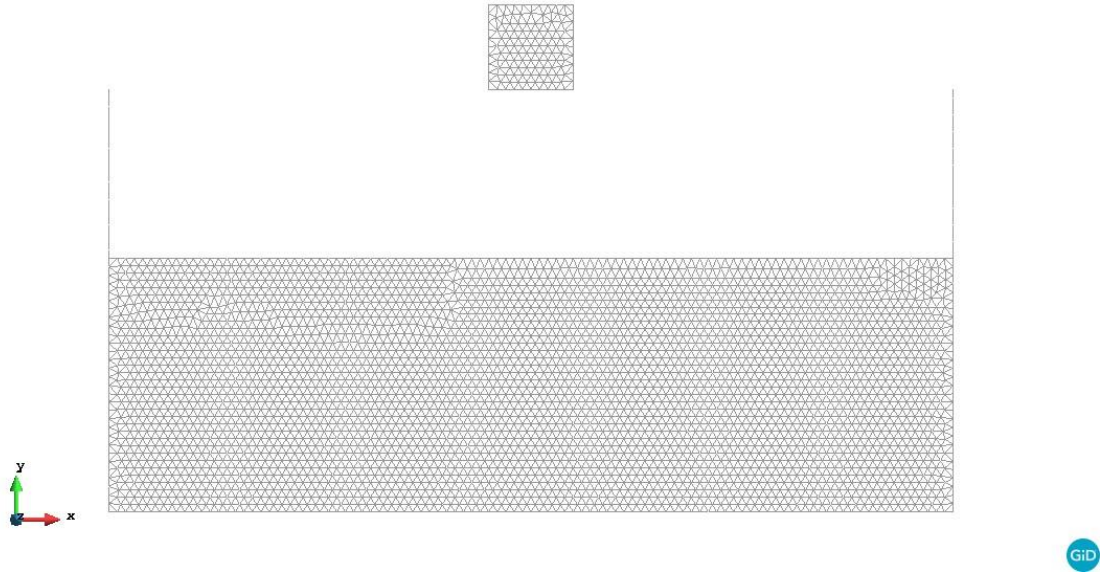

Figure 3.6. Resulting mesh of case 2.

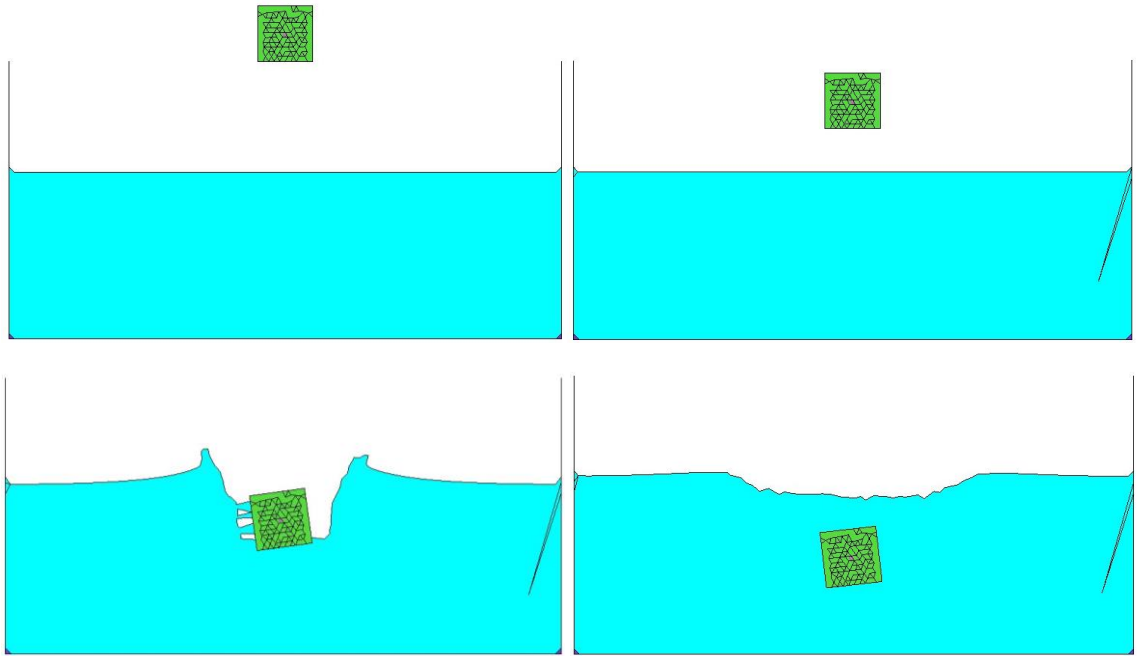

Figure 3.7. Results of the case 2 at different time steps.

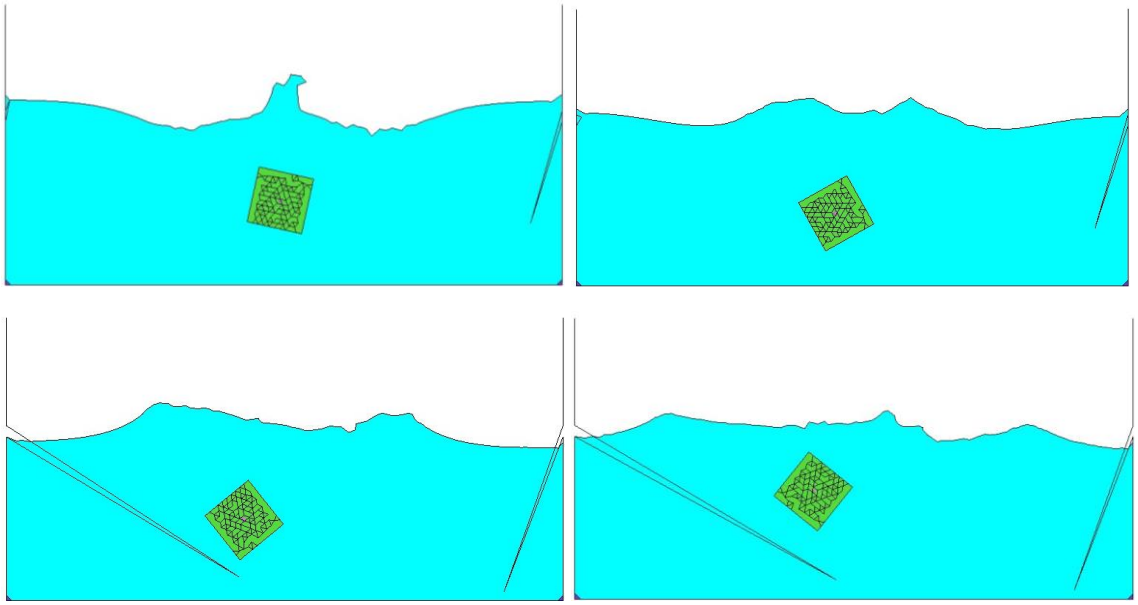

Figure 3.8. Results of the case 2 at different time steps (cont.).

The time steps represented in figure 3.7 are (from top left to bottom right) respectively 0.1s, 0.6s, 1.1s and 1.6s, and the time steps represented in figure 3.8 are respectively 2.1s, 2.6s, 3.1s and 3.6s.

Finally, in the next section is presented the last case of the three analysed.

3.3.3. Case 3: flow of water going in a container partially full of water.

The third and final of the simple cases that are analysed prior to the main problem of this project is a case of a flow of water flowing in a partially full U-shaped container of water. Especially for this case, we will see if the software and the PFEM are a robust method for analysing fluid-structure interaction problems because it implies a lot of water movement. In this case we will see how water drops are formed, which is really interesting in harbour engineering and coastal engineering, mostly when analysing the sea waves crashing into a jetty.

As in the second case, three different layers are created in order to solve properly the problem:

- Boundary layer, which corresponds to the U-shaped container which nodes are located in random points in the plane. Obviously, this layer is a solid with imposed motion, which lasts from the beginning to the end of the analysis of the case, and it restrains any kind of movements in all directions.
- Water layer. This layer represents the water and is a fluid with null surface tension. Like the previous cases, we adopt the viscosity a really small value which allows us to consider it negligible.
- Fluid-in layer. This layer is located where the inflow of water will come. It represents the water flowing in the problem. Again, we neglected the surface tension and the viscosity of water. The inflow velocity we adopted is $(v_x, v_y, v_z) = (5,0,0)$, the inflow surface is 5 and the mesh size is 0.1. Finally, we

set the water to begin flowing at $t = 0$ and last until the analysis of the problem finishes.

The initial shape of the problem can be seen in figure 3.9.

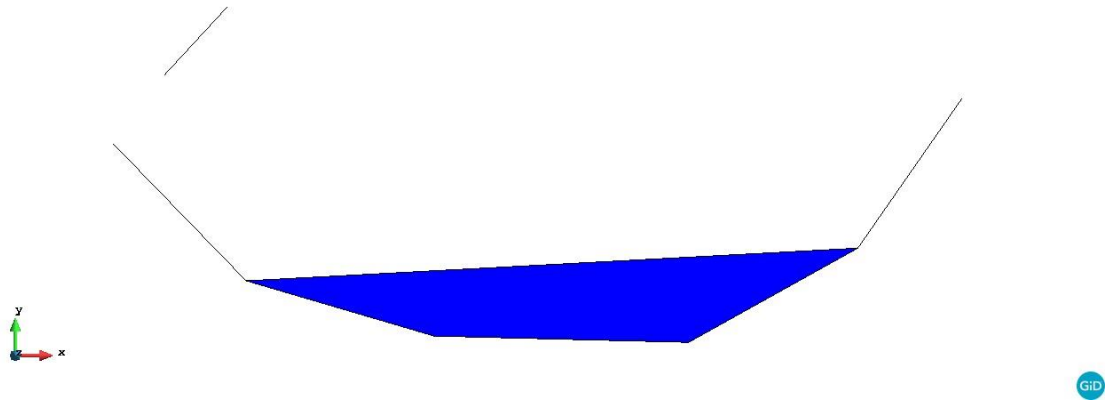

Figure 3.9. Case 3 at t = 0 seconds.

Regarding the mesh parameters, the alpha parameter, as in the other examples, is 1.20, and the mesh size is 0.1. The resulting mesh gives us a total of 865 nodes and 1661 elements. The mesh can be seen in figure 3.10.

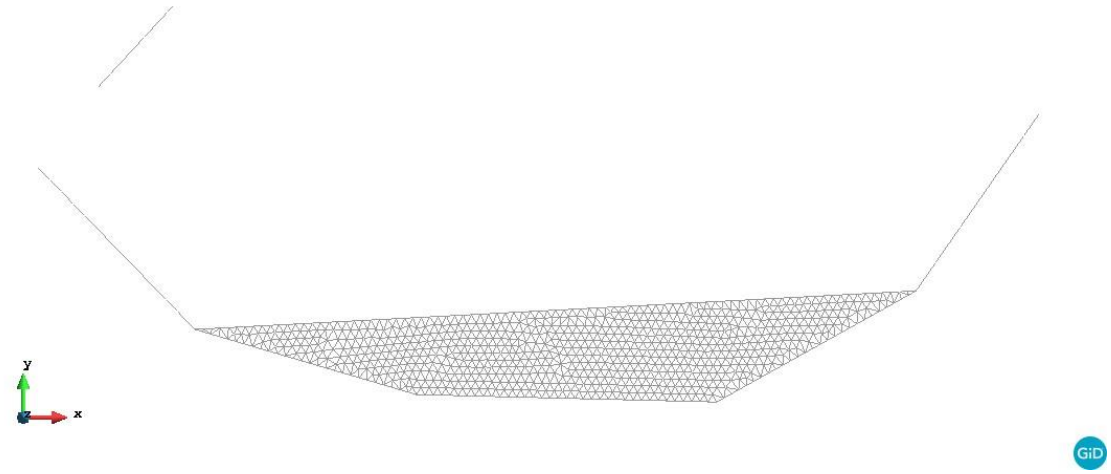

Figure 3.10. Resulting mesh of case 3.

The total time of simulation is 6 seconds and the time step to print results is 0.1 seconds, which means that 60 folders of results will be printed at the end of the calculation process. In figure 3.11 the results at different time steps can be seen.

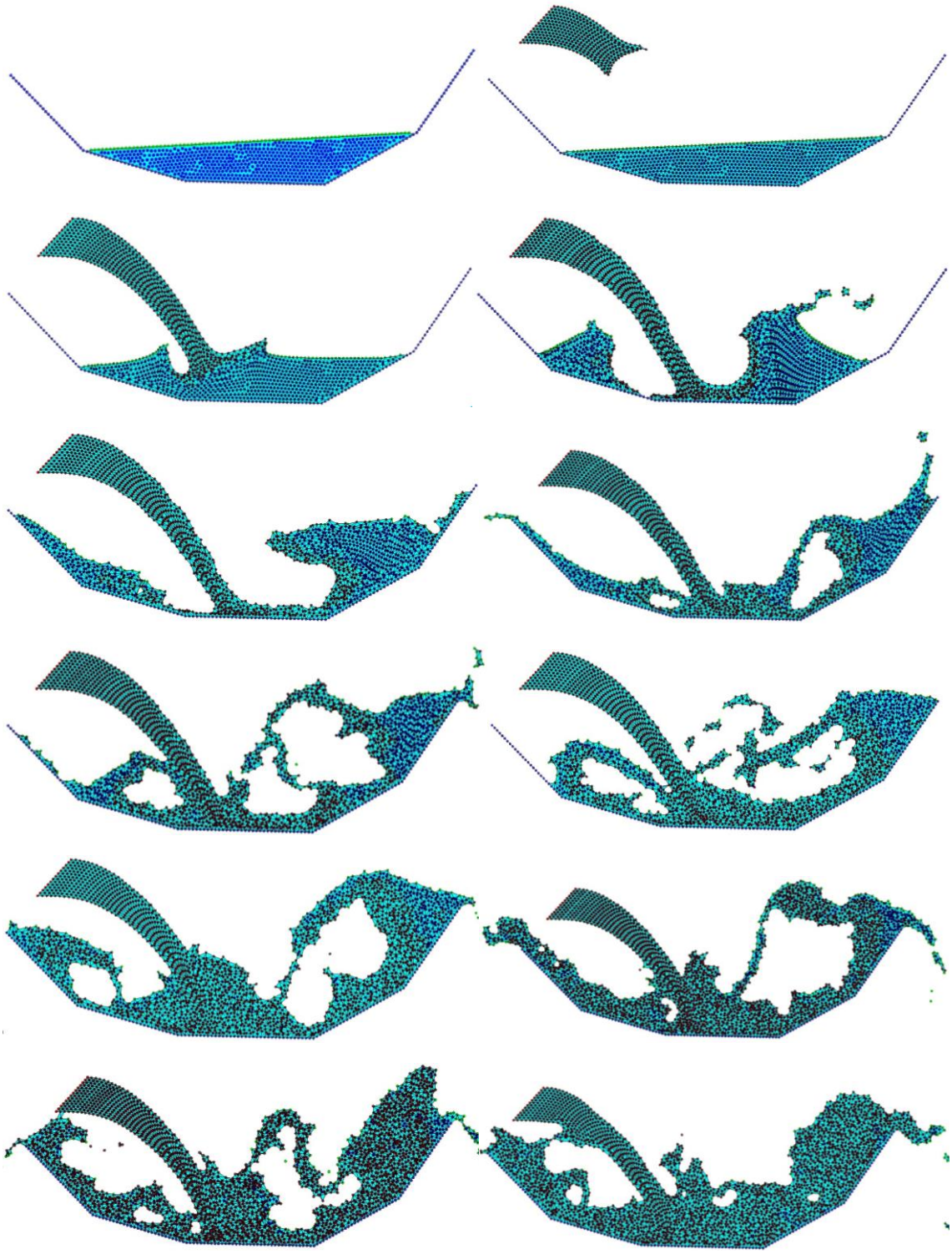

Figure 3.11. Results of case 3 at different time steps.

In figure 3.11, the time steps for each figure (from top left to bottom right) are 0.0s, 0.6s, 1.1s, 1.6s, 2.1s, 2.6s, 3.1s, 3.6s, 4.1s, 4.6s, 5.1s and 5.6s. As mentioned previously, the smaller the mesh size, the better the results will adjust to reality.

4. Experimental model and results.

Tsunamis are one of the most hazardous natural disasters we can find on Earth regarding life and material losses. The most recent one nowadays happened in March 11, 2011, when a huge tsunami hit Japan's north-eastern coast. This tsunami was caused by an earthquake of 9.1 magnitude which epicentre's was located 130 km away from the nearest city, Sendai, Miyagi prefecture.

In the wake of this tsunami, Asai and Chandra (2016)[14] carried out some experiments to see the causes of tsunamis to civil works, such as railways, roads and bridges, among others. They focused on the results of a tsunami that strikes a bridge, and analysed how it behaved through the hit of the tsunami. They chose a simple girder model which is subjected to a dam-break flow. In the experiments, this flow is created when a gate that holds a large amount of water is opened, causing a wave that hits the girder model.

The main aim of this project is to compare the results of the experiments carried out by Asai and Chandra (2016)[14] with the simulation of the experiments computed with the PFEM method to solve fluid-structure interaction problems using the PFLOW software. The experiments explained in the aforementioned paper, were built at a smaller scale than the reality. In figures 4.1 and 4.2 the dimensions on the experiments can be seen. In this paper, three different cases were calculated, depending on the initial height of water. In the experiments, a water column of different height depending on the case we find ourselves in is collapsed when the experiment starts running. Then the water strikes the bridge and brings away the girder of the bridge.

The bridge model consists in two fixed piers which hold a large piece of concrete which is not subjected with the fixed piers by any means, it is just laying on top of the piers by means of gravity (see figure 4.2).

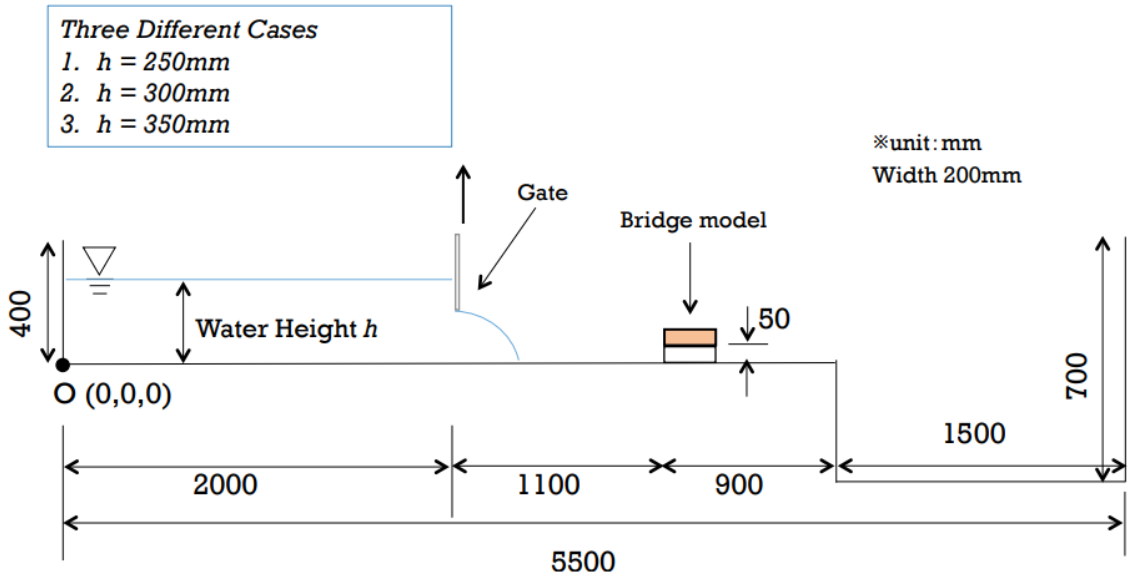

Figure 4.1. Model of the experiment carried out by Asai and Chandra. Source [14].

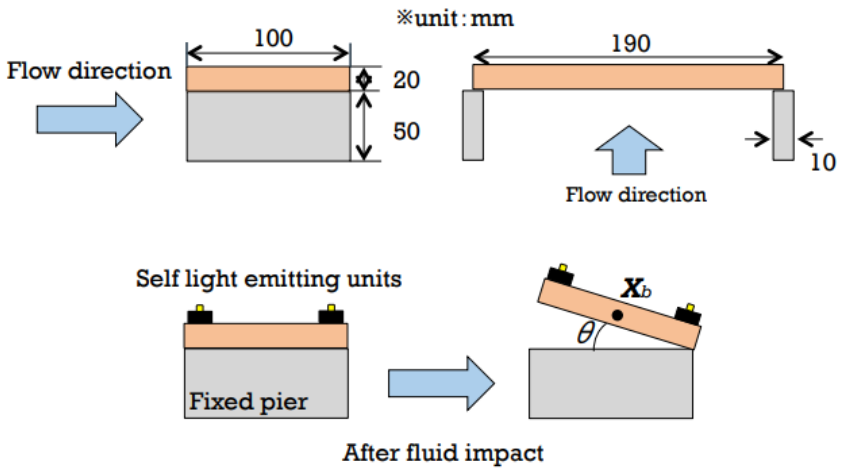

Figure 4.2. Detail of the bridge model and the motion capture system of the experiment carried out by Asai and Chandra. Source [14].

In the experiment, the motion (horizontal and vertical movement and clockwise rotation) of the concrete layer laying on top of the piers was tracked during all the duration of the experiment. As we mentioned, the bridge piers are fixed and the density of the girder is $\rho = 1.161\ g/cm^3$.

Figures 4.3 to 4.11 show the motion of the girder during the experiments. Note that the only data that we take into account is the experimental data not the analysis data.

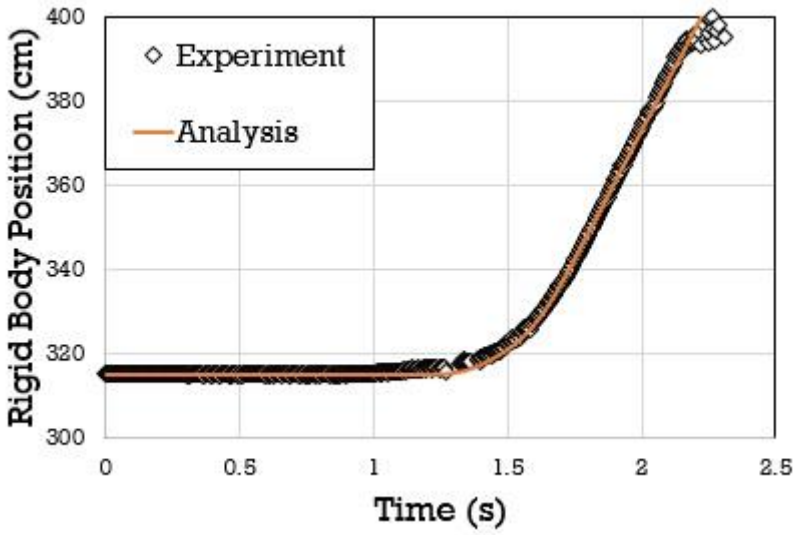

Figure 4.3. Horizontal motion of the girder's centre of gravity for initial water height 250mm. Source [14].

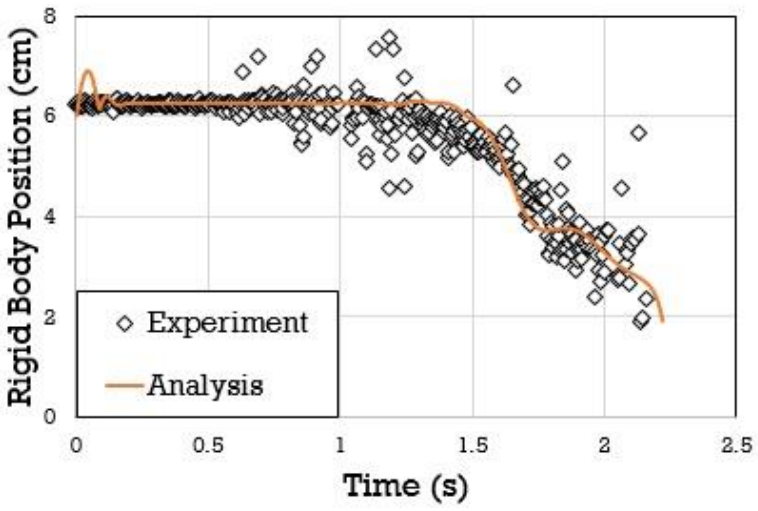

Figure 4.4. Vertical motion of the girder's centre of gravity for initial water height 250mm. Source [14].

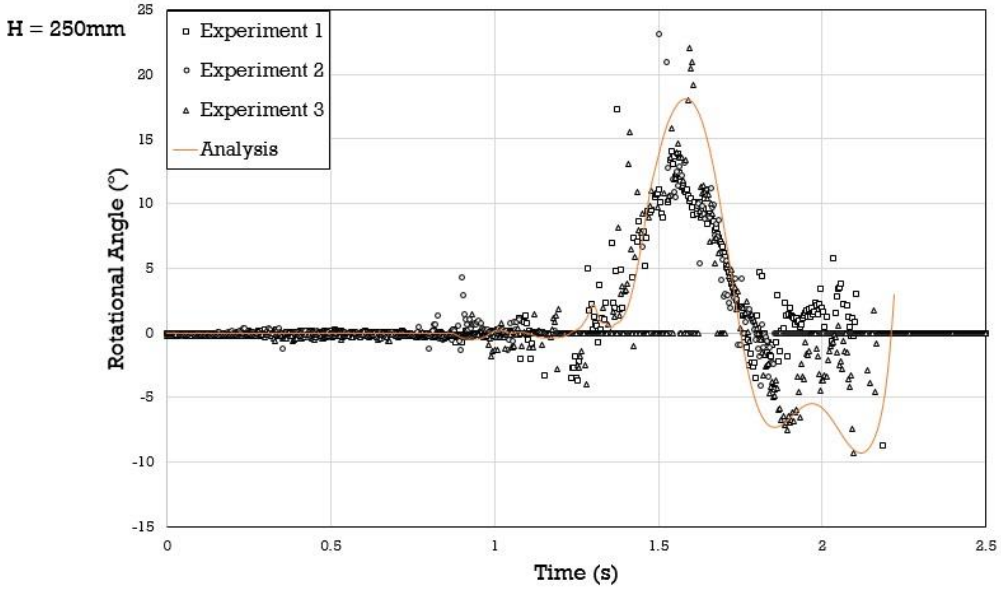

Figure 4.5. Rotational angle of the girder (see figure 4.2) for initial water height 250mm. Source [14].

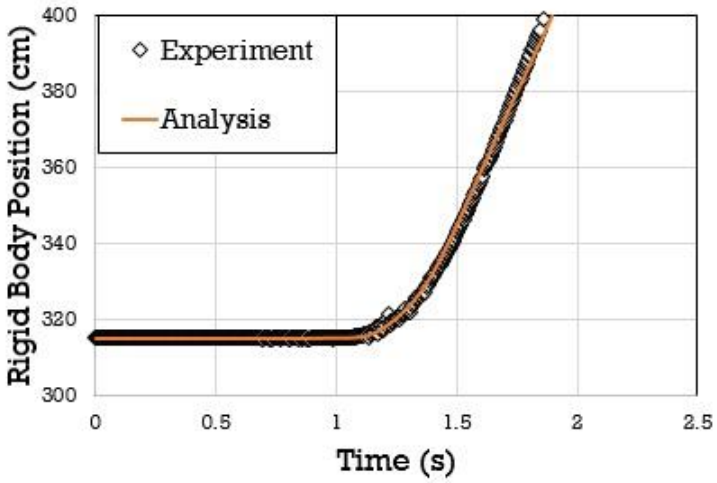

Figure 4.6. Horizontal motion of the girder's centre of gravity for initial water height 300mm. Source [14].

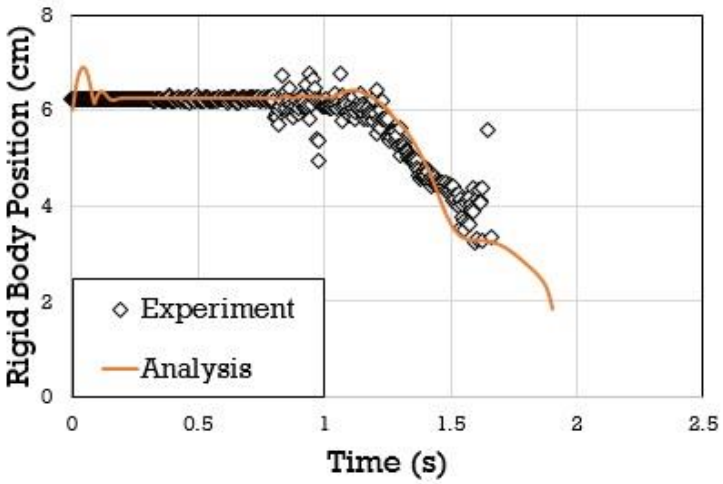

Figure 4.7. Vertical motion of the girder's centre of gravity for initial water height 300mm. Source [14].

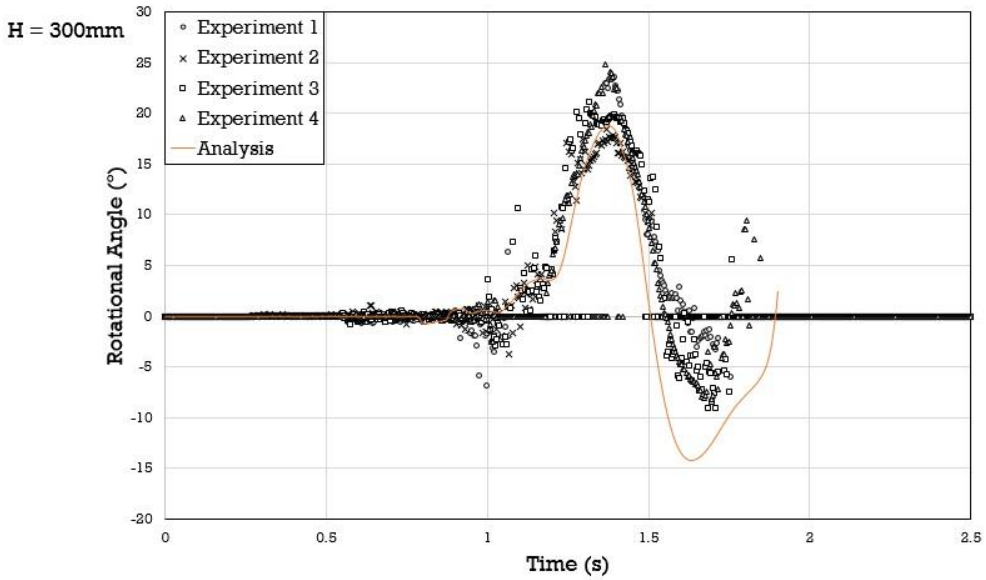

Figure 4.8. Rotational angle of the girder (see figure 4.2) for initial water height 300mm. Source [14].

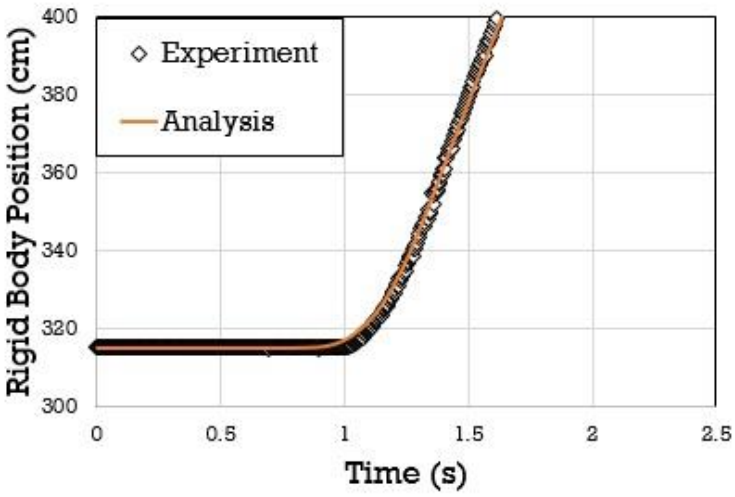

Figure 4.9. Horizontal motion of the girder's centre of gravity for initial water height 350mm. Source [14].

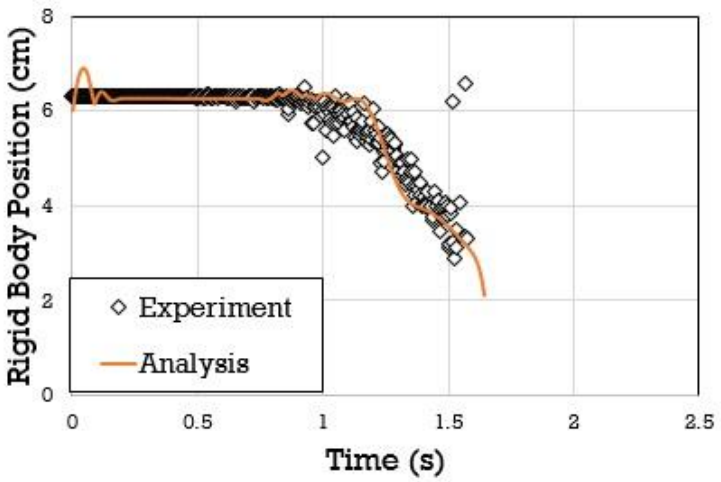

Figure 4.10. Vertical motion of the girder's centre of gravity for initial water height 350mm. Source [14].

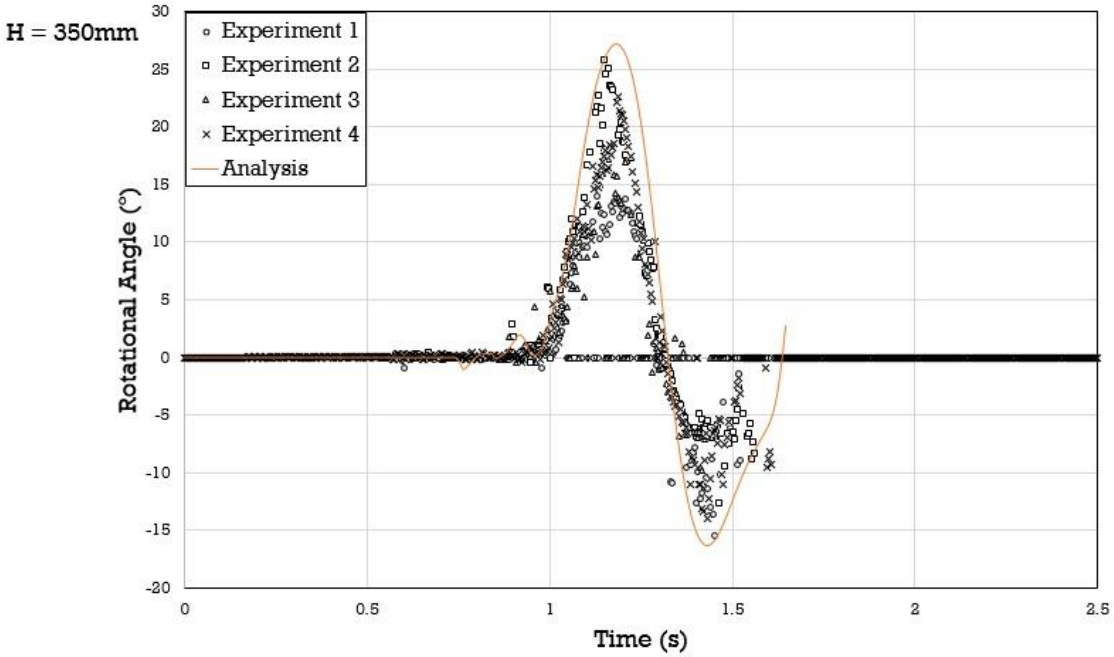

Figure 4.11. Rotational angle of the girder (see figure 4.2) for initial water height 350mm. Source [14].

It is obvious to guess that the higher the initial water height, the bigger the force that water will strike the girder. For the horizontal motion, we can note that the bigger the initial water height, the steeper the straight line after the water hits is, which means that the velocity of water when hitting the girder increases if the initial water height is big. Obviously, this depends on the friction angle between water and the girder, but if we keep it constant for all three water heights, the water will wash out the girder quicker for bigger initial water heights.

A similar thing is happening when looking at the vertical motion of the centre of gravity of the girder. If we focus on the vertical motion against time plots, we can note that the higher the initial water height is, the fewer time the girder will take to be washed out. As an example, for the 250mm initial water height, the last data we have is at around 2.3 seconds, for the 300mm initial water height, the last data from the experiment is at

around 1.7 seconds and for the 350mm initial water height, the last data is at around 1.6 seconds. For the three cases, the pattern of the plot is roughly similar, but as water height increases, the narrower the plot is.

Lastly, for the rotational angle against time plots, we can see as well a similar pattern in all plots but, similarly to the horizontal and vertical motion, as water height increases, the narrower the plot is. In these plots, we can see that when water hits, it creates a clockwise rotation off the girder which is equivalent to when water helps the girder slide through the fixed piers and fall into the water flowing underneath it. Then, when the girder has fallen into the water, makes an anticlockwise rotation which corresponds to when the girder is floating in the water.

All in all, from the experimental data we can see that the higher the initial water height is, the quicker and the bigger the force of water is when washing out the bridge. We see as well that for all three cases, the motion of the girder is very similar, even though in some cases it takes less time to be washed out.

The next point is the simulation of these experiments using the PFEM method to solve fluid-structure interaction problems with the PFLOW software.

5. PFLOW simulations.

This is the most important point of this project because the simulation and comparison of the experiments with the simulations is the main objective. In this part of the project, the simulations of the bridge wash-out phenomenon are presented with the boundary conditions and the problem data, along with the results and motion tracked of the girder of the bridge. In order to validate the PFEM method for solving fluid-structure interaction problems, we need to make a comparison between the experimental results (see section 4) and the simulations presented in this section.

Even though there is data for the three different initial water height, we will only focus on the first of these cases, which corresponds to an initial water height of 250 millimetres. For this initial water height, different simulations varying the mesh size adopted are presented. This will help to understand and see in practice the influence of the mesh size choice. The mesh sizes chosen for this case are 12 millimetres, 10 millimetres and 8 millimetres.

The reason for the choice of just one water height case and to run it with different mesh sizes is to help us to see the importance of the mesh size choice, regarding computational time, accuracy of the results, storage space in the PC, etc. This allows us to see how the girder is behaving with different mesh sizes and how does it influence to the movement of the girder once the wave hits it.

5.1. Analysis model, bridge model and boundary conditions.

The bridge chosen to simulate the wash-out phenomenon is a simple girder model. The analysis model is built in a way that simulates the experimental data of Asai and Chandra (2016)[14], hence the measures of the analysis model are slightly different than in the experimental model (see section 4).

At first, the exact same measures of the real experimental problem of Asai and Chandra (2016)[14] were introduced in the software. Note that the distance between the walls of the container and the girder is just 5 millimetres. When there are two different solid layers in a certain problem, the PFLOW software creates some contact elements (tetrahedrons) of the size of the mesh size and they act as a linking point between the two solid layers. Therefore, for our case, if we work on mesh sizes of less than 5 millimetres there would be no problem at all because these contact elements between the walls and the girder would not exist. However, if we work on mesh sizes greater than 5 millimetres, then these contact elements are created, preventing the flow of water to go through the space between the girder and the walls and, hence, preventing the movement of the girder when the water wave hits it.

As an example, the problem with the exact same measures as the experiments with a mesh size of 12 millimetres was carried out. The results can be seen in figure 5.1.

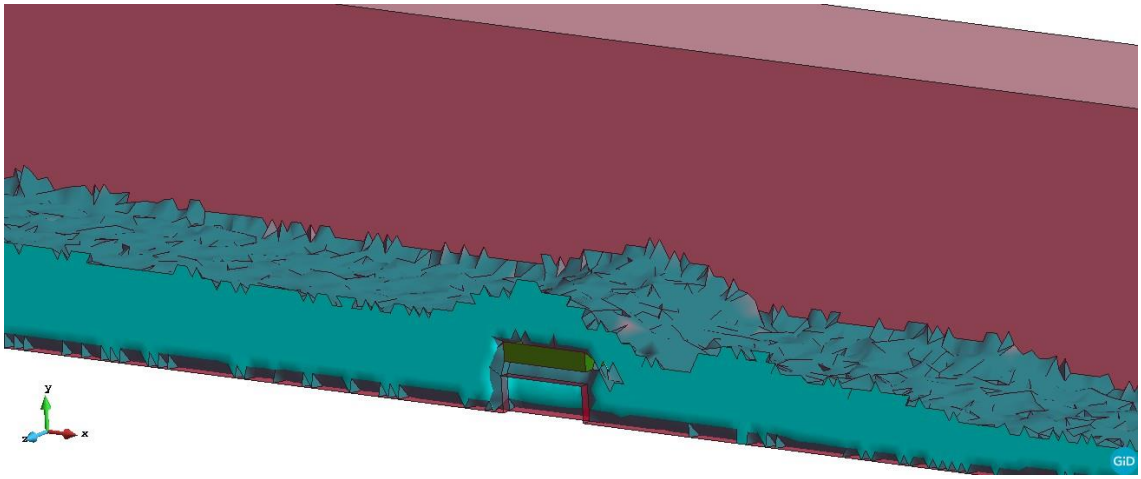

Figure 5.1. Results of the problem with the experimental measures simulated with a mesh size of 12 millimetres at the time step 1.80426 seconds.

In figure 5.1, it can clearly be seen that the results obtained are not correct because the girder is not moving from its initial position. In order to overcome this shortcoming, the dimensions of the analysis model are slightly changed: in the *z* direction, the walls have been expanded 50 millimetres apart from each other. In other words, the front wall of the problem simulated in figure 5.1 is located at $z = 250\ mm$ and the back wall is located at $z = 0\ mm$; and the location of the front wall in the corrected analysis model is at $z = 300\ mm$ and the back wall is at $z = -50\ mm$. Hence, in the *z* direction the measures of the problem have been expanded a total amount of 100 millimetres in order to leave enough space between the walls and the girder for the correct simulation of the problem.

So, the analysis model and a detailed view of the girder can be seen in figures 5.2 and 5.3. Note that the measures of the water layer have been expanded accordingly with the expansion of the container but the measures of the bridge layer have not been changed. This way, the simulation results will be as accurate and accordingly to the experimental results that of Asai and Chandra (2016)[14] presented in their study.

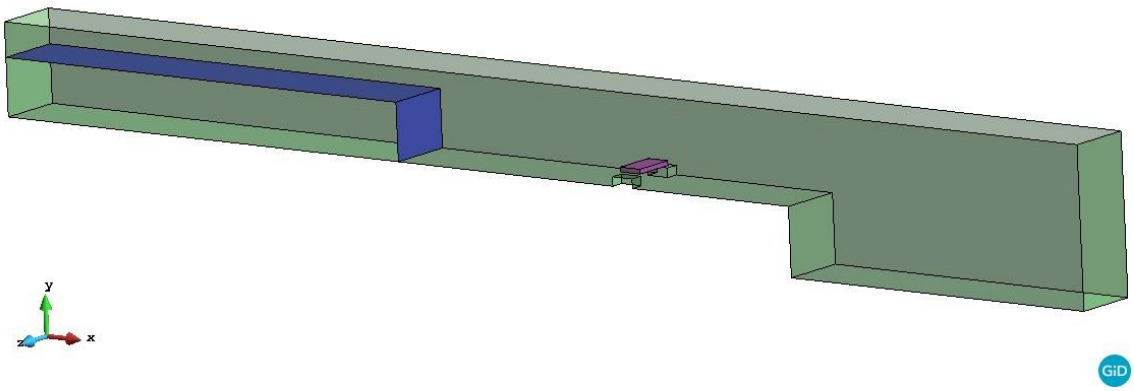

Figure 5.2. Analysis model.

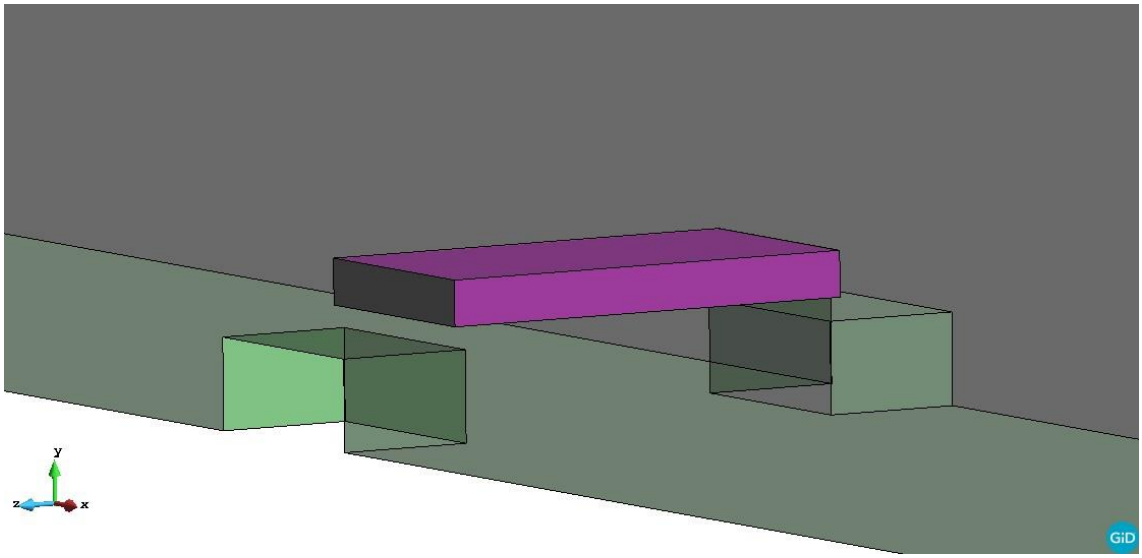

Figure 5.3. Detailed view of the bridge model.

For each mesh size, the measures, bridge model and boundary conditions are the same, the only different asset is the mesh size and therefore the mesh data as well.

For each case, the bridge is located at the same place as in the experiments and depending on the mesh size that is being used, the height of the fixed piers is different. This is because we let the software to create the aforementioned contact elements between the girder and the piers. The distance set between the girder and the piers for each case will be the same than the mesh size set. So, if for instance we work on a 12-millimetre mesh size, the height of the girder is 50 millimetres and the height of the fixed piers is 38 millimetres, and if we work on a 5-millimetre mesh size, the height of the girder is 50 millimetres and the height of the fixed piers is 45 millimetres. This way, the girder is laying over the piers just by means of gravity.

Regarding the boundary conditions of the problem, for each case three different layers are created, a fluid layer for water (blue colour in figure 5.2) and two solid layers for the container of the experiment (green colour) and for the girder (pink colour). Each layer has its own boundary conditions which are explained in the following points:

- Water layer. As the name points out, this layer corresponds to the water in the problem. The only assumptions made for this layer are that there is no surface tension and the viscosity can be neglected (see figure 5.4).

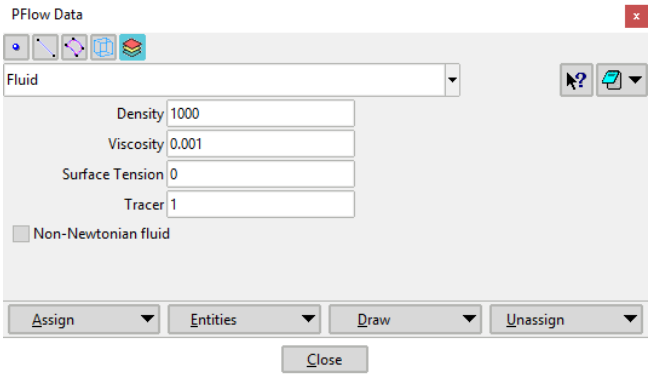

Figure 5.4. Properties of the water layer.

- Structure layer. This layer corresponds to the container where the experiment is held (green colour in figure 5.2). This is a solid layer with imposed motion which does not move throughout the analysis time of the problem. So there is no velocity set nor rotation set to the layer. In Asai and Chandra (2016)[14] the sliding friction coefficient estimated for all the solid layers is $\mu = 0.05$, so the friction angle (θ) is:

$$sin(\theta) = \mu \;\Rightarrow\; \theta = arcsin(0.05) = 2.87 \tag{20}$$

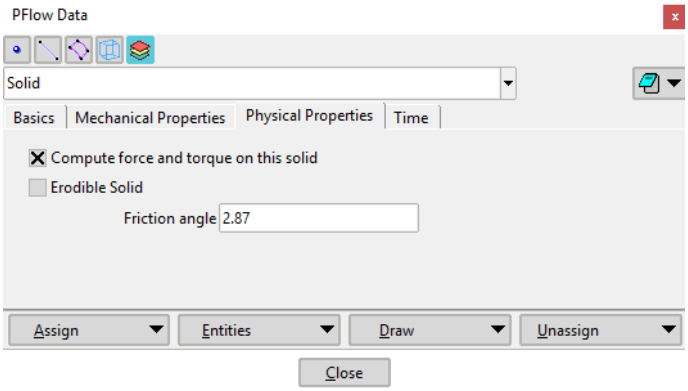

Figure 5.5. Physical properties of the structure layer.

- Bridge layer. This layer corresponds to the girder (pink colour in figure 5.2). The structure and bridge layers had to be separated because the container (structure layer) has no motion throughout the simulation time and the girder (bridge layer) is a mobile solid. For this layer, the mass, principal moments of inertia and the centre of gravity had to be calculated.
  Given the density of the girder which is $\rho = 1.161\ g/cm^3$, the mass (m) can be calculated as the product of the density by the volume:

$$m = \rho \cdot V = 1.161\ g/cm^3 \cdot 19\ cm \cdot 10\ cm \cdot 2\ cm = 0.44118\ kg \tag{21}$$

  Given the measures of the girder in the three directions of the space $x_g = 10\ cm$, $y_g = 2\ cm$ and $z_g = 19\ cm$, the principal moments of inertia can be easily calculated:

$$I_x = \frac{1}{12} \cdot m \cdot \left(y_g^2 + z_g^2\right) = \frac{1}{12} \cdot 0.44118 \cdot (0.02^2 + 0.19^2) = 1.342 \cdot 10^{-3}\ kg \cdot m^2 \tag{22}$$

$$I_y = \frac{1}{12} \cdot m \cdot \left(x_g^2 + z_g^2\right) = \frac{1}{12} \cdot 0.44118 \cdot (0.10^2 + 0.19^2) = 1.695 \cdot 10^{-3}\ kg \cdot m^2 \tag{23}$$

$$I_z = \frac{1}{12} \cdot m \cdot \left(x_g^2 + y_g^2\right) = \frac{1}{12} \cdot 0.44118 \cdot (0.02^2 + 0.10^2) = 0.382 \cdot 10^{-3}\ kg \cdot m^2 \tag{24}$$

  Finally, the centre of gravity of the girder is located at the position in space:

$$(x, y, z) = (3.15, 0.06, 0.1)\ m \tag{25}$$

The friction angle for this layer is the same as for the structure layer and its calculation procedure is the same (see equation 20).

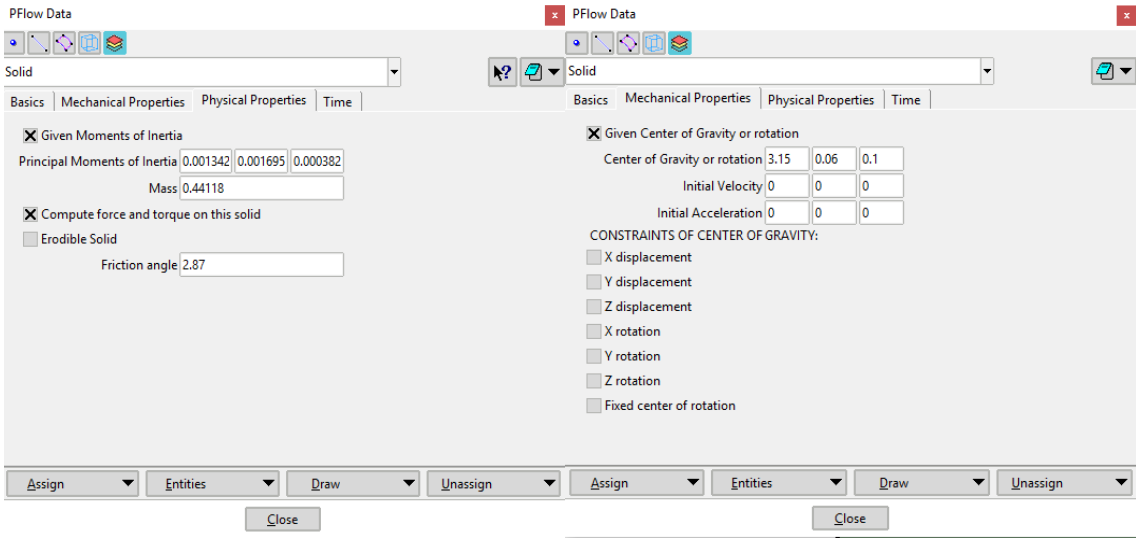

Figure 5.6. Mechanical and physical properties of the bridge layer.

Regarding the problem data, the total time of simulation is set to 4 seconds while the alpha parameter for the alpha shape technique (recognition of free surface) is set to 1.10.

Once all problem data and boundary conditions are presented, the mesh is generated. In the following sections, the mesh is generated with different mesh sizes which will result in different results regarding the accuracy of them. Each of the following sections represent a different mesh size for the mesh generation. For all the mesh sizes, the boundary conditions and problem data are the same.

5.2. Mesh size of 12 millimetres.

5.2.1. Data of the 12-mm size's mesh.

A mesh size of 12 millimetres is the biggest mesh size used in this problem. It is obvious to think that the results resulting from this mesh size might be affected by the fact that the tetrahedron in the mesh are too big. However, the bigger the mesh size, the lesser the accuracy of the results and the lower the computational time will be. In section 3, we talked about the PFEM method and about the fact that for each time step, this method creates a new mesh with the new position of the nodes of the mesh, which position was calculated in the previous time step. So, for each time step, the new position of all nodes of the mesh is calculated and, once calculated, with the new position of all nodes the mesh is created again. This process is repeated for each time step until the simulation time set is reached.

Once the 12-mm mesh is generated, its data can be resumed in the following points.

- Number of nodes: 201.621 nodes.
- Number of triangles: 90.258 triangles.
- Number of tetrahedrons: 866.652 tetrahedrons.
- Number of elements (triangles and tetrahedrons): 956.910 elements.

These data is for the entire mesh, however regarding the different layers, the mesh data can be resumed in table 5.1.

Layer	Water	Structure	Bridge
Tetrahedrons	866.652	0	0
Nodes	156.220	45.441	386
Triangles	37.178	89.490	768
Lines	852	134.931	1.152

Table 5.1. Data by layer of the 12-mm size mesh.

An image of the bridge with the mesh can be seen in figure 5.7.

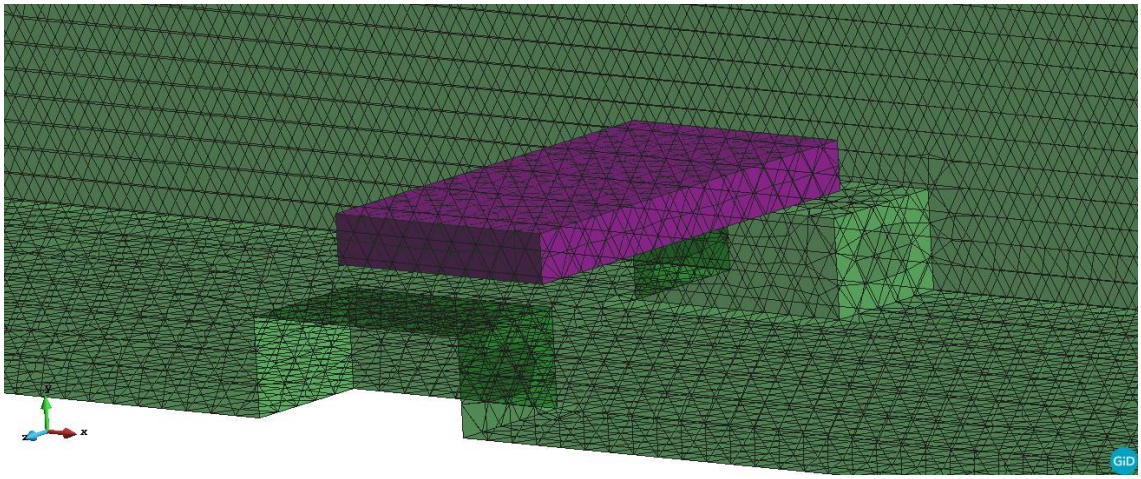

Figure 5.7. Close look of the bridge with the 12-mm mesh.

5.2.2. Results of the 12-mm mesh size case.

In this section, the results with the boundary conditions presented in section 5.1 and with the mesh generated with a mesh size of 12 millimetres are presented.

First and foremost, an example of the output info for a certain time step calculation can be seen in figure 5.8.

```
######-Global Problem-######
********** Running on 1 processor... ********************
Assembling matrices ..............................done!
geo.n.len = 331702
Predictor: VELOCITY (first order frac. step):
VelX: Iteraciones: 1
VelY: Iteraciones: 1
VelZ: Iteraciones: 1
PRESSURE (first order frac.step):
Iteraciones: 53
FMS: Num of Iterations: 1 -- Pressure Error: 0.0427982
Now extending P to contact elements:
Maximo error rel del laplaciano iterativo: 0.00433374  Iteraciones: 14
```

```
P has been extended to contact elements succesfully!
  -  -  -  <SOLID solver> -  -  -
  -  -  -  <   done!   >  -  -  -
Corrector: VELOCITY:
VelX: Iteraciones: 1
VelY: Iteraciones: 1
VelZ: Iteraciones: 1
Corrector: PRESSURE (corrector iteration 1)
Iteraciones: 53
FMS: Num of Iterations: 1 -- Pressure Error: 0.0102035
Now extending P to contact elements:
Maximo error rel del laplaciano iterativo: 0.00445938  Iteraciones: 14
P has been extended to contact elements succesfully!
  -  -  -  <SOLID solver> -  -  -
  -  -  -  <   done!   >  -  -  -
  -  -  -  <SOLID solver> -  -  -
  -  -  -  <   done!   >  -  -  -
Corrector: VELOCITY (corrector iteration 1)
VelX: Iteraciones: 1
VelY: Iteraciones: 1
VelZ: Iteraciones: 1
Corrector: PRESSURE (corrector iteration 2)
Iteraciones: 52
FMS: Num of Iterations: 1 -- Pressure Error: 0.0029613
Now extending P to contact elements:
Maximo error rel del laplaciano iterativo: 0.00445938  Iteraciones: 14
P has been extended to contact elements succesfully!
  -  -  -  <SOLID solver> -  -  -
  -  -  -  <   done!   >  -  -  -
  -  -  -  <SOLID solver> -  -  -
  -  -  -  <   done!   >  -  -  -
Corrector: VELOCITY (corrector iteration 2)
VelX: Iteraciones: 1
VelY: Iteraciones: 1
VelZ: Iteraciones: 1
Trajectories integration .....done!
GP: Num of Iteration: 1 -- Vel Error: 0.00662054 -- Pres Error: 0.0279826
Printing Results:
******************************
        __      _
       /     |  | \
       | __  |  |  |
       \__/  |  |_/

******************************
Results are being written in:  C:/Users/Usuari/Desktop/University/TFG/tfg10.gid/OUTPUT/GID/
np =  331702
Writing resume/backup files:  hecho!
finished.-vol. corr (2)-finished. .....................FINISHED!

Sim. Time: 0.0127456 s, Next  Dt:  0.0013767 s
CPU: 0hs 7min 8s
```

Figure 5.8. Output info for a certain time step of the problem.

The above figure helps us to understand the calculation procedure that the software does for each time step. Regarding the computational time, note that for the time step shown, the calculation lasted 7 minutes and 8 seconds.

In the following figures, a view of the simulation at different time steps can be seen. Note that the red colour represents the structure layer, the green colour is the bridge layer and the blue colour is the water layer.

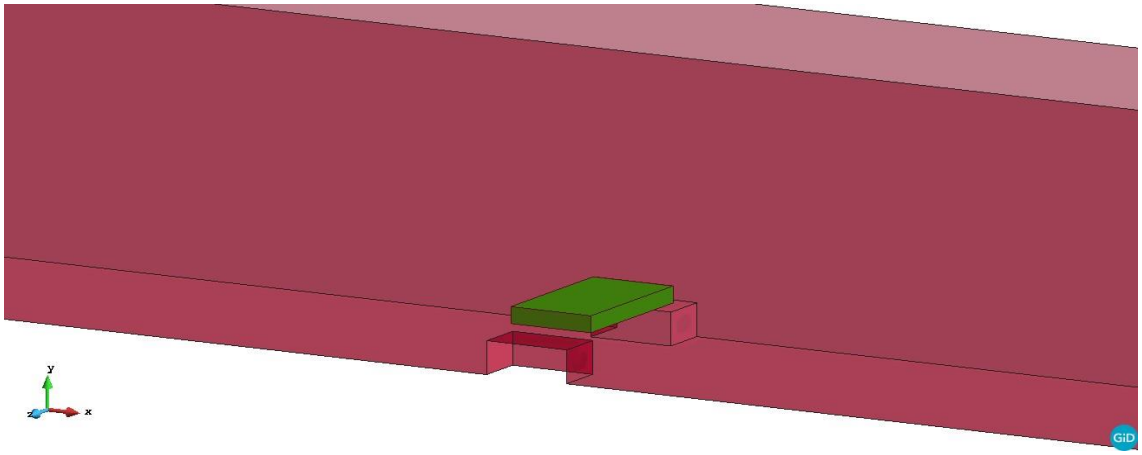

Figure 5.9. View of the simulation with a 12-mm mesh at the time step 0.0001 seconds.

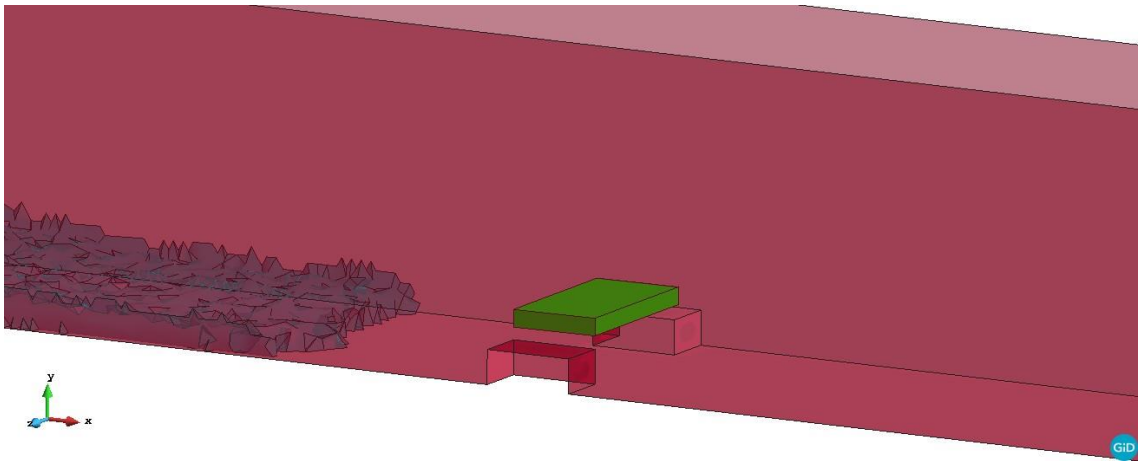

Figure 5.10. View of the simulation with a 12-mm mesh at the time step 0.431736 seconds.

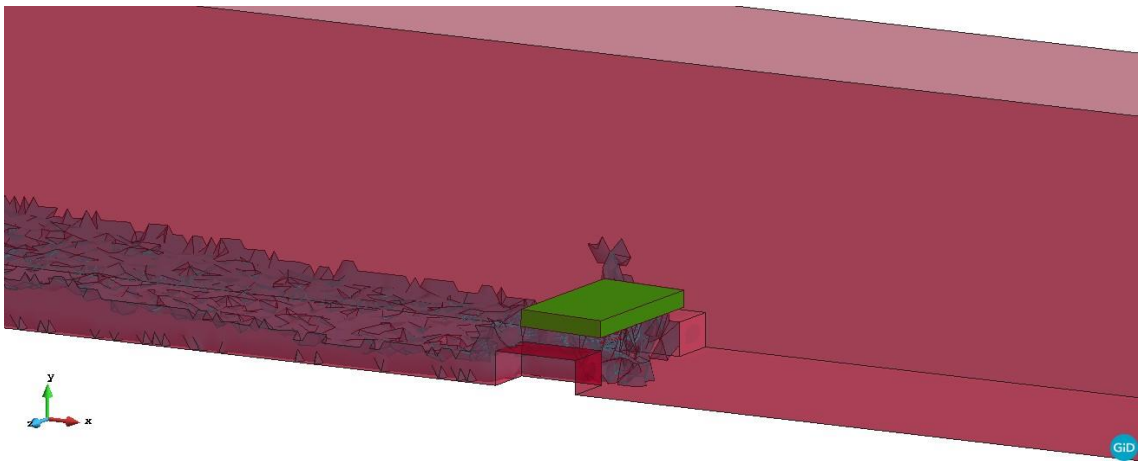

Figure 5.11. View of the simulation with a 12-mm mesh at the time step 0.575485 seconds.

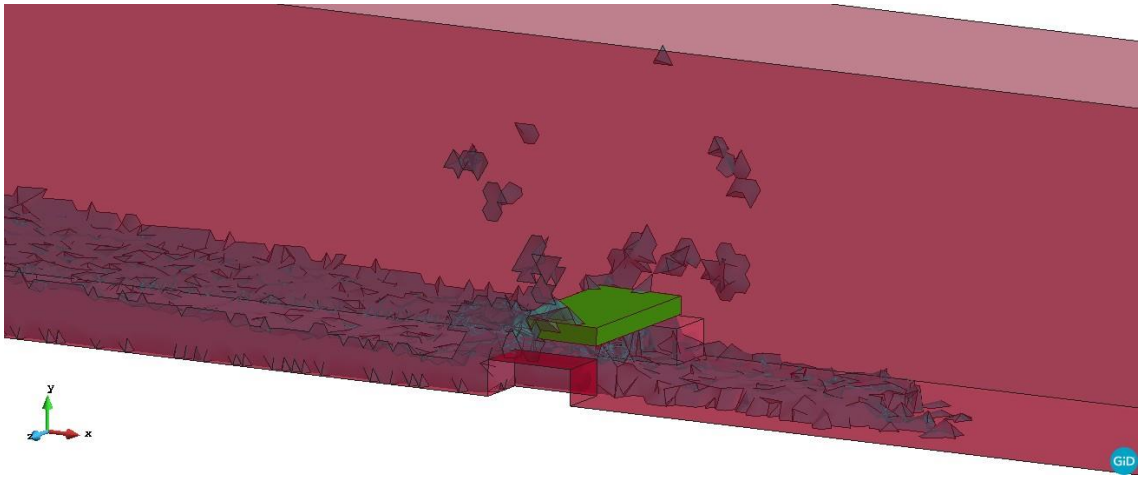

Figure 5.12. View of the simulation with a 12-mm mesh at the time step 0.716340 seconds.

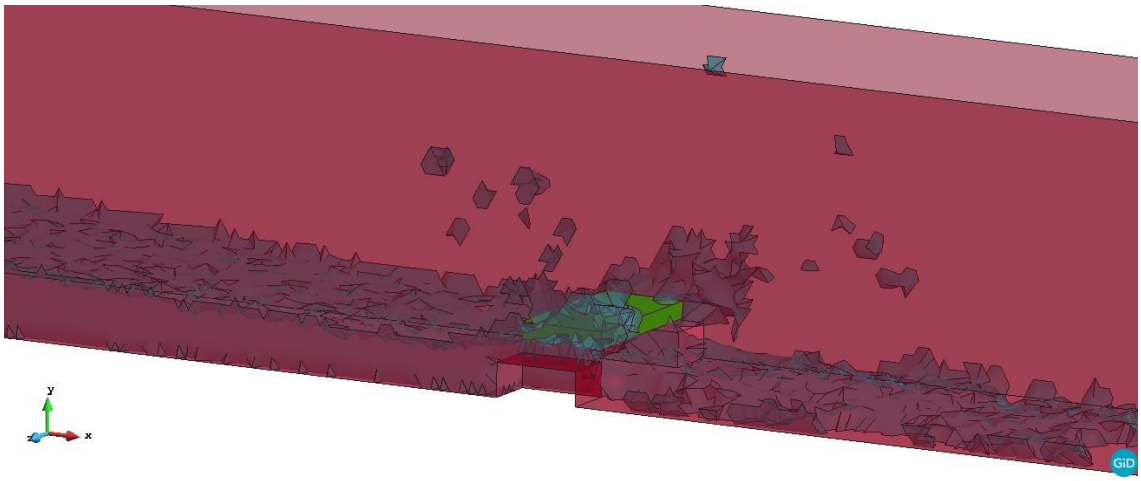

Figure 5.13. View of the simulation with a 12-mm mesh at the time step 0.883367 seconds.

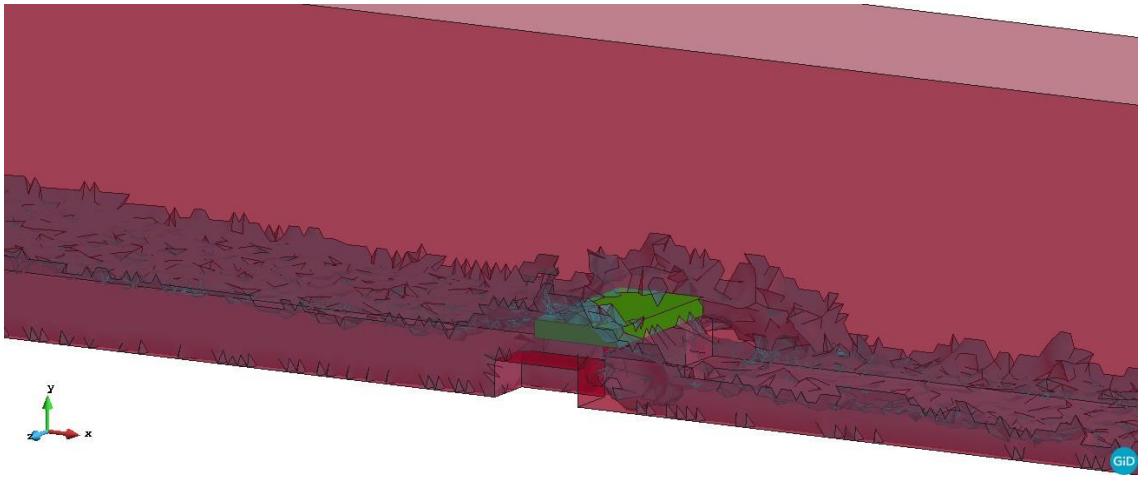

Figure 5.14. View of the simulation with a 12-mm mesh at the time step 1.04401 seconds.

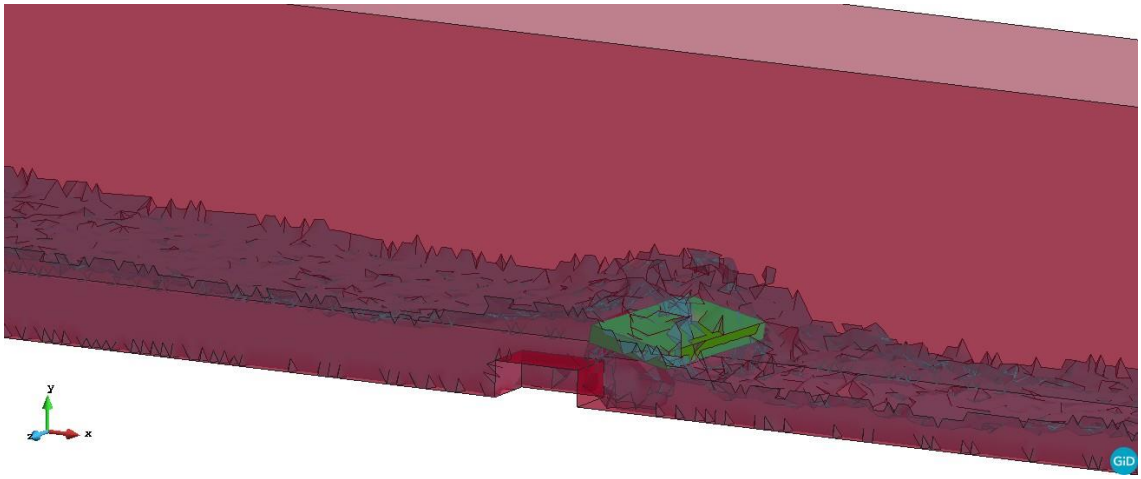

Figure 5.15. View of the simulation with a 12-mm mesh at the time step 1.21834 seconds.

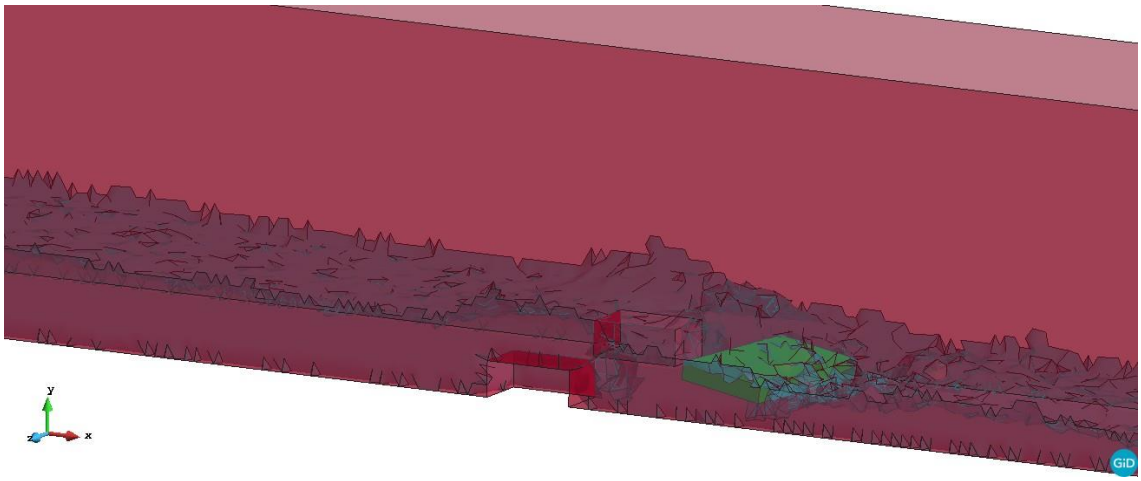

Figure 5.16. View of the simulation with a 12-mm mesh at the time step 1.35937 seconds.

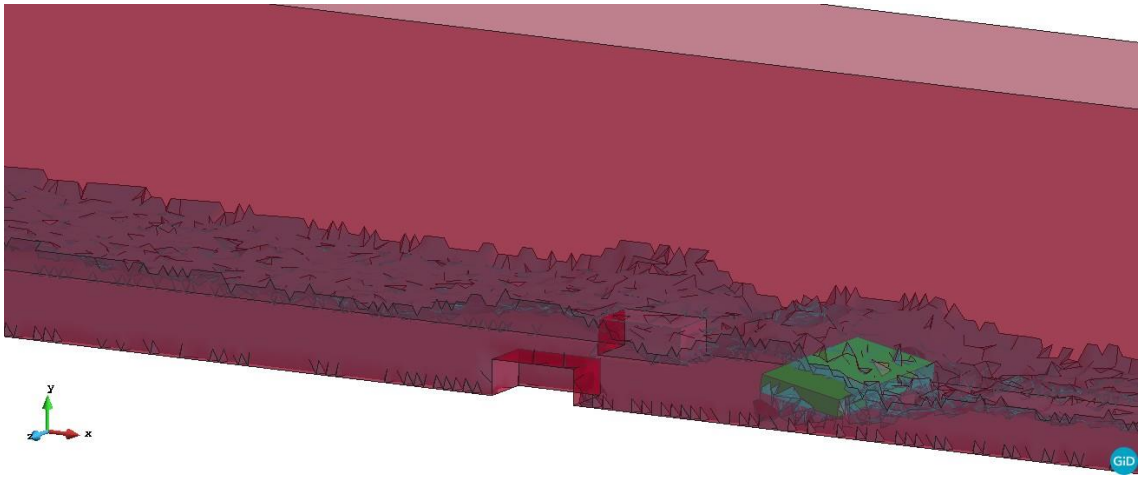

Figure 5.17. View of the simulation with a 12-mm mesh at the time step 1.45394 seconds.

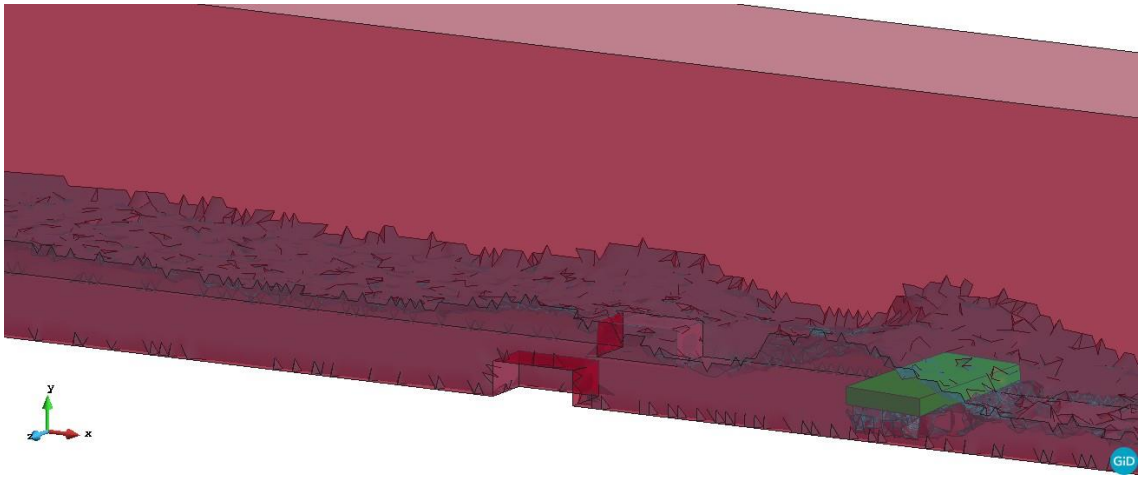

Figure 5.18. View of the simulation with a 12-mm mesh at the time step 1.64126 seconds.

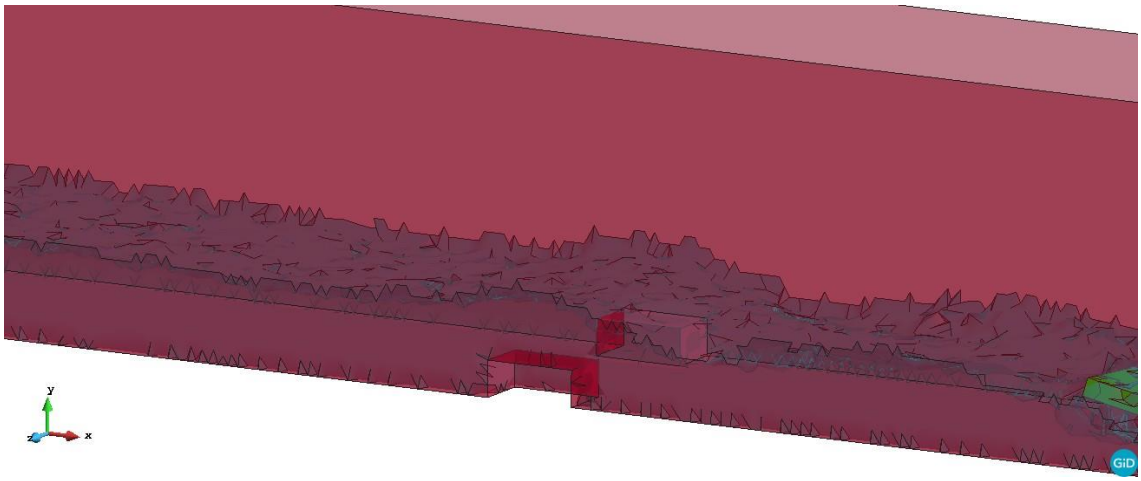

Figure 5.19. View of the simulation with a 12-mm mesh at the time step 1.87710 seconds.

In the previous figures, we can see clearly how the water wave is powerful enough to wash out the girder leaving only the two fixed piers.

Regarding the simulation time, for the 12-mm mesh the software took 2 days and 12 hours to simulate two seconds of the problem. It generated 1036 files of results which is translated into an average of 3 minutes and 28 seconds to calculate one time step.

5.2.3. Motion plots of the girder for the 12-mm mesh size case.

One of the objectives in this project is the validation of the PFEM by means of comparing a real-life experiment with its simulations using the PFOW software, which simulates problems using the PFEM method. Hence, in order to achieve this objective, an x-axis, a y-axis and a rotational angle plot against time are generated for each mesh size. This way, it is easier to compare and judge the accuracy of the simulation compared with reality. The generation of these plots is also beneficent due to the fact that the different mesh size simulations can be compared as well. This will help us to find which mesh size for this problem is better to choose regarding computational time, accuracy of the results, etc.

To generate these plots of the motion of the girder (see section 4), the coordinates of the node corresponding to the centroid of the girder must be tracked along the simulation time. However, the girder of the bridge was created only using nodes, lines and surfaces, which means that no volume was created to the bridge layer. No volume was created since as boundary conditions, we set a mass, principal moments of inertia and a centroid to it. Therefore, when generating the mesh, there was not any node of the mesh close enough to the centroid of the girder for tracking its motion and consider the results accurate enough. The nodes of the mesh were all located in the 6 surfaces of the girder.

To overcome this issue, the two surfaces of the girder contained in the *yz* plane (which measures are 190x20 square millimetres) are considered and the most centric node from each of the two surfaces are taken (see figures 5.20 and 5.21). These two nodes are nodes number 58506 and 58842. At $t = 0$ the coordinates of node 58506 are:

$$x = 3.2\ m \qquad y = 0.0596077\ m \qquad z = 0.105938\ m \tag{26}$$

And the coordinates of node 58842 are:

$$x = 3.1\ m \qquad y = 0.0596077\ m \qquad z = 0.105938\ m \tag{27}$$

Therefore, if we calculate the coordinates as the mean of these two nodes, we find that these coordinates are practically the same than the coordinates of the centroid of the girder, which are:

$$x_c = 3.15\ m \qquad y_c = 0.06\ m \qquad z_c = 0.1\ m \tag{28}$$

This way, for the calculation of the coordinates of the centroid at each time step, the mean position between nodes 58506 and 58842 is calculated. For further details of the calculation see the appendix.

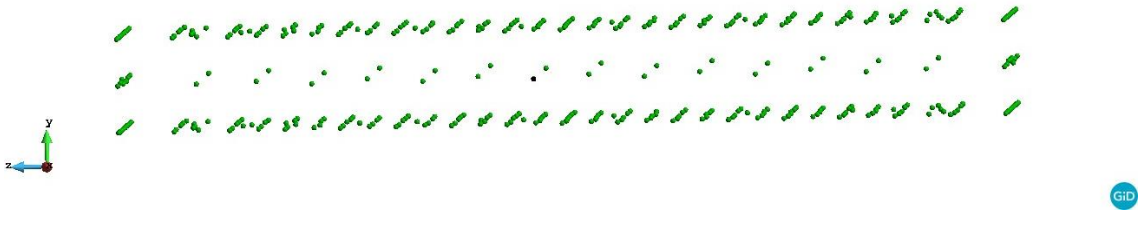

Figure 5.20. Nodes generated in the bridge layer. In black colour node 58506 is highlighted.

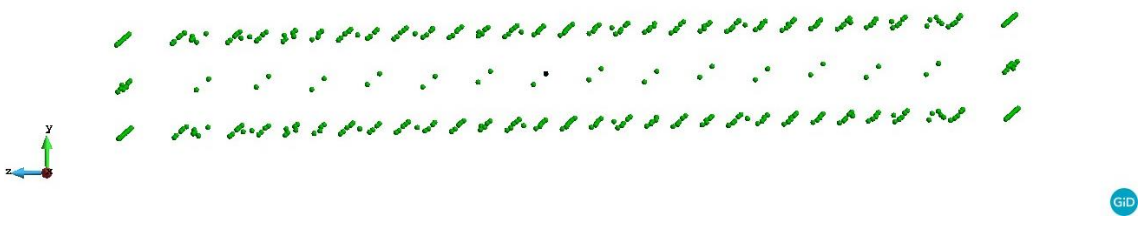

Figure 5.21. Nodes generated in the bridge layer. In black colour node 58842 is highlighted.

For the calculation of the rotational angle at each time step, as in Asai and Chandra (2016)[14] the rotational angle is understood as the angle drawn by the girder with the

horizontal (*xz* plane), the coordinates of nodes 58506 and 58842 are taken and the rotational angle (θ) for every time step is calculated as equation 29 shows.

$$\theta = arcsin\left(\frac{y_2 - y_1}{0.1}\right) \cdot \frac{180}{\pi} \tag{28}$$

where y_2 is the *y* coordinate of node 58842 and y_1 is the coordinate of node 58506.

With the coordinates calculated, an x-axis, y-axis and rotational angle against time plots can be generated. Those can be seen in figures 5.22, 5.23 and 5.24.

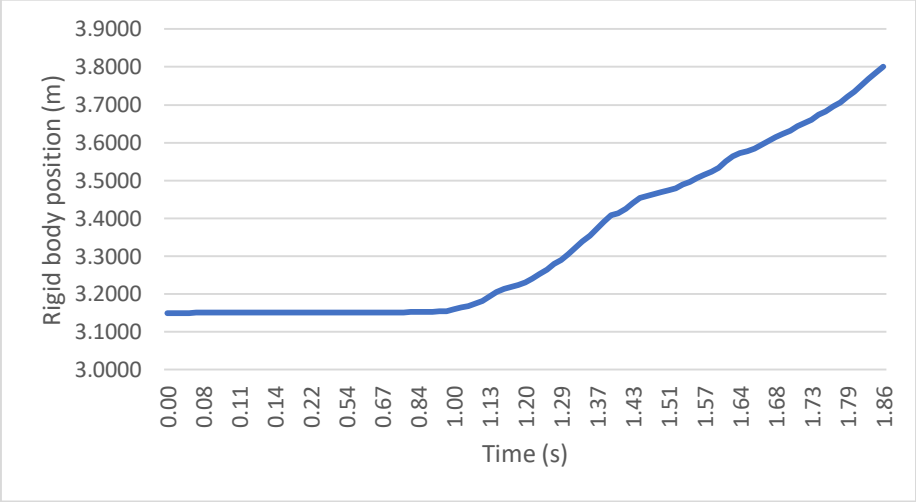

Figure 5.22. Horizontal motion of the rigid body centre of gravity in the simulated case with a 12-mm mesh.

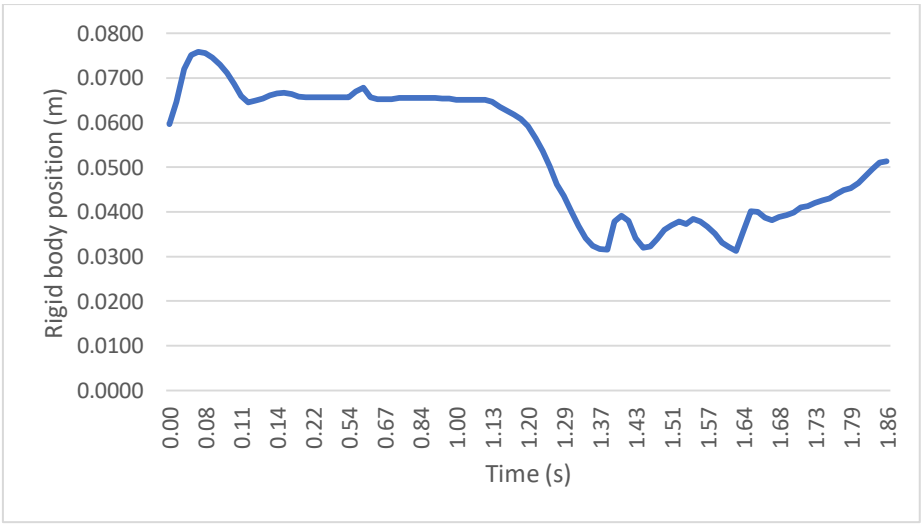

Figure 5.23. Vertical motion of the rigid body centre of gravity in the simulated case with a 12-mm mesh.

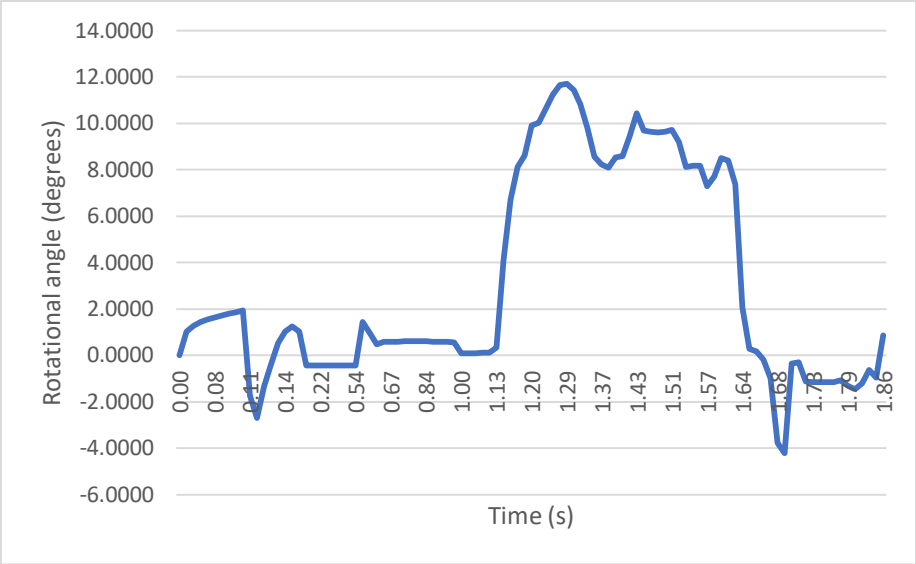

Figure 5.24. Rotational angle of the rigid body centre of gravity in the simulated case with a 12-mm mesh.

Note that in the vertical motion plot, there is a bouncy trajectory at the beginning of the simulation. This is because when the software starts simulating, between two solid layers it creates some contact elements between them which size is the mesh size chosen for the problem. Then, when the simulation reaches the first time step, the girder begins to settle over the piers. It usually takes a very short period of time but, in our case, it always stops way before the water reaches the girder. It can be said that the girder takes some time to settle over these contact elements and, once it has settled over, just gravity links the girder with the two fixed piers.

This phenomenon is only visible in the vertical motion plot, it cannot be perceived in the horizontal motion plot nor in the rotational angle plot.

5.3. Mesh size of 10 millimetres.

5.3.1. Data of the 10-mm size's mesh.

The second of the mesh sizes chosen for the simulation of the problem is a 10-millimetre size mesh. In this case, as the mesh is smaller there will be more nodes and elements in the resulting mesh. Once the 10-mm mesh is generated, its data can be resumed in the following points.

- Number of nodes: 331.553 nodes.
- Number of triangles: 182.962 triangles.
- Number of tetrahedrons: 1.492.673 tetrahedrons.
- Number of elements (triangles and tetrahedrons): 1.675.635 elements.

These data is for the entire mesh, however regarding the different layers, the mesh data can be resumed in table 5.2.

Layer	Water	Structure	Bridge
Tetrahedrons	1.492.673	0	0
Nodes	274.164	83.993	514
Triangles	68.326	166.824	1.024
Lines	23.946	250.816	1.536

Table 5.2. Data by layer of the 10-mm-size mesh.

Note that a change of 2 millimetres in the mesh size results in 718.725 more elements in the mesh, which it translates into both a bigger computational time and a bigger accuracy of the results. A close look of the bridge with the mesh generated can be seen in figure 5.25.

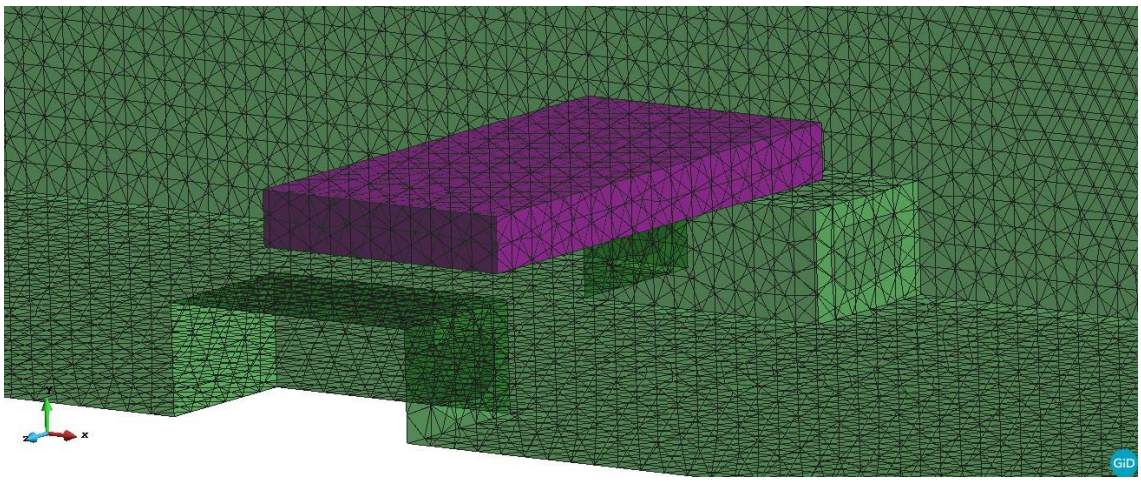

Figure 5.25. Close look of the bridge with the 10-mm mesh.

5.3.2. Results of the 10-mm mesh size case.

Regarding the results of the 10-mm mesh size case, it can easily be seen that the water drops are smaller than in the 12-mm mesh size case. In the following figures the results with the 10-mm mesh can be seen in different time steps of the simulation.

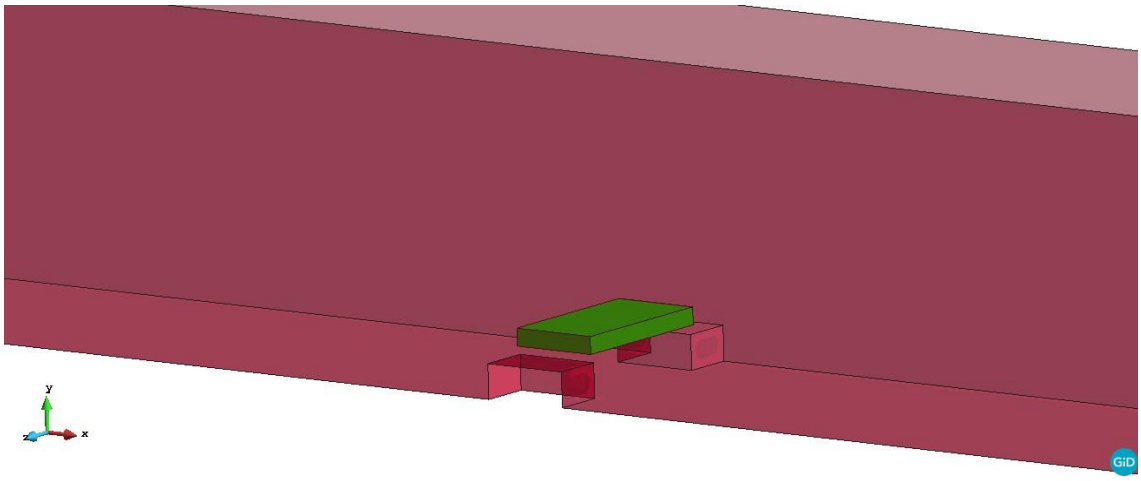

Figure 5.26. View of the simulation with a 10-mm mesh at the time step 0.0001 seconds.

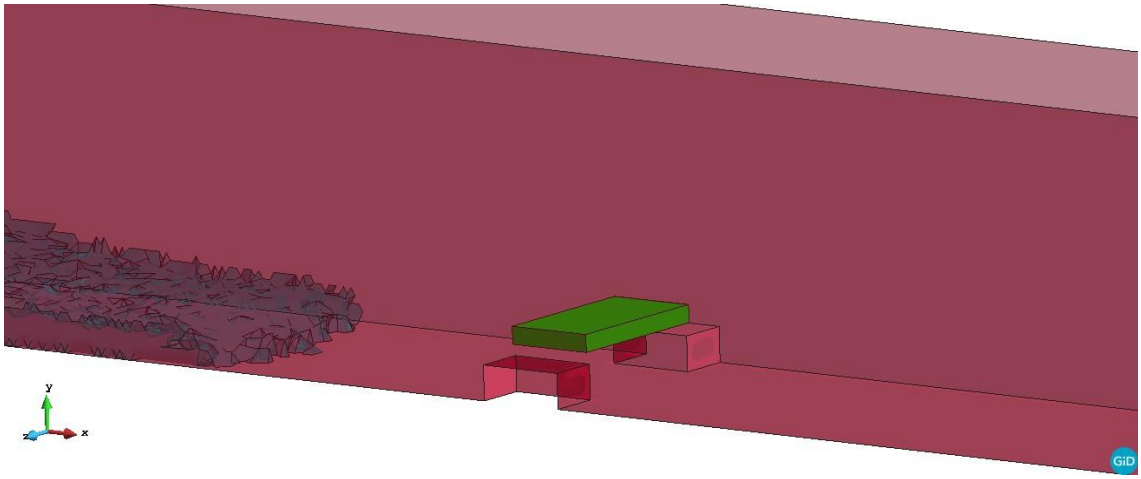

Figure 5.27. View of the simulation with a 10-mm mesh at the time step 0.379383 seconds.

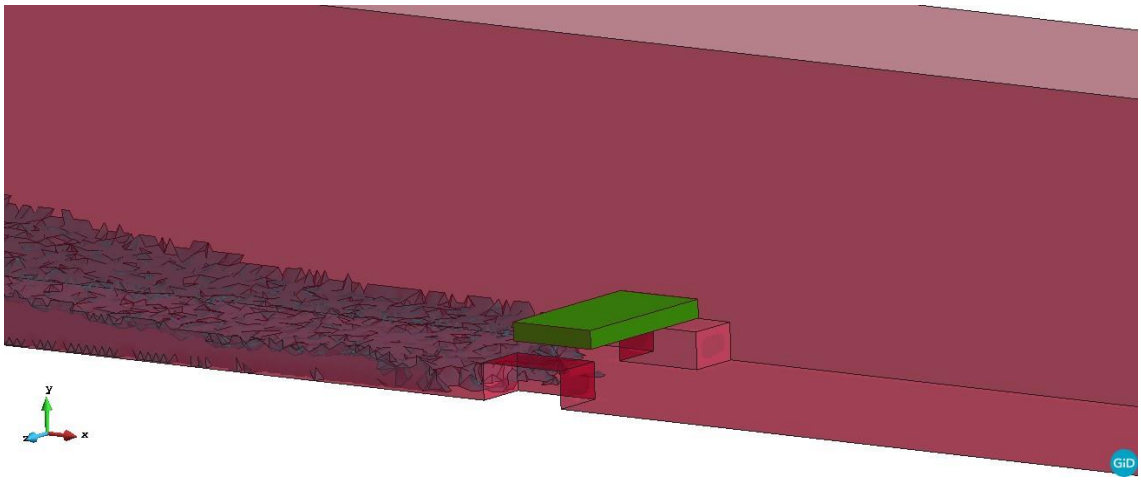

Figure 5.28. View of the simulation with a 10-mm mesh at the time step 0.501177 seconds.

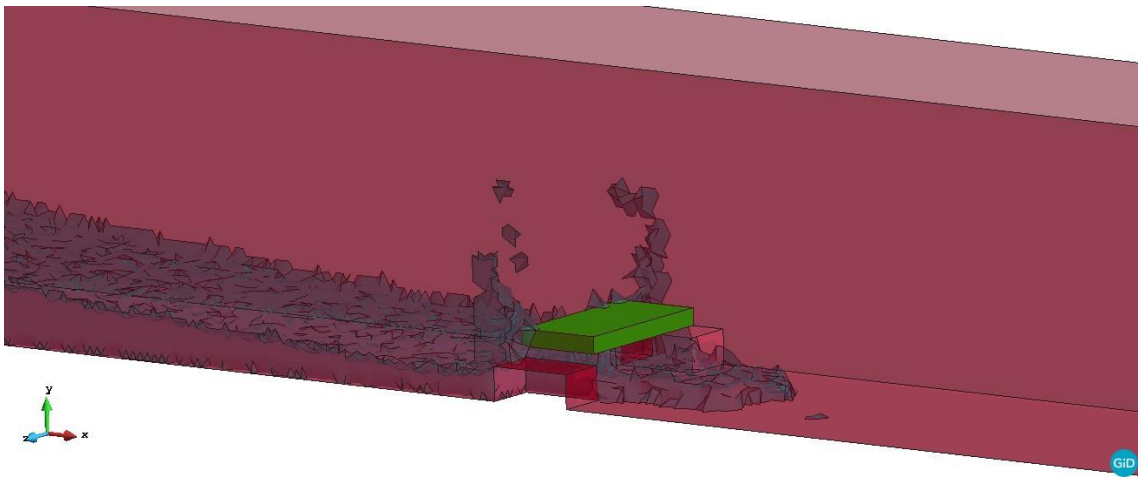

Figure 5.29. View of the simulation with a 10-mm mesh at the time step 0.623464 seconds.

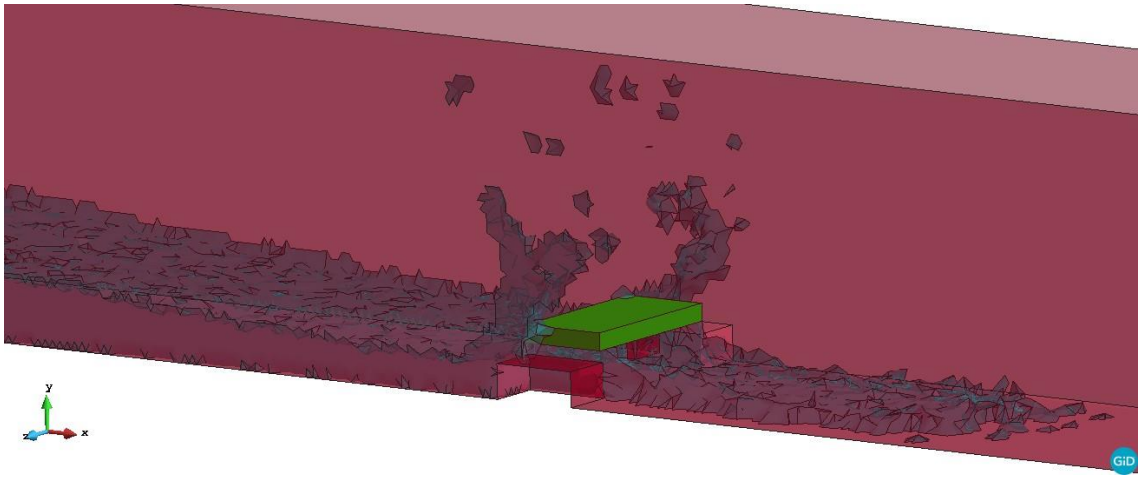

Figure 5.30. View of the simulation with a 10-mm mesh at the time step 0.753604 seconds.

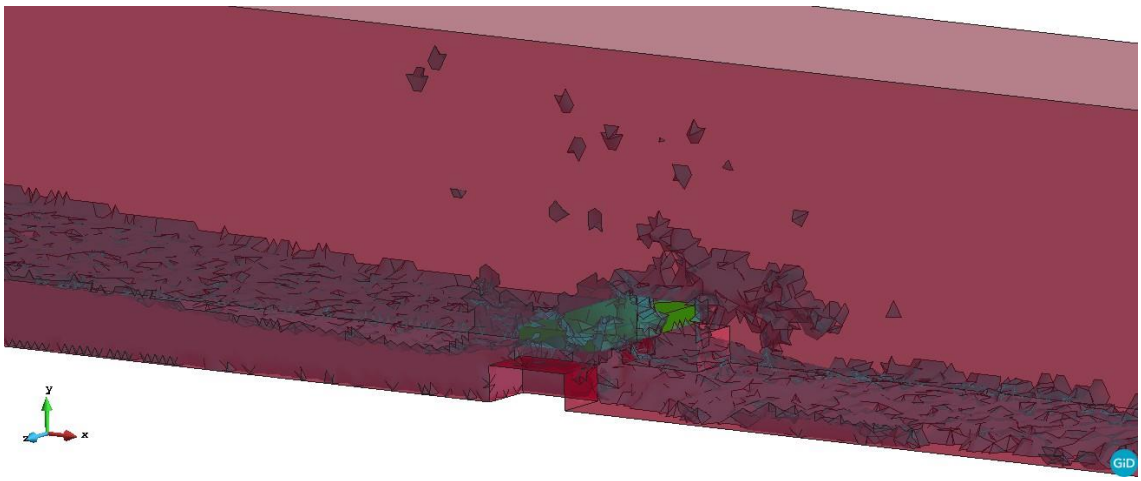

Figure 5.31. View of the simulation with a 10-mm mesh at the time step 0.888153 seconds.

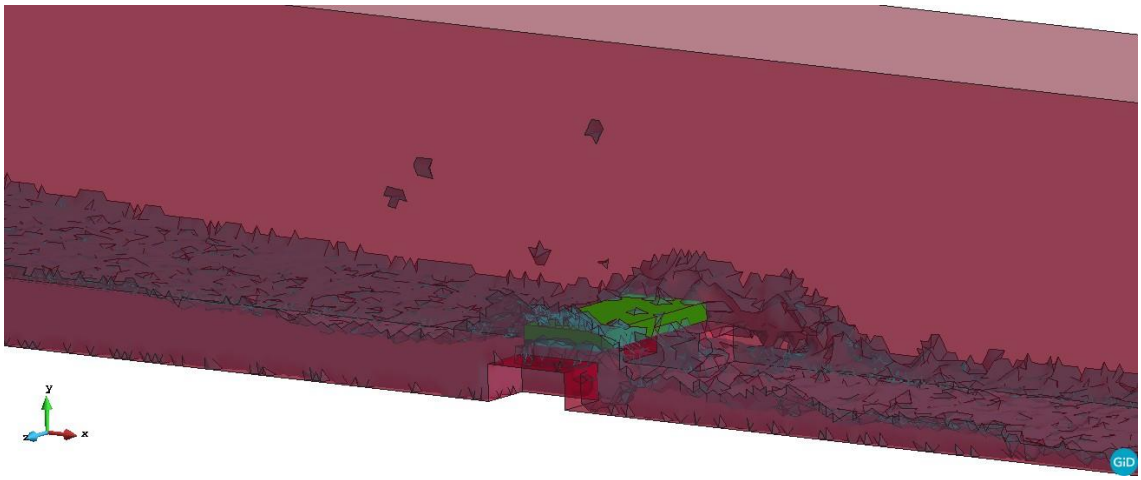

Figure 5.32. View of the simulation with a 10-mm mesh at the time step 1.00339 seconds.

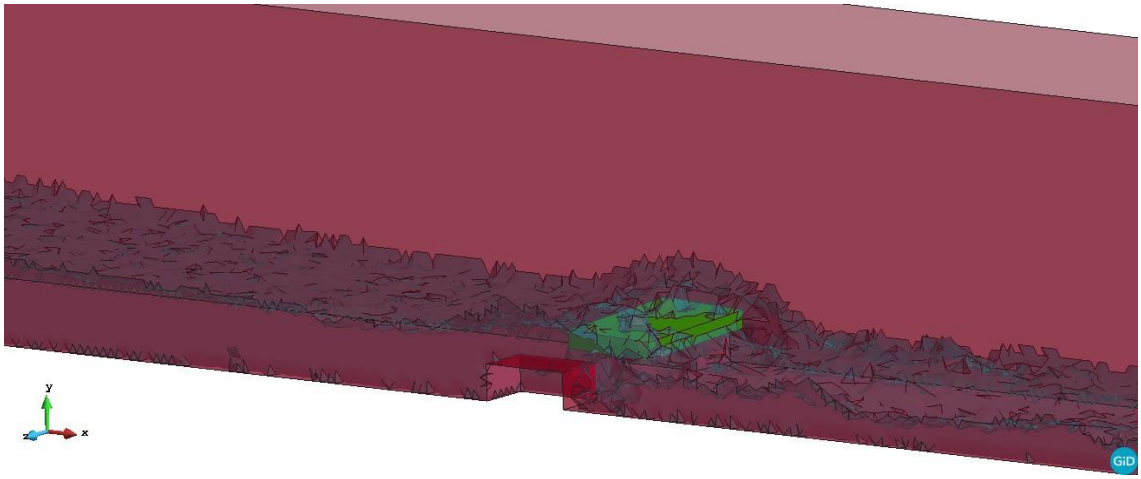

Figure 5.33. View of the simulation with a 10-mm mesh at the time step 1.17482 seconds.

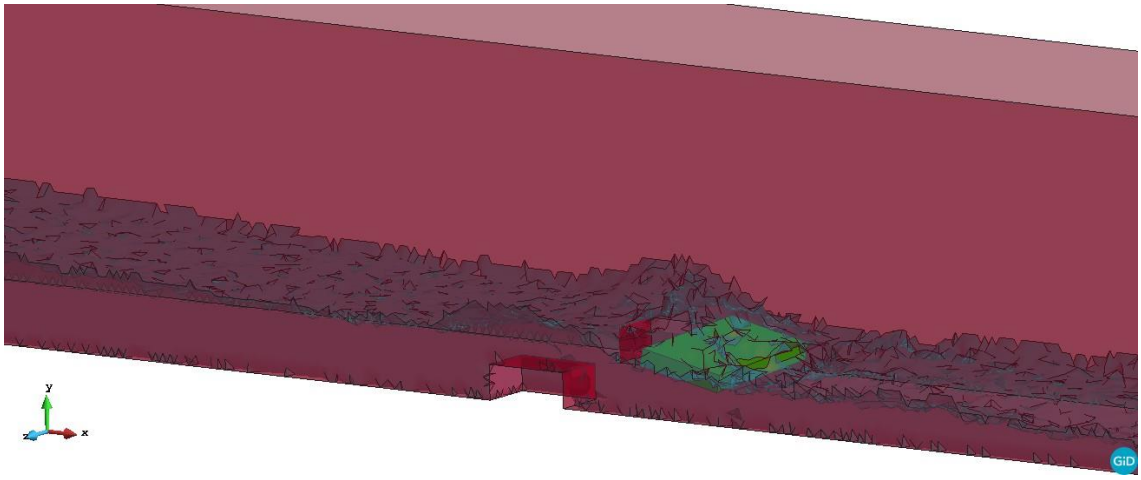

Figure 5.34. View of the simulation with a 10-mm mesh at the time step 1.31174 seconds.

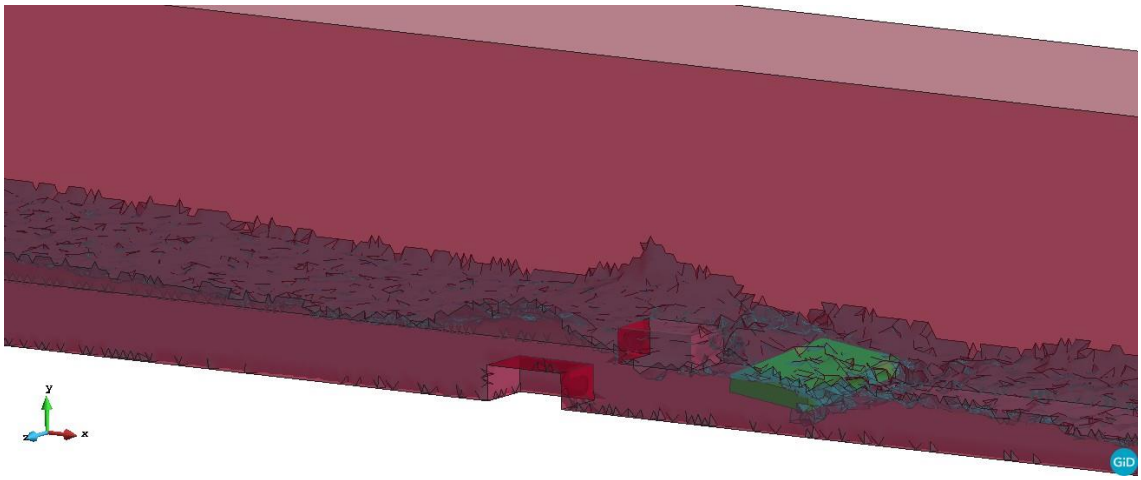

Figure 5.35. View of the simulation with a 10-mm mesh at the time step 1.41897 seconds.

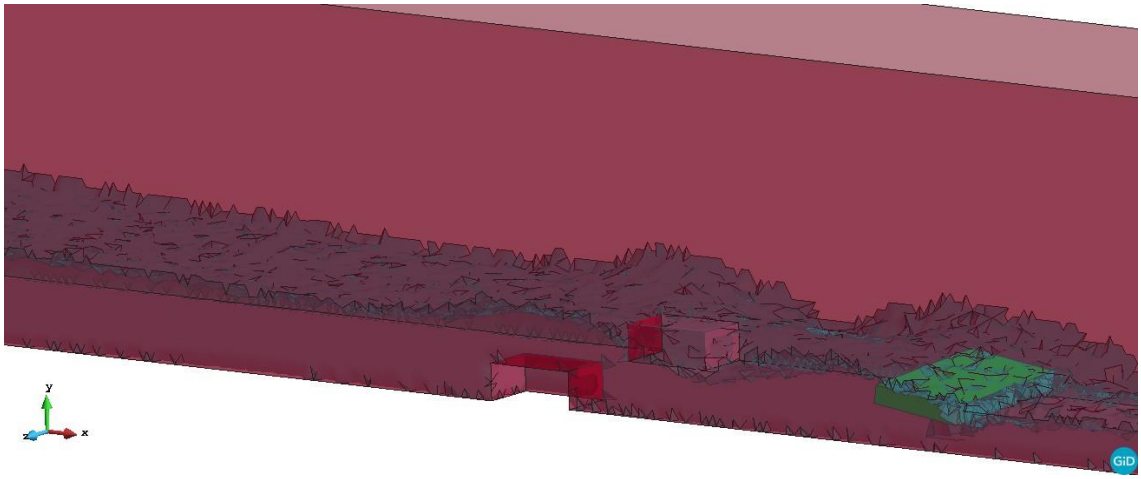

Figure 5.36. View of the simulation with a 10-mm mesh at the time step 1.59665 seconds.

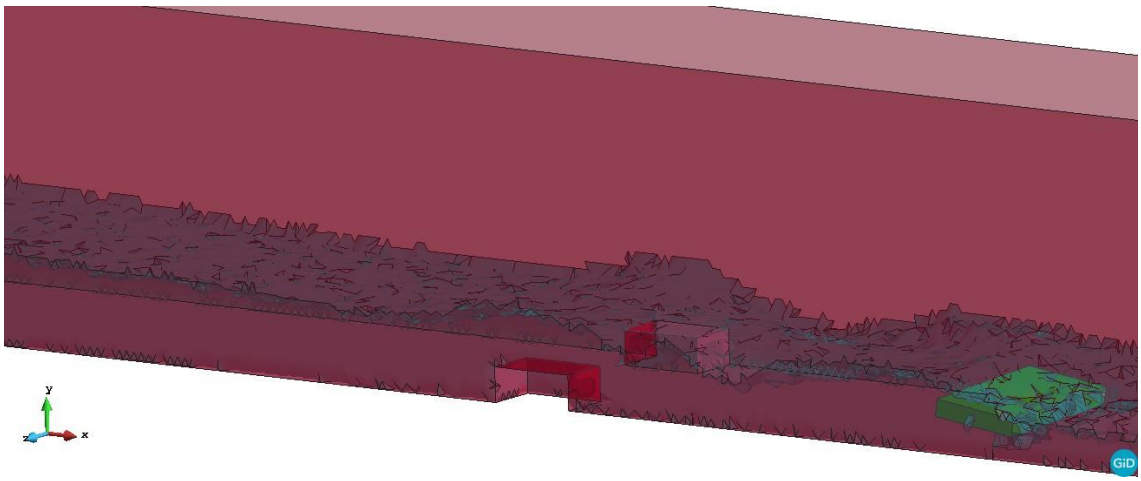

Figure 5.37. View of the simulation with a 10-mm mesh at the time step 1.67985 seconds.

The time spent to simulate 1.7 seconds of the problem for the 10-mm mesh is 4 days and 7 hours. It generated 1032 files of results which is translated into an average of 5 minutes and 59 seconds taken for the software to generate one file of results (one time step).

5.3.3. Motion plots of the girder for the 10-mm mesh size case.

For the generation of the motion of the girder against time plots, a similar thing respect to the 12-mm mesh case is done. In this case from the *yz* plane two nodes are chosen in such a way that the mean coordinates between these two nodes must be as close as possible with respect to the centroid of the girder, which is located as equation 28 shows. The two nodes chosen for this case are node 84022 and node 84477. The coordinates of node 84022 at the initial time step are:

$$x = 3.2\ m \qquad y = 0.0586603\ m \qquad z = 0.1\ m \tag{29}$$

The same way, the coordinates of node 84477 at the initial time step are:

$$x = 3.1\ m \qquad y = 0.0596077\ m \qquad z = 0.1\ m \tag{30}$$

If the mean coordinates between these two nodes is calculated, they result in the closest coordinates possible to the centroid of the girder. This calculation of the mean coordinates between two nodes must be done because, as for the previous case, no volume is created to the bridge layer because there was no need for it.

For the calculation of the rotational angle, the procedure is exactly the same than in the previous case (see equation 28). For further details of the calculation see the appendix.

In figures 5.38 and 5.39, nodes 84022 and 84477 are highlighted.

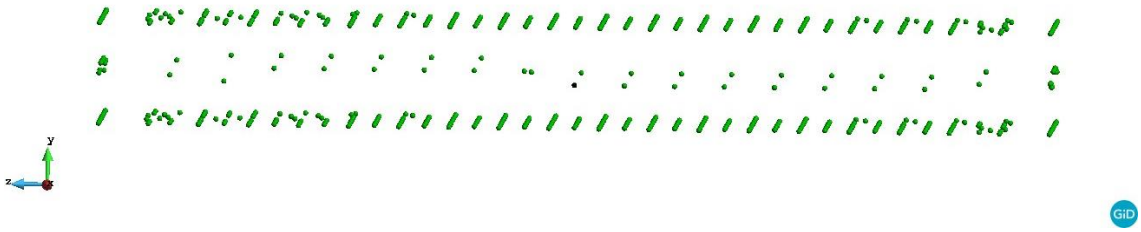

Figure 5.38. Nodes generated in the bridge layer. In black colour node 84022 is highlighted.

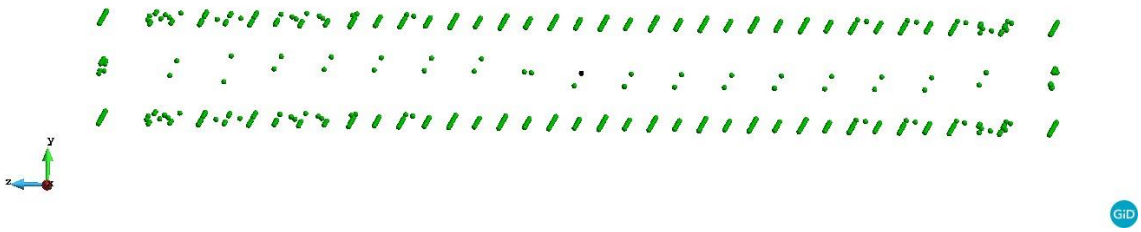

Figure 5.39. Nodes generated in the bridge layer. In black colour node 84477 is highlighted.

In figures 5.40, 5.41 and 5.42 the motion of the girder against time resulting plots can be seen.

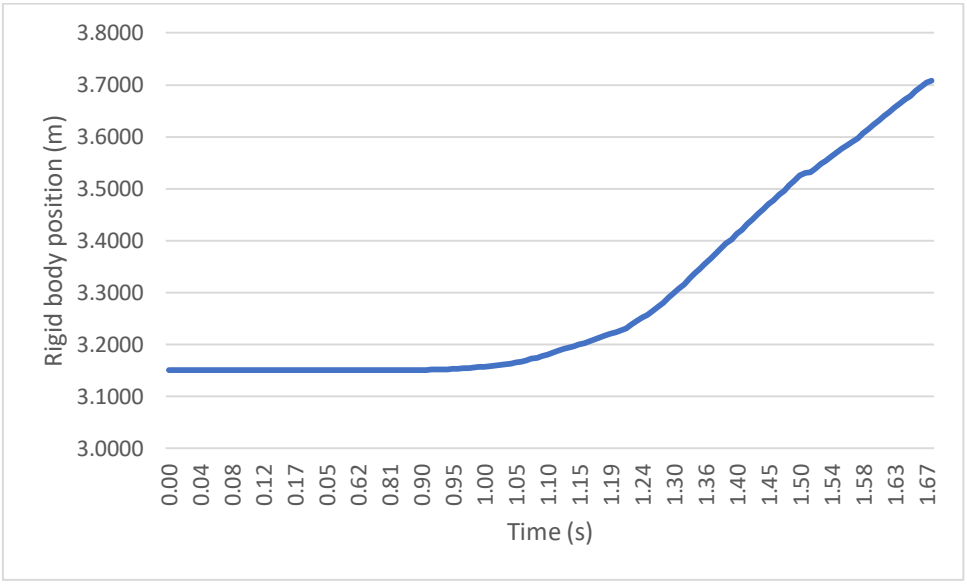

Figure 5.40. Horizontal motion of the rigid body centre of gravity in the simulated case with a 10-mm mesh.

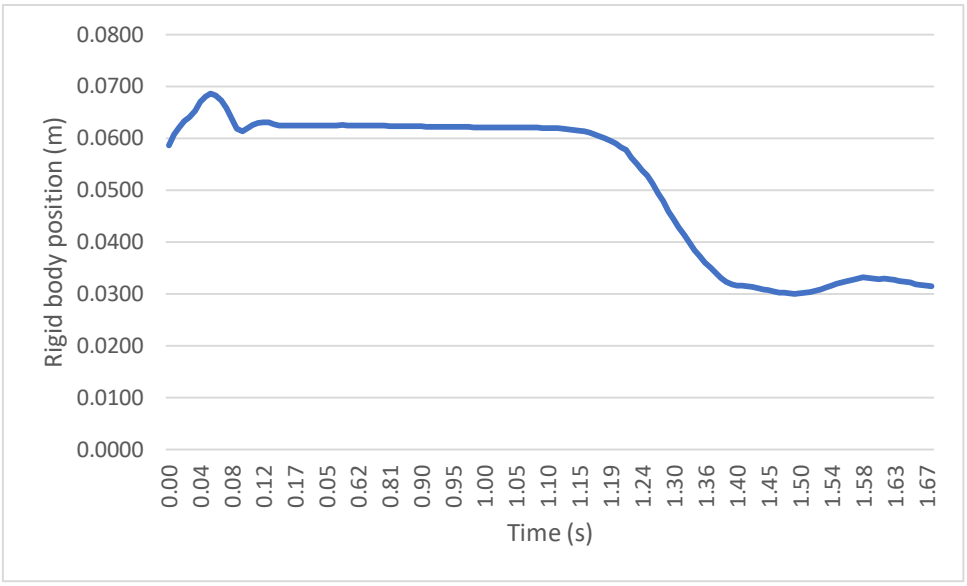

Figure 5.41. Vertical motion of the rigid body centre of gravity in the simulated case with a 10-mm mesh.

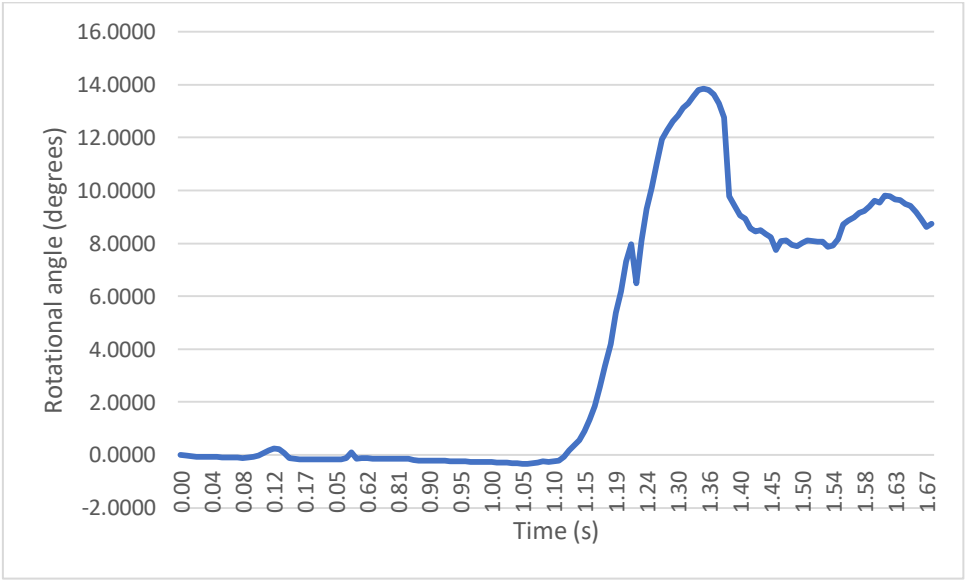

Figure 5.42. Rotational angle of the rigid body centre of gravity in the simulated case with a 10-mm mesh.

Taking a look at the vertical motion plot, a similar thing is happening than the 12-mm mesh size case. There can be observed a bouncy trajectory at the beginning of the simulation due to the creation of the contact elements between the structure layer and the bridge layer, both solid layers.

5.4. Mesh size of 8 millimetres.

5.4.1. Data of the 8-mm size's mesh.

The third of the mesh sizes chosen for solving the problem is a mesh size of 8 millimetres. This will translate into a bigger computational time but will result into a bigger accuracy of the results.

Once the 8-mm mesh is generated, its data can be resumed in the following points.

- Number of nodes: 619.075 nodes.
- Number of triangles: 288.796 triangles.
- Number of tetrahedrons: 2.922.864 tetrahedrons.
- Number of elements (triangles and tetrahedrons): 3.211.660 elements.

These data is for the entire mesh, however regarding the different layers, the mesh data can be resumed in table 5.3.

Layer	Water	Structure	Bridge
Tetrahedrons	2.922.864	0	0
Nodes	528.645	132.210	882
Triangles	108.112	262.968	1.760
Lines	37.697	395.177	2.640

Table 5.3. Data by layer of the 10-mm-size mesh.

A close look of the bridge with the mesh generated can be seen in figure 5.43.

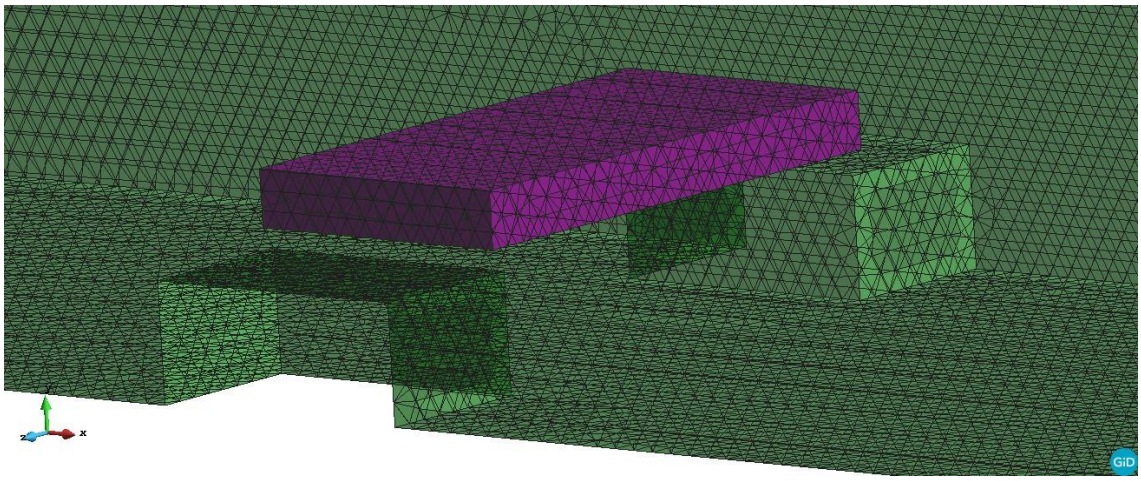

Figure 5.43. Close look of the bridge with the 8-mm mesh.

5.4.2. Results of the 8-mm mesh size case.

In the following figures the results with the 8-mm mesh can be seen in different time steps of the simulation.

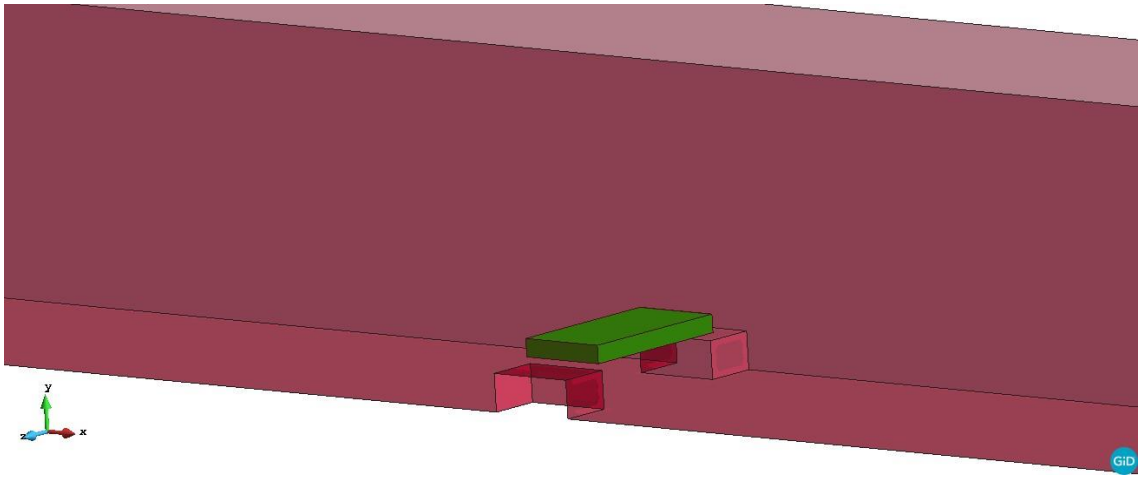

Figure 5.44. View of the simulation with an 8-mm mesh at the time step 0.0002 seconds.

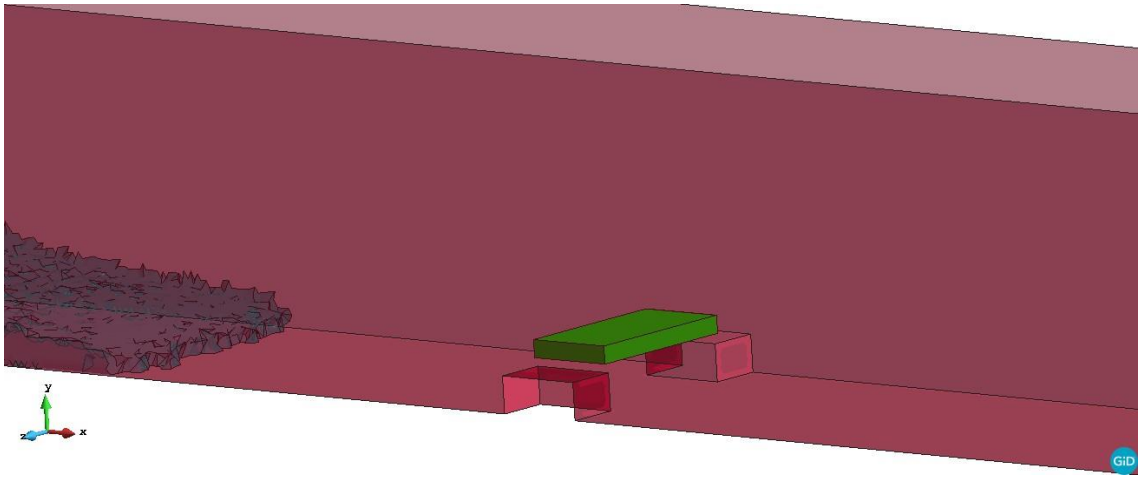

Figure 5.45. View of the simulation with an 8-mm mesh at the time step 0.300063 seconds.

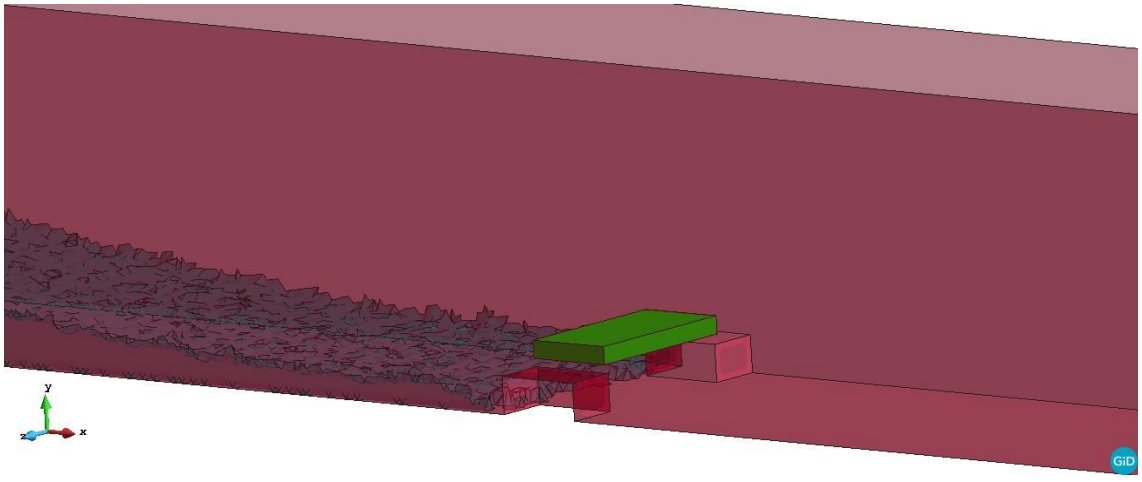

Figure 5.46. View of the simulation with an 8-mm mesh at the time step 0.500079 seconds.

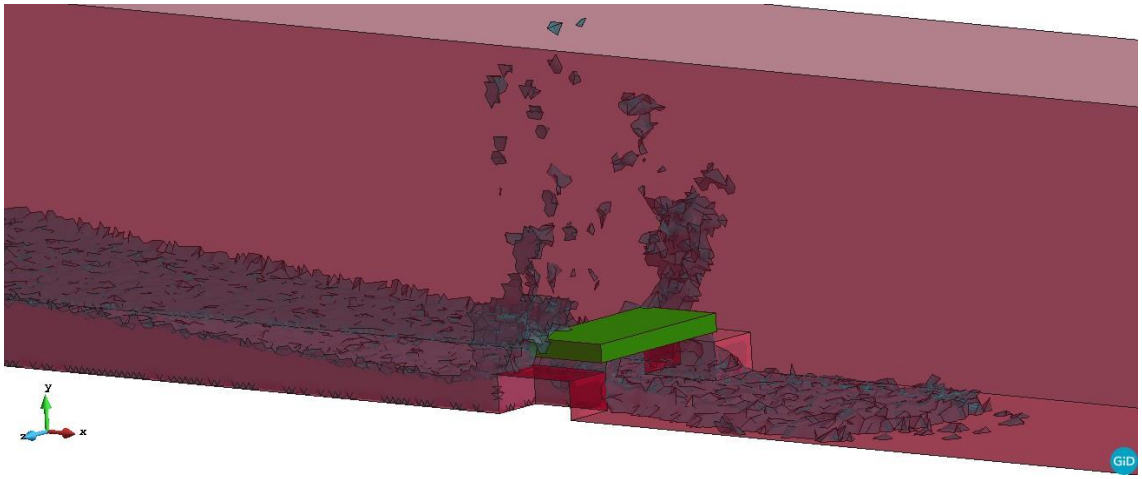

Figure 5.47. View of the simulation with an 8-mm mesh at the time step 0.701003 seconds.

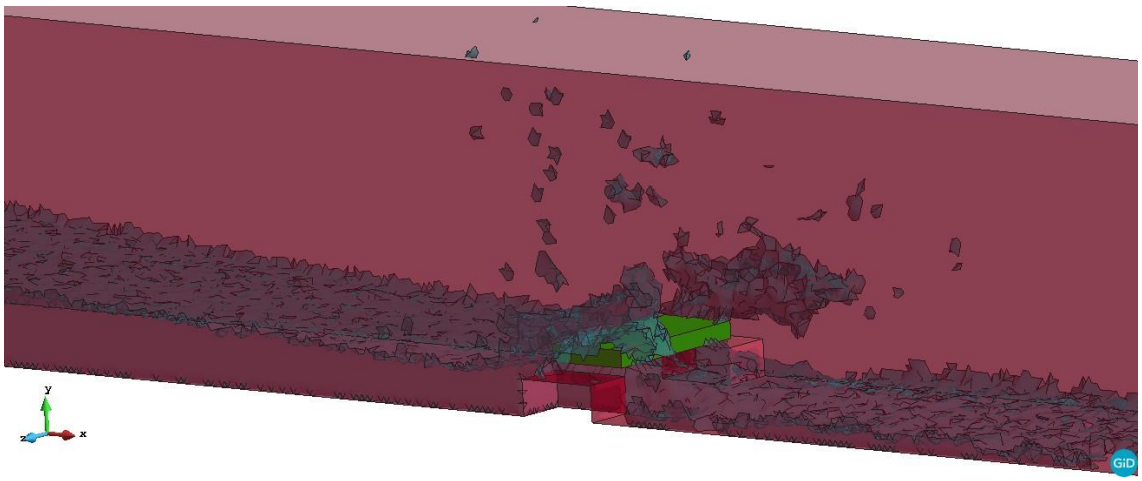

Figure 5.48. View of the simulation with an 8-mm mesh at the time step 0.901245 seconds.

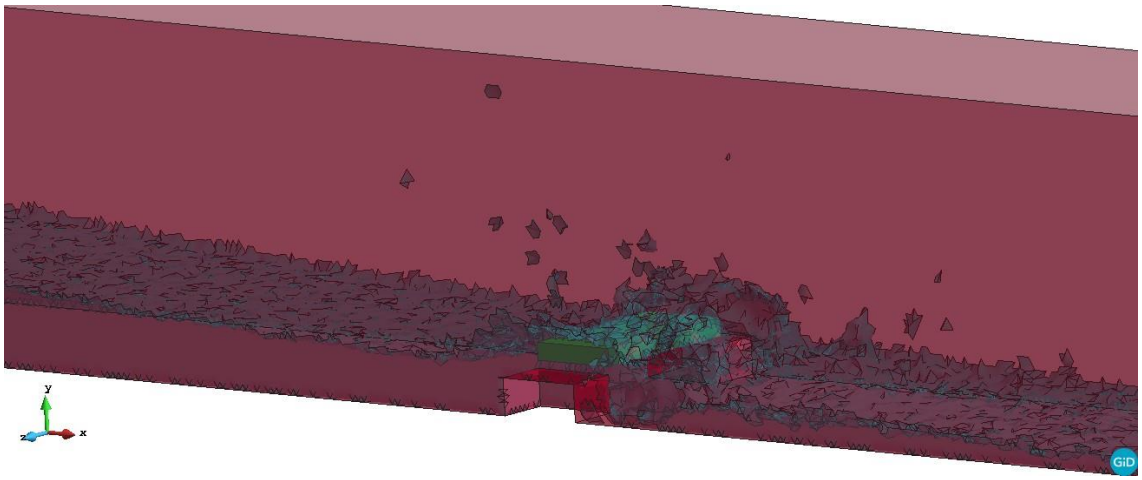

Figure 5.49. View of the simulation with an 8-mm mesh at the time step 1.00113 seconds.

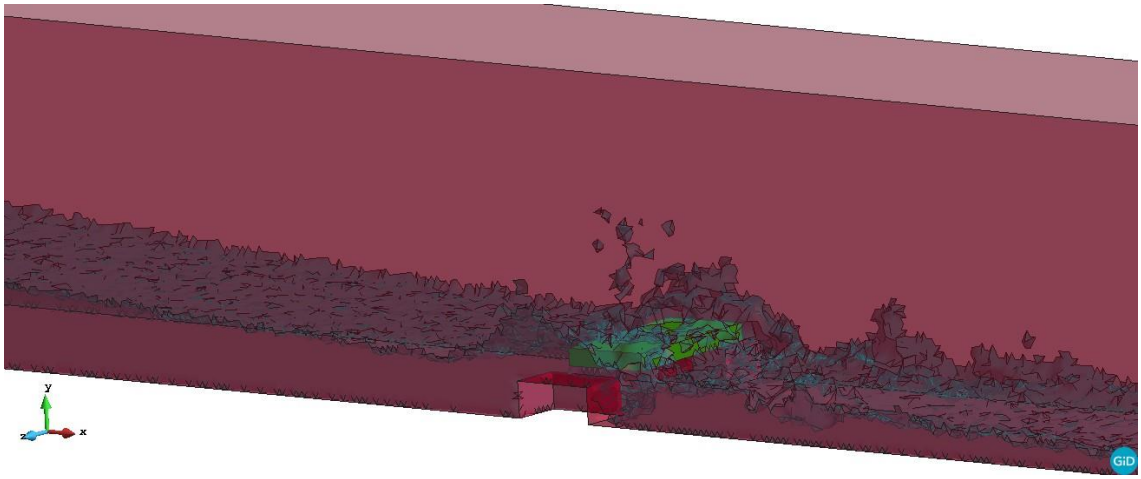

Figure 5.50. View of the simulation with an 8-mm mesh at the time step 1.10076 seconds.

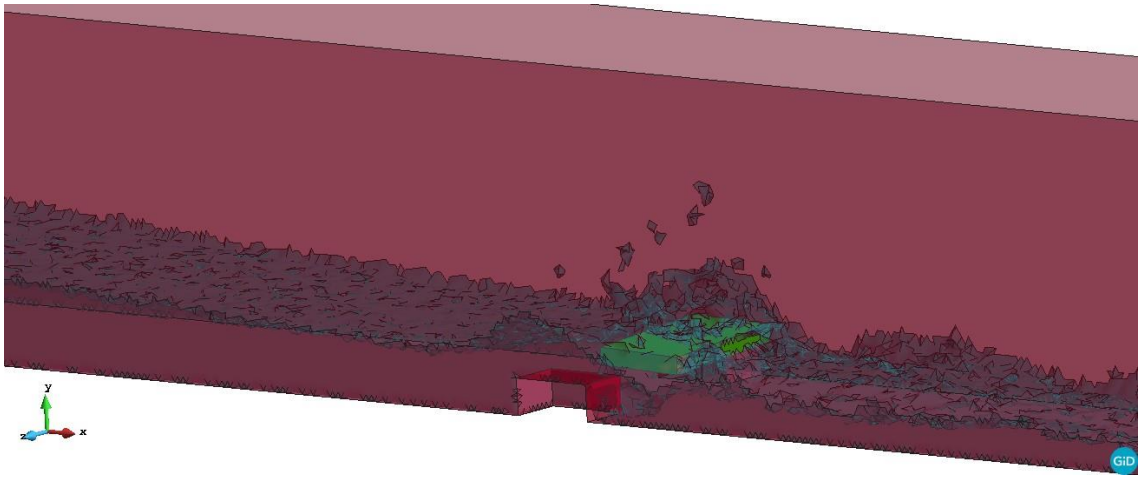

Figure 5.51. View of the simulation with an 8-mm mesh at the time step 1.20033 seconds.

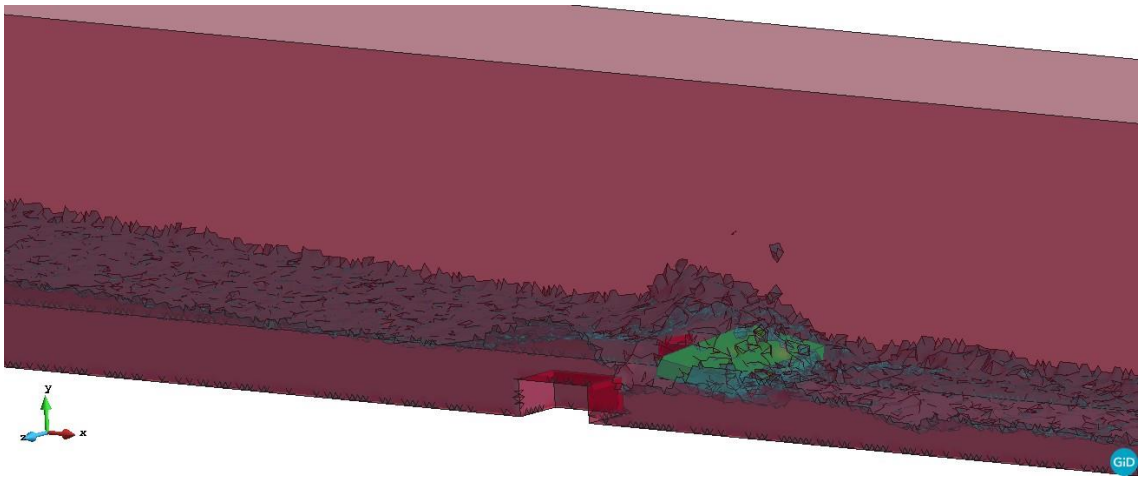

Figure 5.52. View of the simulation with an 8-mm mesh at the time step 1.30013 seconds.

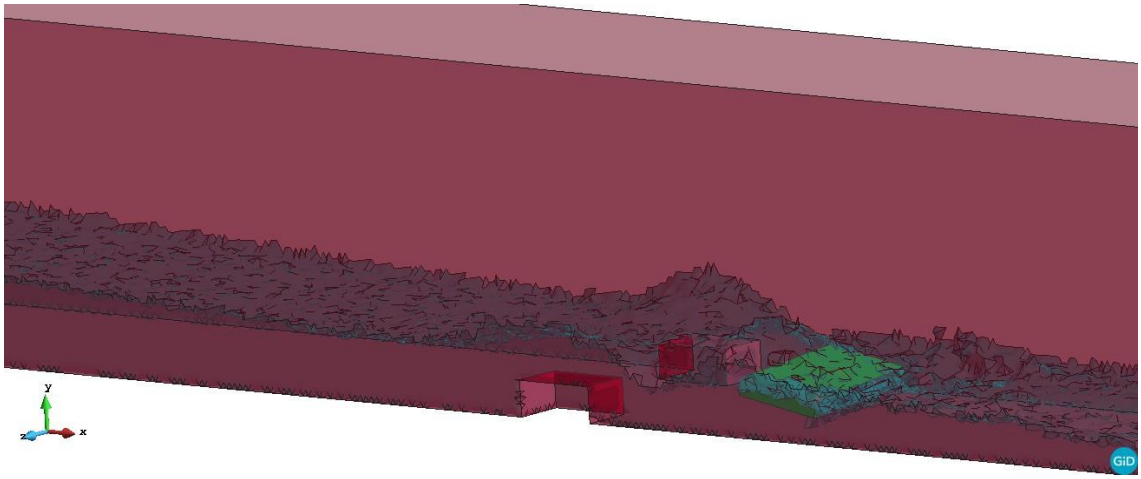

Figure 5.53. View of the simulation with an 8-mm mesh at the time step 1.40131 seconds.

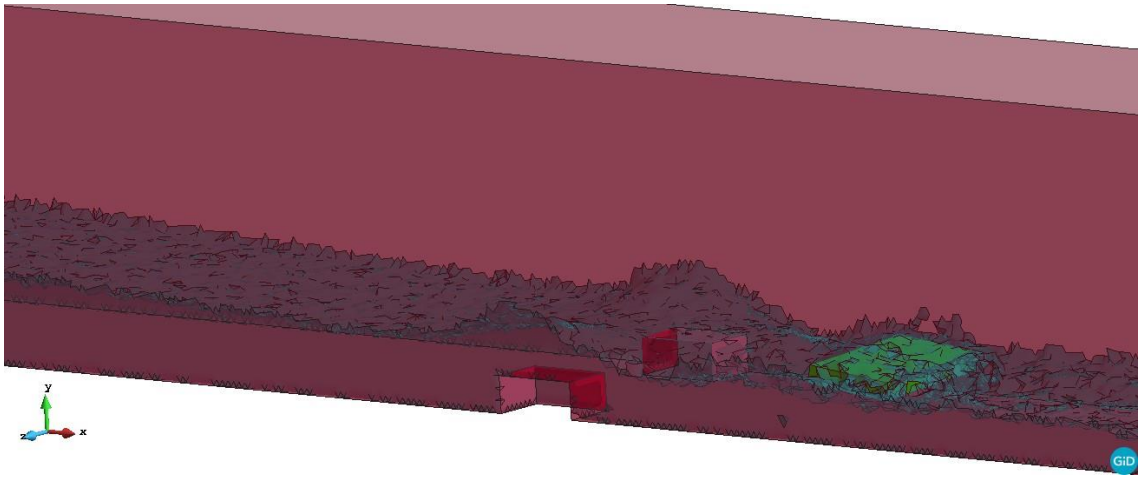

Figure 5.54. View of the simulation with an 8-mm mesh at the time step 1.50012 seconds.

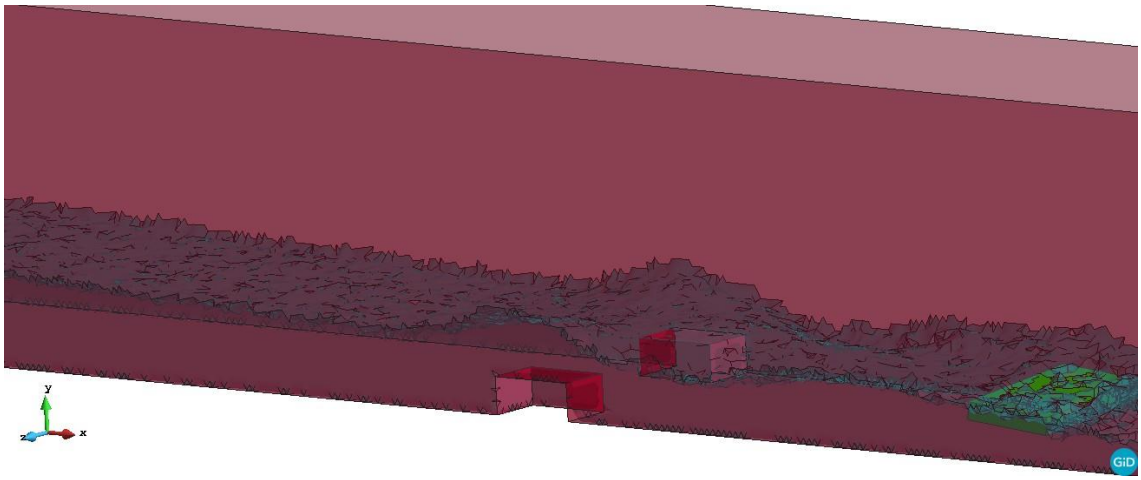

Figure 5.55. View of the simulation with an 8-mm mesh at the time step 1.70014 seconds.

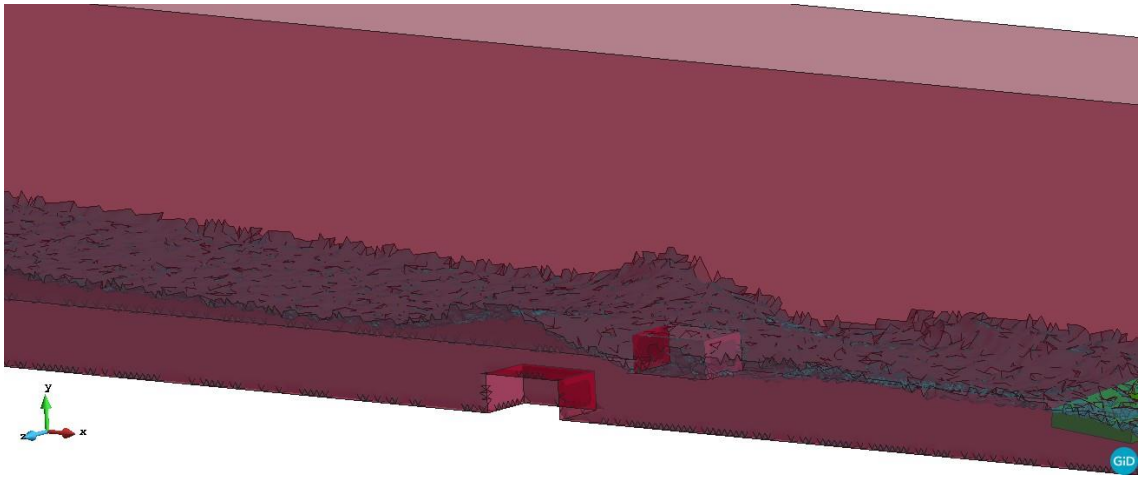

Figure 5.56. View of the simulation with an 8-mm mesh at the time step 1.80064 seconds.

It is known that as the smaller the mesh size is, the bigger the computational time will be. So for the 8-mm mesh size case, to reduce the total computational time, the time step between results was set to 0.1 seconds, and the total time of simulation was set to 2 seconds. Therefore it generated only 19 files of results. The average time the software takes to calculate one time step for this case is 20 minutes, so it would have taken 13.8 days to print 1000 files of results, like in the other cases.

Note that in the appendix, where the calculation of the motion of the centroid of the girder is performed, there are not as time steps calculated for this case than the other two cases.

As there is more time between time steps than the 12 and 10-mm cases the accuracy of the motion plots will not be as high, however, the accuracy of the simulation will be higher than the two previous cases, as the smaller the mesh size, the bigger the accuracy of the results.

5.4.3. Motion plots of the girder for the 8-mm mesh size case.

In this section, the motion of the centroid of the girder is plotted. The difference between this case compared with the 12 and 10 millimetre case is that when the mesh is generated in the two previous cases, in the bridge layer (looking in the *x*-direction) apart from the top and bottom nodes, there is just one row of nodes generated (see figures 5.38 and 5.39). In this case, apart from the top and bottom rows of nodes, the mesh generated two additional rows of nodes between these two. So, for tracking the x-axis and y-axis motion, the mean coordinates of a node from the first row and a node from the second row are calculated. Obviously, these two nodes must not belong to the same surface of the girder. However, for the calculation of the rotational angle, as the *y* coordinate of the two nodes chosen is fairly different, a correction of the rotational angle must be done.

For this case, nodes number 131643 and 132437 are chosen to generate the motion plots. At $t = 0$ the coordinates for node 131643 are:

$$x = 3.2\,m \qquad y = 0.057799\,m \qquad z = 0.103945\,m \tag{31}$$

And the coordinates of node 132437 at the same time step are:

$$x = 3.1\,m \qquad y = 0.0634158\,m \qquad z = 0.102236\,m \tag{32}$$

Therefore, the coordinates calculated of the centroid of the girder are:

$$x_c = 3.15\,m \qquad y_c = 0.0606074\,m \qquad z_c = 0.10309\,m \tag{33}$$

which are fairly similar to the coordinates of the real centroid of the girder (see equation 28).

Regarding the calculation of the rotational angle, a correction must be done due to the difference in the *y* coordinate of the two nodes chosen. So, the rotational angle is calculated (in radians):

$$\begin{aligned}\theta &= arcsin\left(\frac{y_2 - y_1}{0.1}\right) - arcsin\left(\frac{0.0634158 - 0.057799}{0.1}\right) \\ &= arcsin\left(\frac{y_2 - y_1}{0.1}\right) - 0.056\end{aligned} \tag{34}$$

Further information about the calculation of the motion plots can be found in the appendix.

In figures 5.57 and 5.58, nodes 131643 and 132437 are highlighted.

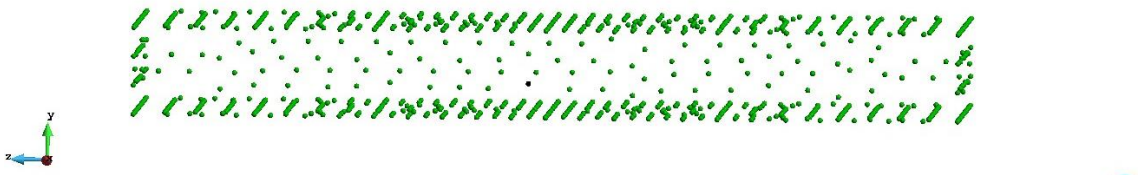

Figure 5.57. Nodes generated in the bridge layer. In black colour node 131643 is highlighted.

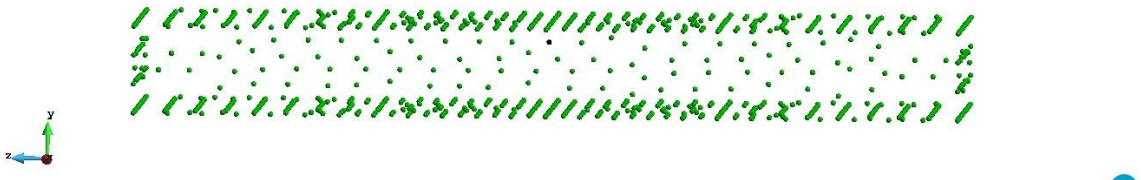

Figure 5.58. Nodes generated in the bridge layer. In black colour node 132437 is highlighted.

The motion plots resulting from those calculations can be seen in figures 5.59, 5.60 and 5.61.

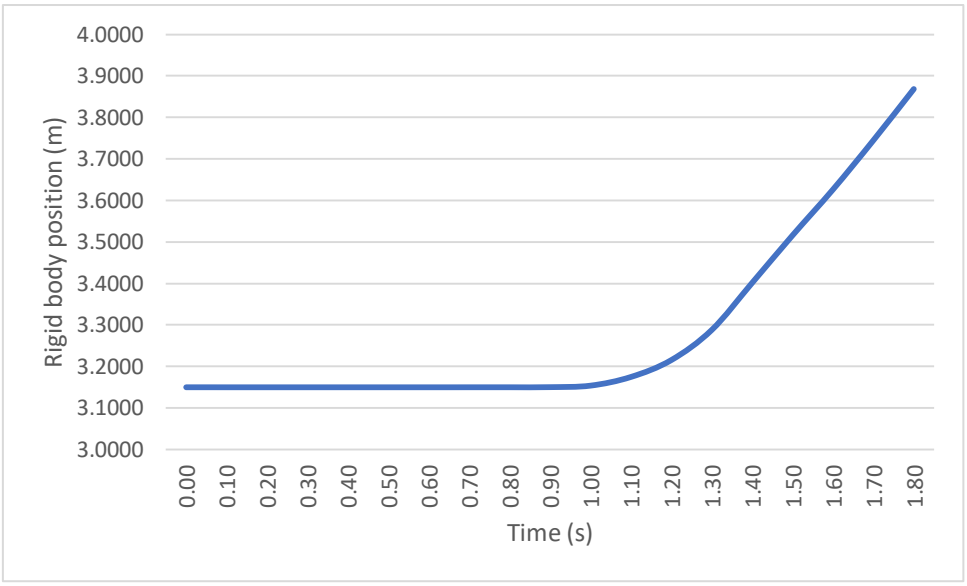

Figure 5.59. Horizontal motion of the rigid body centre of gravity in the simulated case with an 8-mm mesh.

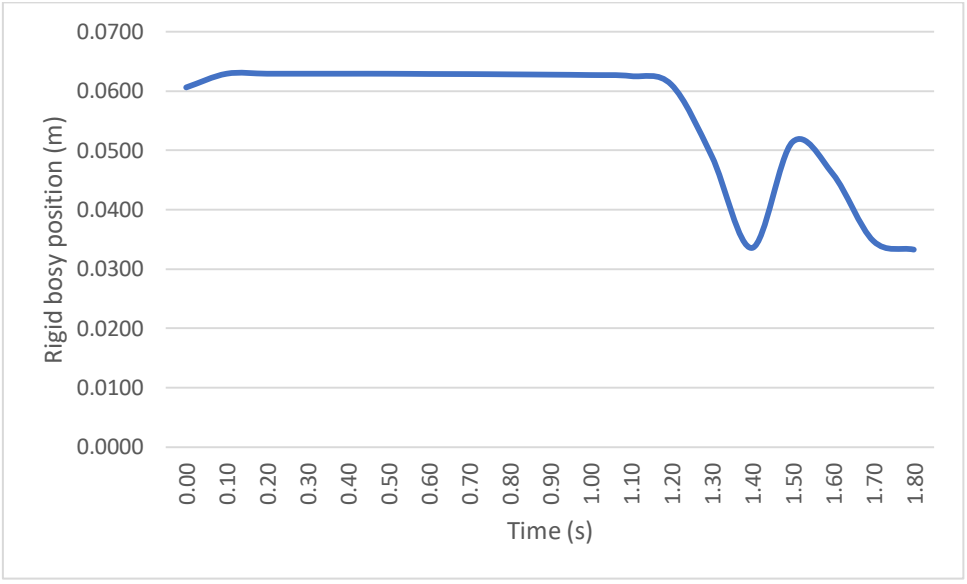

Figure 5.60. Vertical motion of the rigid body centre of gravity in the simulated case with an 8-mm mesh.

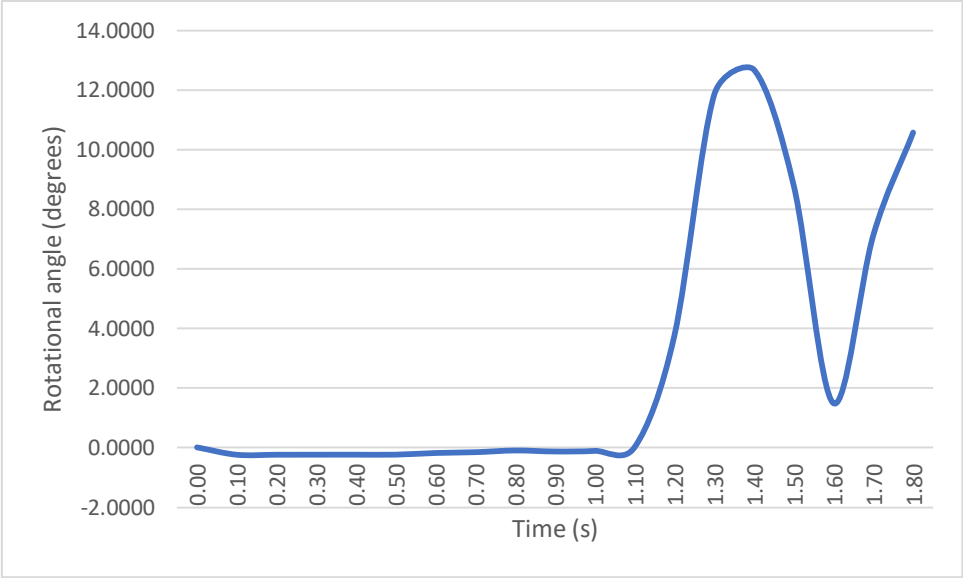

Figure 5.61. Rotational angle of the rigid body centre of gravity in the simulated case with an 8-mm mesh.

As mentioned before, in this case as the computational time was too high and the storage capacity of my computer was not very large, the problem had to be analysed only by printing results every 0.1 seconds. So, in the vertical motion plot, this bouncy effect in the trajectory cannot be perceived because it happens with less than a tenth of a second, which is the time step used in this simulation. Even though it cannot be perceived, the girder also does a kind of bouncy trajectory at the very beginning of the simulation. If we had simulated the problem with a smaller time step it would have been perceived in the vertical motion plot.

6. Comparison of the results obtained.

The most important objective in this project is the validation of the PFEM method by comparing the real-life experiments with the simulations carried out with the different mesh sizes chosen. In the real-life experiments (see section 4), it is mentioned that only the initial water height of 250 millimetres case is considered. Then, 3 simulations with different mesh sizes are carried out with an initial water height of 250 millimetres as well. The simulations try to reproduce the experiments as the same boundary conditions are applied in both the experiments and simulations. This is the same frictional angle, measures of the bridge model, mass, principal moments of inertia, etc.

The methodology for comparing the simulations with the experimental data is by comparing the motion plots of the girder for both the simulated and experimental results. We are using the motion plots as an instrument to validate the PFEM because in Asai and Chandra (2016)[14], the motion plots are the only data that they are facilitating us regarding the experiments they carried out. In fact, this is why we generated the motion plots that can be seen in section 5.

So, in this project, the instrument used to validate the PFEM method is through comparing the experimental motion plots and the generated motion plots of the different simulations carried out and see if they match.

Looking at the motion plots of the 250 millimetres initial water height experiments carried out by Asai and Chandra (2016)[14] (figures 4.3, 4.4 and 4.5), note that the experimental data is represented in the plot as a cloud of points that represent a certain measure in a certain time step. Hence, the experimental data is represented as a scatter plot.

Next, we have to determine the criterion to judge whether if any of the motion plots simulated are a good fit in the scatter plots or not. If for one mesh size the three motion plots are a good fit in the scatter plots, we will consider that the simulation carried out is well adequate to the reality and therefore, the PFEM is validated. If the *x* and *y*-axis motion plots fit well but the rotational angle plot does not, we will discuss if the problem simulated is adequately adapted to reality. We must take into account when comparing the real-life experiments with the simulations, that there is a wide range of different motions that the girder might perform when is being washed out. Plus, we must also consider the correction in the measures of the problem that makes it compatible with the software. This correction consisted in the expansion of the container of the problem (structure layer) 50 millimetres in both *z* and –*z* direction (see page 27). It had to be done because the girder was too close to the walls of the container and the software created some contact elements between the girder and both walls, which restrained the movement of the girder when the water was hitting it.

Moreover, the mesh size is a key point when comparing the real-life experiments with the simulations as the smaller the mesh size, the bigger the accuracy and the adequacy

of the results to reality. If a big mesh size is used, the results might be different than what is happening in real life.

Having all the above considerations in mind, we can compare the real-life experiments with the simulated results with the different mesh sizes.

6.1. Comparison between the experimental and simulated results.

In this section, the experimental results that can be seen in Asai and Chandra (2016)[14] are compared with each mesh size simulated in the software. Firstly, the comparison of the motion plots of the girder of the 12-mm mesh size case with the experimental data is accomplished.

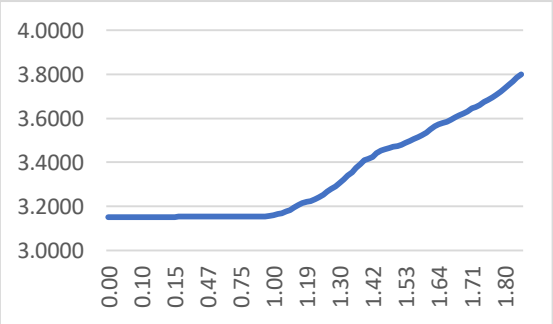

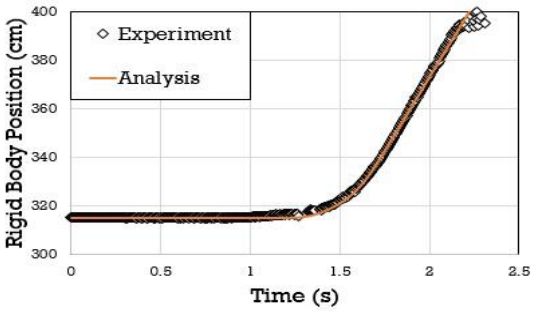

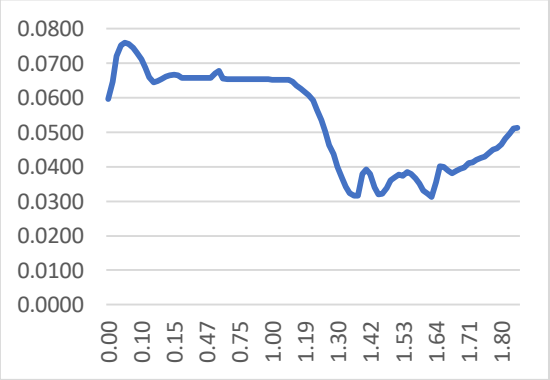

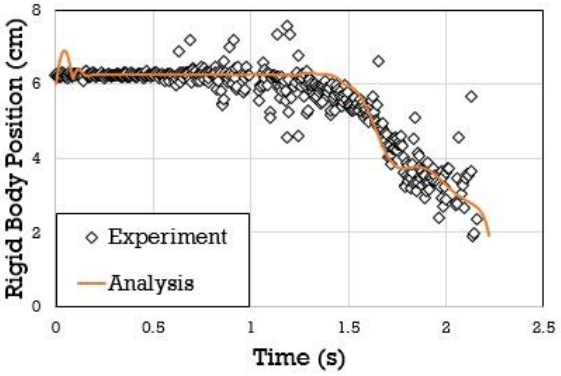

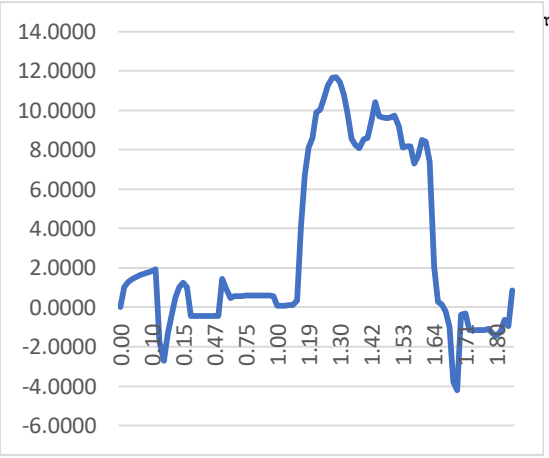

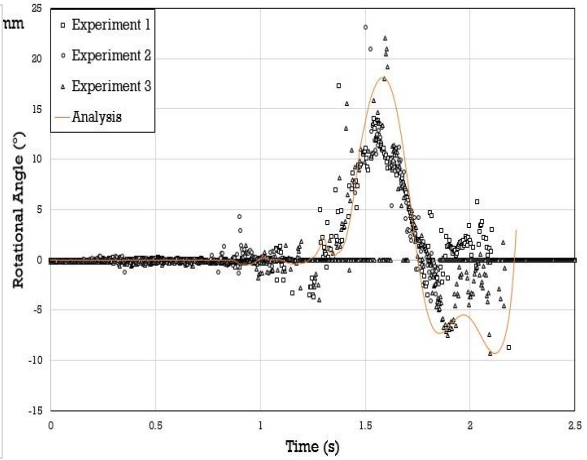

Figure 6.1. Comparative motion plots of the girder in the simulated 12-mm mesh size case (left) and the experiments (right) (source [14]). These are the horizontal motion plots (top), the vertical motion plots (middle) and the rotational angle plots (bottom).

Taking a look at the horizontal motion plot, we can affirm that they look fairly similar especially in the velocity the girder is moving in both cases. However, we see a small difference in terms of the initiation of the movement of the girder: in the simulated case, the motion begins at about 1 second after the water its movement but in the experimental case, the movement does not begin until 1.3 seconds after the initiation of the movement of water. This might be because the mesh size is too big for since it creates water drops that are bigger than in real life. Actually, this water drops the software creates are a tetrahedron of 12-millimetre sides. Obviously, in reality, water drops do not adopt any shape in particular, they are changing bodies through time. The PFEM does not allow that because it is a method for solving fluid-structure interaction problems that require a creation of a mesh of a certain size and, therefore, it does not allow to create elements smaller than the mesh size set.

Another fact to comment about this difference of time when the water is hitting the girder between the two cases is that, in the simulation we began with a prism of water that at $t = 0$ was not moving, and when the simulation started, it collapsed and travelled towards the bridge model washing it out. However, the difference with the experiments rely on the fact that having a perfect prism of water is impossible unless we have a 4-sided container that holds it. So in the experiments, the methodology for holding the prism of water was by means of a mobile gate which held the water until the experiment started. Once the experiment started, they removed in a very quick way the gate, letting the water flow through the bridge. As the gate was removed very fast, it was considered that the gate was removed in a time step negligible, which means that in an infinitesimal time step, the gate was removed. This is why in the simulations there is not any layer compared to the gate in the experiments because there is no need to create it. Rather than creating a new layer to the problem, in the simulations a prism of water is created in a way that is not moving until the simulation starts.

It was considered that this was a good way to simulate the experiments, but it seems that for the 12-mm mesh size case in the simulation the water washes out the bridge 3 tenths of a second before in the experiments, and a mixture of the two reasons presented above can be the possible explanations for it.

Regarding the horizontal motion of the girder plots, it is interesting to mention that in the experimental case, the scatter plot it does not differ much from an imaginary straight line that corresponds to the velocity that the girder is moving through the wave. Plus, as it is a straight line, it denotes that the velocity which the girder is moving through the wave is constant, and is equal to the slope of the line.

Moving on, if we focus on the vertical motion plots, in the experimental results plot we note that there is more dispersion in the scatter plot than in the horizontal motion plot, which means that there is a bigger allowance in the plots of simulations calculated.

At the first sight, both plots look fairly similar except in two small sections, which are at the beginning of the plot and at the end of it. The reason why in the experimental plot at the beginning there is no vertical movement but in the simulation plot there is, is due to the contact elements that are mentioned in early sections of the project. In the simulation, due to this contact elements the girder takes some time to settle over the fixed piers because, in fact, in the simulation, the girder does not settle over the piers themselves, it actually settles over the contact elements created over the piers. This is why in the simulations we let a small gap between the piers and the girder. So, at first stages of the simulation the girder settles over the piers and, then keeps a constant vertical position through time until water washes out the bridge.

The second interval in the plots where they differ a bit from each other is the final part (until 1.8 seconds). While in the experiment plot the girder has a descending tendency, the simulation plot descends until 1.64 seconds when the vertical position of the girder is raising. This fact may be once again due to the big size of the mesh, which affects the accuracy of the results. As mentioned previously, there are a wide range of possible motions that the girder might perform, but a sudden rise of the centroid of the girder cannot be possible due to the shape of the container of the problem, which is flat through the entirety of simulation.

Despite these two disagreements on the motion plots, we can conclude that they look very similar and that in terms of vertical motion, the simulation emulates correctly the reality.

Lastly, in the experimental rotational angle plot, we note that even though the scatter plot is dispersed, the tendency line can be well defined. At the first stages of the simulation, we note that both plots differ from each other. In fact, at simple sight, the two plots are not as similar as the horizontal and vertical motion plots. What is happening at the beginning of the simulation is that the girder of the bridge is settling over the two fixed piers. We will see later on that the smaller the mesh size is, the easier for the girder to settle over the piers and, therefore, the lesser time it will take to not move and finish to settle. So, in this case, due to the big size of the mesh and, hence, the contact elements, the girder is doing lots of movements before the water hits it. This early disagreement in the plots is due to this reason, because the bridge is settling over the piers and it takes some time and some strange movements to do so.

After 1 second of simulation, both plots are quite similar: they both rise the rotational angle to 10 to 12 degrees and then it lowers again to 0 degrees. The only difference between them might be the velocity they rise the rotational angle. In the simulation plot, the angle is risen very fast, while in the experimental plot the angle rises in a softer way.

Despite this small disagreement and the differences between both plots at the beginning of the simulation, we can conclude that the three motion plots of the 12-mm mesh size case are similar to the experimental plots and, therefore, for this mesh size

the PFEM is validated. The simulation is a good representation of reality, despite the small lack of accuracy.

Secondly, the comparison between the motion plots of the girder of the experiments and the 10-mm mesh size simulation is carried out. In figure 6.2 the comparison between the motion plots can be seen.

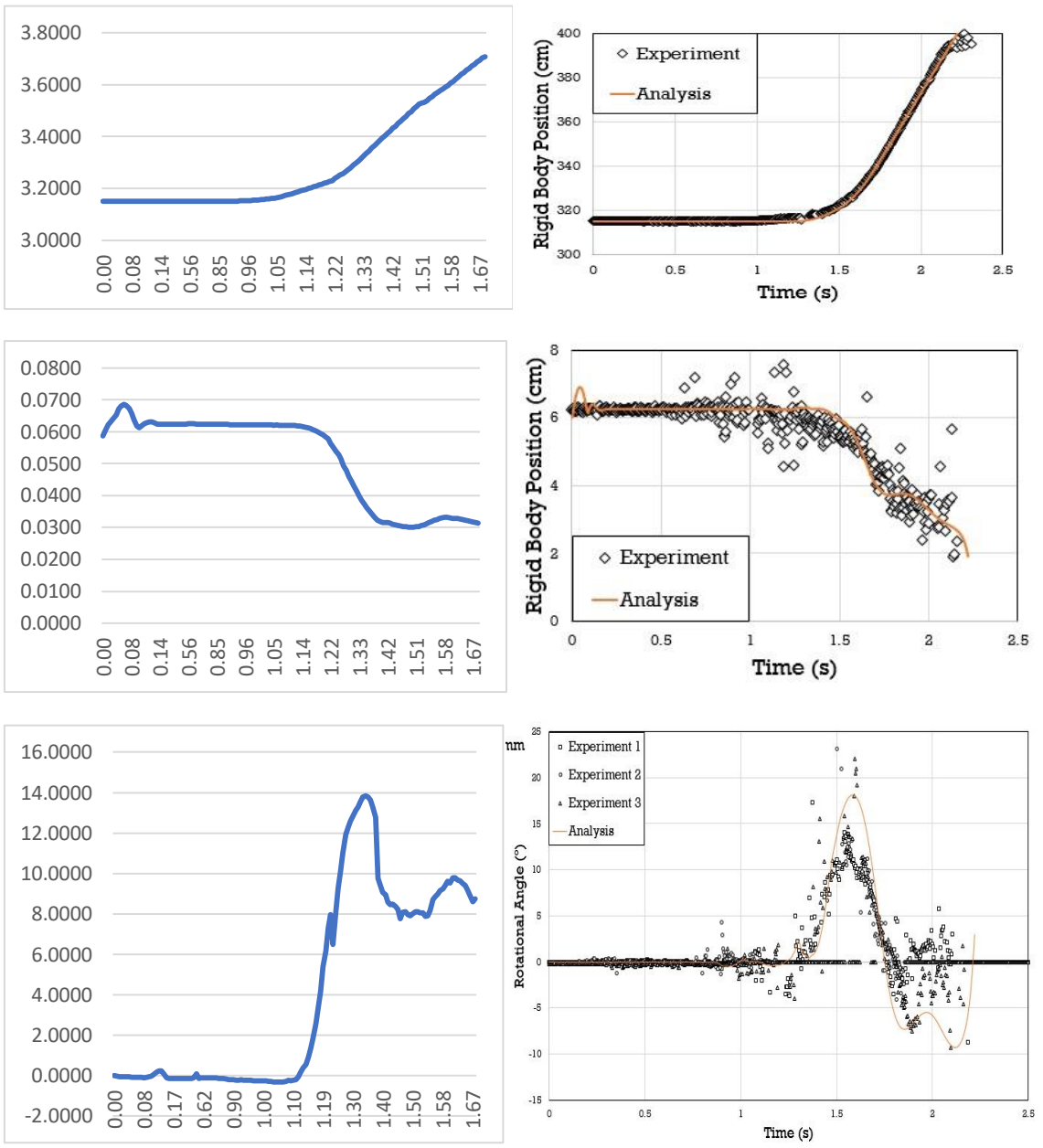

Figure 6.2. Comparative motion plots of the girder in the simulated 10-mm mesh size case (left) and the experiments (right) (source [14]). These are the horizontal motion plots (top), the vertical motion plots (middle) and the rotational angle plots (bottom).

Firstly, the comparison of both horizontal motion of the girder plots with naked eye, we see that they are similar to each other. Even though the cloud of points in the experimental plots follow a clear and unequivocal path, the simulation plot does so as well. However, if we focus on when does the girder initiate its movement in the horizontal direction, we conclude that for the simulated case, it begins it movement at

around 1.05 seconds after the initiation of the simulation and for the experimental case, the girder begins to move at around 1.3 seconds, which means that there is a difference of 0.25 seconds between the initiation of the movement of the girder. This is a similar thing than the comparison with the 12-mm mesh size. The two possibilities for this difference in the plots might be the mesh size, which might be too big for the problem that we simulated, or might be due to the consideration that a collapse of the water prism is a similar thing than the removal of a gate in an infinitesimal amount of time.

This earlier arrival of water to the girder might also be caused by the fact that we considered water a fluid with zero viscosity, which is actually not true. Water in real life has a low viscosity value that depends on its temperature. In fact, at 25 degrees Celsius, the viscosity value is around 0.9[18], instead of the value of 0 that we adopted in the boundary conditions. The viscosity of a fluid is a measure of its resistance to deformation. So, a fluid with low viscosity will take a shorter amount of time to pass through a small hole than a viscous fluid. Therefore, a fluid with 0 viscosity will move through the container of the problem at a higher velocity than a viscous fluid. This way, even though there is a small difference between the viscosities of the water in the experiment and the water in the simulation, the time when the water hits the bridge can be slightly affected. This might be another reason of this disagreement in when the water hits the girder of the bridge.

Secondly, focusing on the vertical motion plots, we see that they are very similar except in two areas. The first interval where both the experimental and the simulation plot are in disagree is at the beginning of the simulation or experiment. There, in the experimental plot, we see that vertically speaking, there is no movement at all of the girder, while in the simulation plot, we see that in the first tenth of a second the girder does a bouncy trajectory in the vertical direction. A similar thins was happening in the previous case, where in the experimental plot the girder was not vertically moving while in the simulation plot it clearly was. In the previous case, we suggested an explanation for this phenomenon, and this is the appearance of contact elements in the simulation between the solid surfaces that are in contact with each other. These contact elements act like a spring that at $t = 0$ are in compression due to the weight of the girder itself. Once the simulation has begun to run, the contact elements that act like a spring apply a force upwards to the girder that rejects it. So the reason why this bouncy trajectory appears in the simulation plot is due to the contact elements, which act like a spring. Once the girder has settled over the two fixed piers, the vertical movement is zero until the water washes out the bridge.

There is also a discordant thing when comparing both the experimental vertical motion plot and the simulation vertical motion plot, and this is the time when the vertical coordinate begins to lower its value or, which is the same, when the girder by the action of water falls off the two fixed piers. Even though the scatter plot of the experimental data is allowing a wide range of possible motions, there is none of them that locates the vertical coordinate of the girder at 3 centimetres 1.4 seconds after the initiation of the simulation. This difference of time might be as well due to either the size of the mesh or

the consideration in the simulation that water is a fluid with zero viscosity, which is not in its entirety true.

Even though there is a small time difference between the simulated and experimental results, we can conclude that both plots look fairly the same and have the same shape, which is good for the validation of the PFEM method.

The last comparison needed to do between the experimental results and the simulated data with the 10-mm mesh is the comparison of the rotational angle plot. For this case, it stands out in the simulation plot that, while in the experimental data the rotational angle is below 0 in any point in the experiment, the rotational angle stays always with a positive value. This fact is because in the simulation plot we only have data from 0 to 1.67 seconds after the initiation of the simulation, while in the experimental plot we can find data until 2.25 seconds. If we take a close look at the experimental plot, actually the rotational angle value is always positive until 1.67 seconds, which makes both plots look very similar. It would be interesting to have data of the simulation up until 2.25 seconds after the initiation of the simulation, but, regardless, both plots look a lot like each other.

All in all, the 10-mm mesh size case fits in every plot we generated as they all three are very similar. We can conclude saying that the 10-mm mesh size case simulation is an accurate representation of reality and making the PFEM method a good methodology for solving fluid-structure interaction problems. Note how the plots for this case are more similar to the experiment plots than the 12-mm mesh size case simulation plots, which were as well similar to the experimental plots, but not quite as much as in this case.

Lastly, the comparison between the 8-mm mesh size simulation plots with the experimental plots must be carried out. Before presenting the plots, we must remember that as a matter of time and storage space in the computer, for this case we only simulated with a time step of 0.1 seconds during 2 seconds, which resulted in just 20 files of results. Due to this, note beforehand that the accuracy of the simulation plots is lower than the previous simulation plots that we generated. In figures 6.3 and 6.4, the comparison of the simulation plots and the experimental plots can be seen.

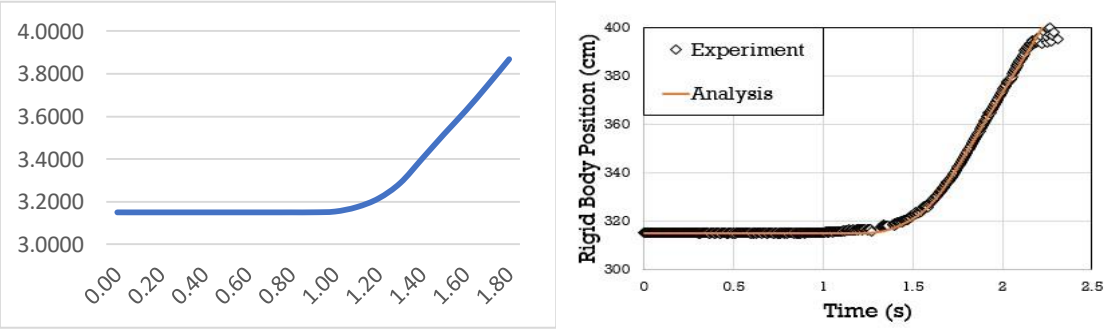

Figure 6.3. Comparative motion plots of the girder in the simulated 8-mm mesh size case (left) and the experiments (right) (source [14]). These are the horizontal motion plots (top), the vertical motion plots (middle) and the rotational angle plots (bottom).

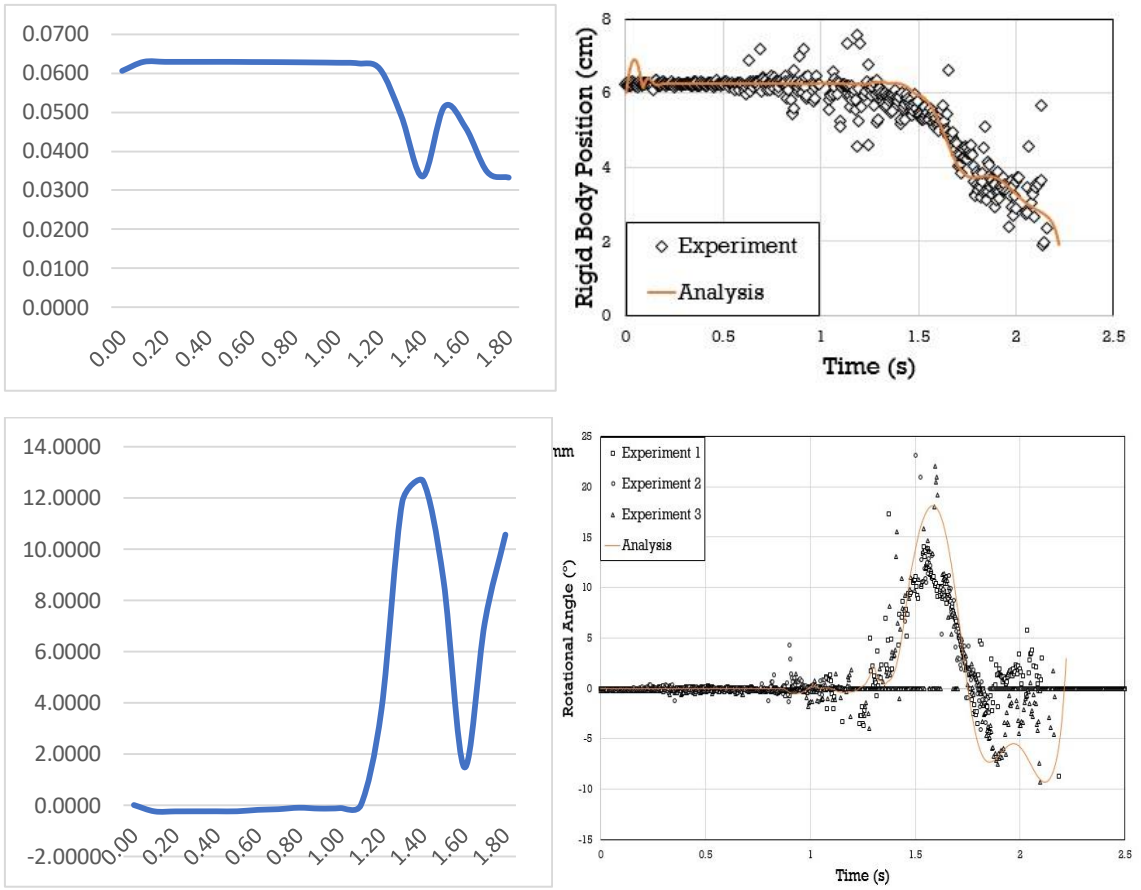

Figure 6.4. Comparative motion plots of the girder in the simulated 8-mm mesh size case (left) and the experiments (right) (source [14]). These are the horizontal motion plots (top), the vertical motion plots (middle) and the rotational angle plots (bottom) (cont.).

In the horizontal motion plots, we saw in the two previous cases with bigger mesh sizes, that water was hitting the girder some tenths of a second before the experimental results said so. However, it is interesting to see that in this case, for the smallest mesh size simulated, the water hits the bridge at the same time in both the experimental and simulated plots. In the two previous cases it is as well mentioned that this difference in the hitting time of the wave might be due to a couple of possible reasons, which are the assumption of the null viscosity of water in the simulated case when in reality water has some viscosity as a fluid, and the fact that the mesh size might be too large. So, watching the results and comparing them, even if it's a really small change in the time when the wave is hitting the bridge, we can conclude that the mesh size affects the motion of water and its velocity through the container of the problem. This reason is proved by the data that we have generated via the horizontal motion plots, but it is possible that a mixture of the two aforementioned reasons would be the cause of this delay in the hitting time of the wave.

Regarding the similarity with the experimental plot, we can conclude that they both look similar to each other, in fact, the 8-mm mesh size case horizontal motion plot, out of the three is the one that fits most in the experimental data. This is very important for the following section, where a comparison between the motion plots of the different mesh sizes is made.

In the vertical motion plots, a difference can be seen with the other simulations regarding the bouncy trajectory at the beginning of the simulation. It is mentioned that for running this case, a time step of 0.1 seconds had to be set due to the computational time and the storage space. In the other cases, the bouncy trajectory of the vertical coordinate took place in less than a tenth of second, so in this case, there is no data regarding this trajectory but, however, it is certainly known that the girder of the bridge does exactly the same bouncy trajectory than in the other cases. This is known because otherwise the simulation would not have worked properly and the girder would not have moved at all.

Despite the value at $t = 1.4$ seconds, the simulated plot fits really well at the experimental plot, once again being the best fit out of the three mesh sizes simulated.

Lastly, in the rotational angle plots, there is one time step where the plots do not match quite well but regardless the simulation plot fits really well to the scatter plot from the experiments. Again, out of the three mesh sizes analysed, this motion plots from the simulation data fit really well to the experimental data.

All in all, we can conclude in this section that the smaller the mesh size is, the bigger the accuracy of the results will be but, in return, we will have a much bigger computational time in the simulation. So, all of the three mesh sizes match a real life problem but the smaller the mesh size, the better the simulation of reality. With this being said, the conclusion is that as all the three mesh sizes match a real-life experiment so the software is robust in terms of simulate the reality and, therefore, the PFEM method for solving fluid-structure interaction problems is a robust methodology as well.

6.2. Comparison between the simulated results regarding the mesh size's choice.

Even though the main objective of the project was to validate the PFEM method by comparing the experimental data with the simulations carried out, the second major objective in this project was to compare the different mesh sizes generated and simulated and discuss their differences and adequation in this problem that we worked on. Comparing the results of the different simulations focusing on the mesh size generated is also beneficent for future problems analysed with this same software or with the PFEM. This section is not only focused on the results, it is also focused on the generation process of the mesh and its data.

In the previous section, it is proven how the smallest mesh size used is the one that fits best in the experimental plots, even though all simulations fit well in the motion scatter plots. In table 6.1, a comparative overview of the mesh data for each mesh size can be viewed.

	12 millimetres	10 millimetres	8 millimetres
Nodes	201.621	331.553	619.075
Triangles	90.258	182.962	288.796
Tetrahedrons	866.652	1.492.673	2.922.864
Elements	956.910	1.675.635	3.211.660
Generation time (s)	107	202	1047

Table 6.1. Comparison of mesh data regarding the mesh size.

What stands out most in this comparative table, is the fact that the generation of the 8-mm mesh in this problem lasts 5 times more than the 10-mm mesh and 10 times more than the 12-mm mesh. This is really important when choosing the mesh size because the computational time might be too large. In these cases, a choice between the best accuracy possible and a big computational time must be done. Remember that in the 12-mm mesh size simulation, one file of results lasted on average 208 seconds, while in the 10-mm mesh size simulation, one file of results, equivalent to the calculation of one time step, lasted on average 359 seconds. However, in the 8-mm mesh size simulation, a single time step calculation lasted about 1260 seconds, which is a big difference between the two bigger mesh sizes cases.

So, the 8-mm mesh is giving us the best accuracy and the best simulation of reality when looking at the motion plots of the girder, but price to pay is the bigger computational time when generating the results, which comes out to be between 4 and 5 times higher for a single time step than in the 10-mm mesh size case. When discussing which mesh size is the best fit in the problem analysed in this project, both the computational time and the accuracy of the results must be taken into account.

In this section, a comparison between the motions of the girder plots generated must be done as well, in order to compare the different motions that each mesh size is performing to the girder. In figure 6.5, a comparison between the horizontal motions of the girder can be seen between the three mesh sizes generated and simulated.

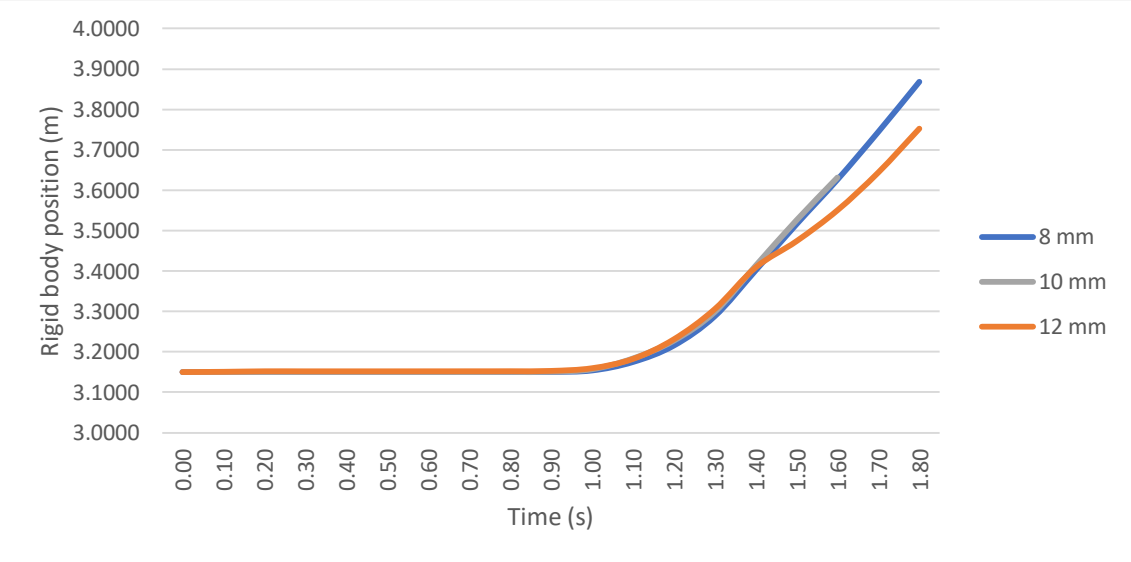

Figure 6.5. Comparison of the horizontal motion of the rigid body centre of gravity between the three mesh sizes simulated.

Analysing figure 6.5, note that all three mesh sizes follow a similar path. In the experiments carried out, the horizontal motion was very similar in all cases, which means that the scatter plot was not disperse at all. This is why the horizontal movement is very similar in all cases. However, the 12-mm mesh size case differs from the other two cases at around 1.4 seconds, where it adopts a different path and changes the rigid body position to 1 centimetre. We mentioned that the horizontal motion plot in the 12-mm mesh simulation was a good fit in the experimental data so, even though the 12-mm horizontal motion plot differs 1 centimetre at the end of the simulation from the other two simulations, they are all a robust simulation of reality.

In the previous section, it is mentioned as well that the best fit in the experimental data was the 8-mm mesh size case. Despite this fact, in figure 6.5 it can be seen that the 10-mm trajectory does not differ much from the 8-mm trajectory, which makes the 10-mm trajectory a good fit in the experimental data. So both the 10-mm mesh size case and the 8-mm mesh size case are an accurate representation of reality in terms of the horizontal motion of the girder.

The horizontal motion plot of the experimental data was not disperse at all but, however, the vertical motion and rotational angle plots are very disperse. For this reason it is possible that the comparison between the three mesh size cases, the trajectories of motion might disagree from one another. In figure 6.6, a comparison of the vertical motion trajectories of all mesh size cases can be seen.

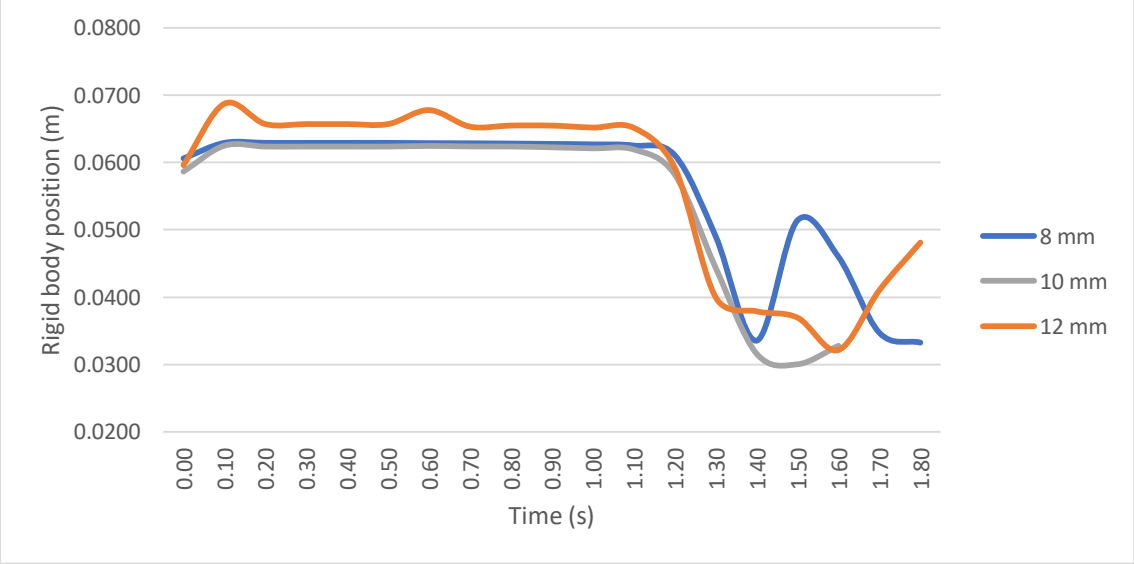

Figure 6.6. Comparison of the vertical motion of the rigid body centre of gravity between the three mesh sizes simulated.

A similar thing is happening in figure 6.6 as in the horizontal motion comparative plot: both the 10-mm and 8-mm mesh size simulations are very similar but the 12-mm mesh size is not. Although it is mentioned that the 12-mm mesh size motion plots are all fairly similar to the experimental scatter plots, in this comparative plot the 12-mm mesh size simulation disagrees in the majority of the simulation time. The 12-mm vertical motion is really different especially before the wave hits the girder of the bridge. This fact might

be due to the mesh size, which might mean that this mesh size is too big for the problem analysed in this project. However, the three cases agree in when the water is hitting the bridge, which means that they all agree in when the girder falls by the action of the wave from the two fixed piers.

The mesh size that fit best to the experimental data is the 8-mm mesh size, but looking at the comparative plot, the 10-mm mesh size case does not differ much from the 8-mm mesh size case, so both cases are a good fit of the experimental data and, hence, they both represent accurately the reality, except at the final stages of the simulation, where it is easier to find different trajectories of the vertical motion of the girder.

So far, it does not seen worth to generate an 8-mm mesh for the problem even though it is the most accurate representation of reality. The big computational time makes it less competitive than the 10-mm mesh. Moreover, the trajectories of both the 8-mm and 10-mm mesh size simulations seem very similar, so, so far, the 10-mm mesh size seems the optimal mesh size to choose for this problem of the project.

The last motion plot to analyse is the rotational angle of the girder plot. This scatter plot for the experimental case, is the most disperse plot out of the three. Hence, this means that a wide range of possible motions can be performed by the girder once the water wave hits it. In figure 6.7, a comparison between the rotational angle of the different mesh sizes can be seen.

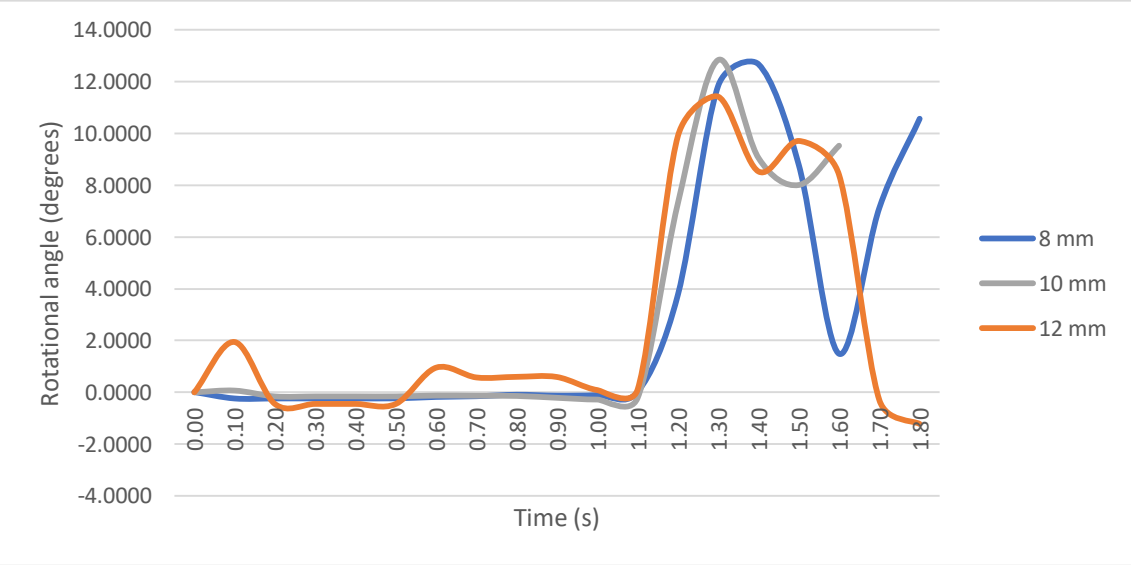

Figure 6.7. Comparison of the rotational angle of the rigid body centre of gravity between the three mesh sizes simulated.

In figure 6.7, focusing on the interval of time before the water wave hits the bridge (around 1.1 seconds), it can be seen how the 12-mm mesh size simulation differs from the two other simulations and does not keep a constant value throughout the initiation of the simulation until the water wave reaches the girder. The reason why in the 12-mm trajectory is not constant, is because the girder of the bridge is settling over the two fixed piers via the contact elements that work as a spring. For the 12-mm mesh size simulation, it took longer time and bigger movements the girder to settle over the piers.

On the other hand, the 10-mm and 8-mm trajectories keep a near zero value throughout the initial stages of the simulation, which makes the two simulations more realistic than the 12-mm mesh size simulation.

In the experimental plot, after the hit of the girder, the scatter plot allows the simulations various possibilities in the rotational angle motion. However, an average trajectory can be drawn in the plot, and this average trajectory is a sudden rise of the rotational angle until 10 to 12 degrees, and then the angle lowers its value to negative values. In the comparison plot, it can be seen that all three simulations rise the value of the rotational angle and then lower it, but they all do it in different ways. It is mentioned in the previous section that, despite one time step, the 8-mm mesh size simulation is the one that best fits in the experimental rotational angle scatter plot. It looks like none of the other simulations follow the same path than the 8-mm mesh but it can be assumed that all the trajectories are quite similar.

As all the simulations trace similar trajectories, it can be said that regarding the rotational angle motion, all three cases are a good representation of reality. The only simulation that looks the less like reality is the 12-mm mesh size simulation, which before the hit of the water wave draws a changing trajectory that in real life is not happening. Once again, the 10-mm mesh size simulation is really similar to the 8-mm mesh size case, and this fact happened in the three motion plots. Therefore, the differences in terms of results between the 8-mm mesh size simulation and the 10-mm mesh size simulation are very small.

All in all, in the three motion plots all the simulations are similar to each other. However, the simulation that differs the most from the others is the 12-mm mesh size case, which leads us to think that this mesh size applied in this problem is too big to generate results with big accuracy. On the other hand, either the 10-mm mesh and the 8-mm mesh trajectories are really similar, which means that both gives us results with great accuracy and so for the calculation of the problem in terms of results, any of these mesh sizes would give us credible results.

7. Conclusions.

After an extensive period of time working on the PFLOW software and investigating the functioning basics of the PFEM, it can be established that it is a robust and solid methodology for solving fluid-structure interaction problems. The generation of the mesh using the Delaunay tessellation and adopting an optimal alpha parameter in the alpha shape technique, make the PFEM a competitive tool for the solving of fluid-structure interaction problems. Simple two dimensional examples have been solved in order to demonstrate the well-functioning of both the software and the PFEM method.

However, the shortcoming of the PFEM is the fact that it is a method that requires a mesh to be solved and, this fact, requires as well a bigger computational time than some other meshless methods. The biggest part of the computational time relies on calculate the new position of all nodes and then draw again the mesh for the next time step. On the other hand, the fact that the PFEM requires a mesh to calculate makes it a more accurate methodology for solving these kind of problems.

Having all these above facts taken into account, it can be concluded that, if chosen the optimal and right mesh size for the generation of the mesh, the PFEM is a really good and competitive method for solving fluid-structure interaction problems of all kind. Even though it would be interesting to study the optimal mesh size to use for any problem, it is out of the scope of this project. In this project the only focus is on the simulation of the bridge wash out phenomenon.

The software used to simulate the problems with the PFEM method is the PFLOW software. If a good knowledge of the functioning of the PFEM is provided, then it can be said that PFLOW is a good user-friendly software, especially in the post-processing, where streamlines, graphs, contour fills, etc. can be generated. In the pre-processing, the PFLOW is also a competitive software and user-friendly, because there are numerous boundary conditions that can be introduced depending on which kind of solid or fluid is needed to be generated.

However, some problems appeared when trying to simulate the bridge wash out problem on the software with the exact same measures than in the experiments. This problem was related to the girder of the bridge, which was too close to the container walls and generated some contact elements that restrained the movement of the girder from its initial position. The software did not warn of this error in the design of the problem, so some time was spent without knowing the reason why the girder was not moving. Finally, the contact element could be seen in the post process, where there is a wide range of possible display options for the well analysis of the problem.

The 2D examples generated have the function to validate the PFEM when simple problems are solved with this methodology. The problems were specifically selected to have water in them in order to visualize how the PFEM works when there is fluid and solid in the same problem.

The main objective in the project was to validate the PFEM method by comparing some simulations calculated with the experimental data provided. So, the quality of the experimental data must be high in order to compare it with the simulations generated. It can be said that the experimental data chosen in this project is high quality, because the data is three scatter plots that define the motion of the girder of the bridge, which results in an easy comparison of experimental and simulated plots. However, there are no imager nor videos of the experiments carried out, which would be a great extension of the information of the experiments but, regardless, the experimental data has allowed the easy comparison and, hence, validation of the PFEM.

As mentioned, the PFEM will be validated if all three motion plots for all simulations agree in shape to the experimental scatter plots. The 12-mm mesh size plots were fitting good in the experimental plots but in some regions or intervals, the simulated plots differed from the actual motion drawn in the experiments. Even though the 12-mm mesh size simulation is the quickest one to calculate, their results are not as accurate as expected, therefore for this problem, a mesh size of 12 millimetres is not the optimal size to choose.

It is interesting and surprising at the same time to see that the 8-mm mesh size simulation plots are very similar to the 10-mm mesh size simulation plots. Even though there is a 2-millimetre difference on the mesh size, it looks like the behaviour of the girder is the same for both cases. Plus, the trajectories in the motion plots are both very similar to the scatter plots generated in the experimental analysis.

So, as both the 10-mm mesh size and the 8-mm mesh size simulations are a good representation of reality (as the motion plots of the girder are very similar to the experimental data), two conclusions arise from this fact. The first of these conclusions is which mesh size is the optimal to choose for the generation of this problem. As for the 8-mm mesh size simulation, the computational time rises to 5 times the computational time of the 10-mm mesh size simulation, and despite the better accuracy of the 8-mm mesh size plots, the optimal mesh size to generate and calculate for this specific problem is the mesh size of 10 millimetres. This size is chosen in terms of computational time efficiency and accuracy of the results, which are the two main parameters in the simulation of real-life problems.

The second of the two conclusions arisen takes into account the PFEM. Despite the less accuracy of the 12-mm mesh size simulation, both the 10.mm and 8-mm mesh size simulations have come out to be really good representations of the experiments carried out. With these good fit of reality, it can be said that the PFEM method for solving fluid-structure interaction problems is validated thanks to both the simple two-dimensional examples, and the main problem simulated with different mesh sizes and analysed how the girder of the bridge is behaving throughout the simulation of the problems.

References

[1] Oñate, E., Idelsohn, S.R., Del Pin, F., Aubry, R. (2014). The particle finite element method. An Overview. *International Journal of Computational Methods.* 1(2): 267-307.

[2] Idelsohn, S.R., Calvo, N., Oñate, E. (2003). Polyhedrization of an arbitrary 3D point set. *Computer Methods in Applied Mechanics and Engineering.* 192(22-24): 2649-2667.

[3] Oñate, E., Celigueta, M. A., Idelsohn, S.R., Salazar, F., Suárez, B. (2012). Fluid-soil-structure interaction analysis with the particle finite element method. *Bytes and Science.* 103-114.

[4] CIMNE. *PFEM.* Retrieved March 2019 from http://www.cimne.com/pfem/default.asp.

[5] Oliver, X., Agelet de Saracibar, C. (2017). *Continuum Mechanics for Engineers. Theory and Problems.* 2nd edition.

[6] CIMNE. *Kratos Multiphysics' wiki.* Retrieved April 2019 from http://kratos-wiki.cimne.upc.edu/index.php/Shape_Functions.

[7] Edelsbrunner, H., Mücke, E. P. (1999). Three dimensional Alpha Shapes. *ACM Transactions on Graphics.* 13(1): 43-72.

[8] Oñate, E., Idelsohn, S.R., Celigueta, M.A., Rossi, R., Marti, J., Carbonell, J.M., Ryzakov, P., Suárez, B. (2011). Advances in the particle finite element method (PFEM) for solving coupled problems in engineering. *Particle-based methods. Computational methods in applied sciences.* 25: 1-49.

[9] Zienkiewicz, O.C., Taylor, R.L. (2000). *The finite element method.* 5th edition, 3 Volumes, Butterworth-Heinemann.

[10] Idelsohn, S.R., Oñate, E., Calvo, N., Del Pin, F. (2003). The meshless finite element method. *International Journal for Numerical Methods in Engineering.* 58(6): 893-912.

[11] Idelsohn, S.R., Marti, J., Limache, A., Oñate, E. (2008). Unified Lagrangian formulation for elastic solids and incompressible fluids: Application to fluid-structure interaction problems via the PFEM. *Computer Methods in Applied Mechanics and Engineering.* 197: 1762-1776.

[12] *GiD. The personal pre and post processor.* Retrieved April 2019 from https://www.gidhome.com/.

[13] *GiD User Manual.* Retrieved April 2019 from https://www.gidhome.com/support/gid-manuals/.

[14] Asai, M., Chandra, B. (2016). Numerical prediction of bridge wash-out during natural disaster by using a stabilized ISPH method.

[15] Miyagawa, Y., Asai, M. (2016). Multi-scale bridge wash out simulation during tsunami by using a particle method. *MATEC Web Conferences.* 47, 02019.

[16] Chandra, B., Asai, M. (2016). Verification and validation of the fluid-rigid body interaction simulation by the smoothed particle hydrodynamics method. *Proceedings of Computational Engineering Conference.* 21.

[17] Chandra, B., Asai, M., Oya, T. (2016). A study of bridge wash-out simulation during tsunami using a particle method considering frictional contact.

[18] Anton Paar Wiki. *Viscosity of Water.* Retrieved September 2019 from https://wiki.anton-paar.com/en/water/.

Appendix

Table of coordinates of node 58506 and node 58842 and the calculation of the coordinates of the centroid of the girder for different time steps for the 12-mm mesh case.

	Node 58506		Node 58842					
Dt (seconds)	**x (m)**	**y (m)**	**x (m)**	**y (m)**	**Mean x (m)**	**Mean y (m)**	**Rot Angle (rad)**	**Rot Angle (deg)**
0.0001	3.2000	0.0596	3.1000	0.0596	3.1500	0.0596	0.0000	0.0000
0.0201	3.2002	0.0638	3.1002	0.0655	3.1502	0.0647	0.0176	1.0103
0.0401	3.2003	0.0710	3.1003	0.0732	3.1503	0.0721	0.0222	1.2745
0.0560	3.2004	0.0740	3.1004	0.0765	3.1504	0.0752	0.0249	1.4290
0.0674	3.2005	0.0746	3.1005	0.0773	3.1505	0.0759	0.0269	1.5391
0.0765	3.2005	0.0742	3.1006	0.0770	3.1505	0.0756	0.0284	1.6279
0.0850	3.2006	0.0731	3.1006	0.0760	3.1506	0.0745	0.0298	1.7098
0.0923	3.2006	0.0715	3.1007	0.0746	3.1506	0.0731	0.0311	1.7808
0.0993	3.2007	0.0696	3.1007	0.0728	3.1507	0.0712	0.0323	1.8486
0.1064	3.2007	0.0670	3.1008	0.0704	3.1507	0.0687	0.0339	1.9449
0.1133	3.2008	0.0674	3.1008	0.0644	3.1508	0.0659	-0.0304	-1.7405
0.1197	3.2007	0.0669	3.1008	0.0622	3.1508	0.0645	-0.0474	-2.7136
0.1259	3.2008	0.0661	3.1008	0.0637	3.1508	0.0649	-0.0236	-1.3538
0.1310	3.2010	0.0658	3.1010	0.0651	3.1510	0.0655	-0.0069	-0.3931
0.1372	3.2011	0.0657	3.1011	0.0666	3.1511	0.0661	0.0090	0.5160
0.1428	3.2013	0.0656	3.1013	0.0674	3.1513	0.0665	0.0176	1.0081
0.1489	3.2014	0.0655	3.1014	0.0677	3.1514	0.0666	0.0219	1.2548
0.1577	3.2016	0.0656	3.1016	0.0674	3.1516	0.0665	0.0176	1.0094
0.1696	3.2019	0.0661	3.1019	0.0654	3.1519	0.0658	-0.0076	-0.4338
0.1818	3.2019	0.0661	3.1020	0.0653	3.1519	0.0657	-0.0078	-0.4480
0.2225	3.2019	0.0661	3.1019	0.0653	3.1519	0.0657	-0.0078	-0.4479
0.2777	3.2019	0.0661	3.1019	0.0653	3.1519	0.0657	-0.0078	-0.4478
0.3202	3.2019	0.0661	3.1019	0.0653	3.1519	0.0657	-0.0078	-0.4477
0.3627	3.2019	0.0661	3.1019	0.0653	3.1519	0.0657	-0.0078	-0.4476
0.4741	3.2019	0.0661	3.1019	0.0653	3.1519	0.0657	-0.0078	-0.4476
0.5439	3.2019	0.0661	3.1019	0.0653	3.1519	0.0657	-0.0078	-0.4473
0.5721	3.2018	0.0658	3.1019	0.0683	3.1519	0.0670	0.0252	1.4410
0.5913	3.2020	0.0670	3.1020	0.0686	3.1520	0.0678	0.0166	0.9531
0.6144	3.2021	0.0653	3.1021	0.0661	3.1521	0.0657	0.0080	0.4602
0.6340	3.2021	0.0648	3.1021	0.0658	3.1521	0.0653	0.0100	0.5754
0.6682	3.2020	0.0648	3.1020	0.0658	3.1520	0.0653	0.0100	0.5741
0.7038	3.2020	0.0648	3.1020	0.0658	3.1520	0.0653	0.0100	0.5754
0.7475	3.2021	0.0650	3.1021	0.0660	3.1521	0.0655	0.0105	0.6024
0.7776	3.2021	0.0650	3.1021	0.0660	3.1521	0.0655	0.0105	0.6044
0.8128	3.2022	0.0650	3.1022	0.0660	3.1522	0.0655	0.0105	0.5990
0.8390	3.2022	0.0650	3.1022	0.0660	3.1522	0.0655	0.0105	0.5991

0.8727	3.2023	0.0650	3.1023	0.0660	3.1523	0.0655	0.0103	0.5924
0.9119	3.2029	0.0650	3.1029	0.0660	3.1529	0.0655	0.0103	0.5920
0.9421	3.2040	0.0650	3.1040	0.0660	3.1540	0.0655	0.0103	0.5876
0.9700	3.2055	0.0649	3.1055	0.0659	3.1555	0.0654	0.0098	0.5623
1.0032	3.2095	0.0651	3.1095	0.0653	3.1595	0.0652	0.0015	0.0872
1.0334	3.2149	0.0651	3.1149	0.0653	3.1649	0.0652	0.0015	0.0872
1.0505	3.2190	0.0651	3.1190	0.0652	3.1690	0.0652	0.0015	0.0873
1.0743	3.2256	0.0651	3.1256	0.0653	3.1756	0.0652	0.0018	0.1032
1.0955	3.2323	0.0651	3.1323	0.0652	3.1823	0.0651	0.0018	0.1035
1.1282	3.2441	0.0644	3.1441	0.0650	3.1941	0.0647	0.0060	0.3446
1.1584	3.2559	0.0600	3.1562	0.0671	3.2060	0.0636	0.0713	4.0866
1.1746	3.2629	0.0568	3.1638	0.0685	3.2134	0.0626	0.1171	6.7089
1.1860	3.2685	0.0547	3.1697	0.0688	3.2191	0.0617	0.1415	8.1049
1.1952	3.2735	0.0533	3.1749	0.0682	3.2242	0.0608	0.1501	8.6012
1.2007	3.2800	0.0506	3.1818	0.0678	3.2309	0.0592	0.1728	9.9009
1.2233	3.2908	0.0479	3.1926	0.0653	3.2417	0.0566	0.1747	10.0118
1.2387	3.3015	0.0444	3.2036	0.0628	3.2526	0.0536	0.1851	10.6081
1.2557	3.3142	0.0405	3.2165	0.0600	3.2653	0.0502	0.1962	11.2406
1.2732	3.3283	0.0362	3.2308	0.0563	3.2796	0.0462	0.2031	11.6375
1.2853	3.3388	0.0335	3.2413	0.0537	3.2900	0.0436	0.2040	11.6880
1.3023	3.3544	0.0301	3.2568	0.0499	3.3056	0.0400	0.1994	11.4242
1.3189	3.3705	0.0275	3.2726	0.0462	3.3216	0.0368	0.1886	10.8071
1.3352	3.3880	0.0256	3.2898	0.0426	3.3389	0.0341	0.1710	9.7997
1.3500	3.4041	0.0249	3.3057	0.0398	3.3549	0.0324	0.1493	8.5569
1.3669	3.4225	0.0245	3.3239	0.0388	3.3732	0.0317	0.1437	8.2311
1.3851	3.4415	0.0245	3.3428	0.0386	3.3921	0.0316	0.1411	8.0869
1.4003	3.4580	0.0305	3.3594	0.0453	3.4087	0.0379	0.1489	8.5327
1.4057	3.4632	0.0317	3.3647	0.0467	3.4140	0.0392	0.1500	8.5927
1.4174	3.4742	0.0298	3.3758	0.0462	3.4250	0.0380	0.1645	9.4256
1.4348	3.4902	0.0250	3.3921	0.0431	3.4412	0.0341	0.1818	10.4176
1.4493	3.5031	0.0236	3.4047	0.0404	3.4539	0.0320	0.1693	9.6975
1.4599	3.5088	0.0239	3.4104	0.0406	3.4596	0.0323	0.1682	9.6352
1.4774	3.5129	0.0256	3.4145	0.0423	3.4637	0.0339	0.1677	9.6068
1.4969	3.5190	0.0277	3.4206	0.0444	3.4698	0.0360	0.1682	9.6354
1.5065	3.5231	0.0285	3.4248	0.0454	3.4739	0.0370	0.1695	9.7124
1.5187	3.5294	0.0298	3.4309	0.0458	3.4801	0.0378	0.1603	9.1819
1.5339	3.5383	0.0303	3.4395	0.0444	3.4889	0.0374	0.1414	8.1018
1.5458	3.5461	0.0314	3.4473	0.0456	3.4967	0.0385	0.1425	8.1632
1.5586	3.5551	0.0307	3.4562	0.0449	3.5056	0.0378	0.1426	8.1696
1.5705	3.5640	0.0303	3.4650	0.0430	3.5145	0.0367	0.1274	7.2967
1.5811	3.5724	0.0284	3.4735	0.0418	3.5230	0.0351	0.1342	7.6864
1.5943	3.5832	0.0257	3.4845	0.0405	3.5338	0.0331	0.1484	8.5004
1.6136	3.5998	0.0249	3.5010	0.0395	3.5504	0.0322	0.1466	8.4004
1.6307	3.6135	0.0248	3.5145	0.0376	3.5640	0.0312	0.1288	7.3780
1.6406	3.6221	0.0337	3.5228	0.0373	3.5724	0.0355	0.0361	2.0689

1.6450	3.6268	0.0400	3.5276	0.0404	3.5772	0.0402	0.0047	0.2666
1.6522	3.6342	0.0398	3.5350	0.0401	3.5846	0.0400	0.0027	0.1539
1.6617	3.6439	0.0390	3.5446	0.0386	3.5942	0.0388	-0.0035	-0.2028
1.6724	3.6545	0.0389	3.5552	0.0372	3.6048	0.0381	-0.0171	-0.9808
1.6821	3.6640	0.0421	3.5648	0.0355	3.6144	0.0388	-0.0661	-3.7889
1.6907	3.6724	0.0430	3.5733	0.0357	3.6228	0.0393	-0.0735	-4.2123
1.6998	3.6818	0.0402	3.5820	0.0395	3.6319	0.0399	-0.0064	-0.3662
1.7122	3.6941	0.0413	3.5943	0.0408	3.6442	0.0410	-0.0053	-0.3031
1.7194	3.7012	0.0424	3.6015	0.0404	3.6514	0.0414	-0.0199	-1.1416
1.7289	3.7110	0.0430	3.6113	0.0410	3.6611	0.0420	-0.0201	-1.1496
1.7405	3.7231	0.0436	3.6234	0.0416	3.6733	0.0426	-0.0201	-1.1506
1.7496	3.7329	0.0440	3.6332	0.0420	3.6830	0.0430	-0.0202	-1.1547
1.7612	3.7454	0.0451	3.6457	0.0431	3.6956	0.0441	-0.0203	-1.1616
1.7716	3.7566	0.0459	3.6569	0.0440	3.7067	0.0449	-0.0188	-1.0745
1.7855	3.7716	0.0465	3.6719	0.0442	3.7217	0.0453	-0.0230	-1.3182
1.7978	3.7848	0.0477	3.6851	0.0452	3.7349	0.0464	-0.0254	-1.4533
1.8139	3.8022	0.0492	3.7025	0.0470	3.7524	0.0481	-0.0213	-1.2220
1.8295	3.8189	0.0501	3.7193	0.0490	3.7691	0.0496	-0.0109	-0.6249
1.8449	3.8352	0.0519	3.7355	0.0503	3.7854	0.0511	-0.0168	-0.9631
1.8588	3.8499	0.0506	3.7501	0.0521	3.8000	0.0514	0.0150	0.8574

Table of coordinates of node 84022 and node 84477 and the calculation of the coordinates of the centroid of the girder for different time steps for the 10-mm mesh case.

	Node 84022		**Node 84477**					
Dt (seconds)	**x (m)**	**y (m)**	**x (m)**	**y (m)**	**Mean x (m)**	**Mean y (m)**	**Rot Angle (rad)**	**Rot Angle (deg)**
0.0001	3.2000	0.0587	3.1000	0.0587	3.1500	0.0587	0.0000	0.0000
0.0127	3.2000	0.0607	3.1000	0.0607	3.1500	0.0607	-0.0006	-0.0337
0.0169	3.2000	0.0621	3.1000	0.0620	3.1500	0.0621	-0.0010	-0.0574
0.0204	3.2000	0.0633	3.1000	0.0632	3.1500	0.0633	-0.0011	-0.0624
0.0230	3.2000	0.0641	3.1000	0.0640	3.1500	0.0641	-0.0011	-0.0642
0.0275	3.2000	0.0654	3.1000	0.0653	3.1500	0.0653	-0.0012	-0.0674
0.0354	3.2000	0.0671	3.1000	0.0670	3.1500	0.0670	-0.0013	-0.0731
0.0424	3.2000	0.0681	3.1000	0.0679	3.1500	0.0680	-0.0014	-0.0780
0.0537	3.2000	0.0687	3.1000	0.0685	3.1500	0.0686	-0.0015	-0.0859
0.0623	3.2000	0.0683	3.1000	0.0681	3.1500	0.0682	-0.0016	-0.0921
0.0700	3.2000	0.0673	3.1000	0.0671	3.1500	0.0672	-0.0017	-0.0975
0.0774	3.2000	0.0658	3.1000	0.0656	3.1500	0.0657	-0.0018	-0.1027
0.0845	3.2000	0.0639	3.1000	0.0637	3.1500	0.0638	-0.0019	-0.1077
0.0906	3.2000	0.0619	3.1000	0.0618	3.1500	0.0619	-0.0016	-0.0904
0.0966	3.2000	0.0614	3.1000	0.0612	3.1500	0.0613	-0.0012	-0.0661
0.0103	3.2000	0.0619	3.1000	0.0619	3.1500	0.0619	-0.0005	-0.0265
0.1084	3.2000	0.0624	3.1000	0.0626	3.1500	0.0625	0.0012	0.0684

0.1137	3.2000	0.0628	3.1000	0.0631	3.1500	0.0629	0.0028	0.1613
0.1196	3.2000	0.0629	3.1000	0.0633	3.1500	0.0631	0.0041	0.2327
0.1247	3.2000	0.0628	3.1000	0.0632	3.1500	0.0630	0.0040	0.2284
0.1304	3.2000	0.0626	3.1000	0.0628	3.1500	0.0627	0.0015	0.0852
0.1357	3.2000	0.0625	3.1000	0.0623	3.1500	0.0624	-0.0021	-0.1227
0.1443	3.2000	0.0625	3.1000	0.0622	3.1500	0.0624	-0.0027	-0.1548
0.1501	3.2000	0.0625	3.1000	0.0622	3.1500	0.0624	-0.0027	-0.1575
0.1657	3.2000	0.0625	3.1000	0.0622	3.1500	0.0624	-0.0027	-0.1573
0.2546	3.2000	0.0625	3.1000	0.0622	3.1500	0.0624	-0.0027	-0.1570
0.2983	3.2000	0.0625	3.1000	0.0622	3.1500	0.0624	-0.0027	-0.1568
0.0362	3.2000	0.0625	3.1000	0.0622	3.1500	0.0624	-0.0027	-0.1567
0.4066	3.2000	0.0625	3.1000	0.0622	3.1500	0.0624	-0.0027	-0.1566
0.4355	3.2000	0.0625	3.1000	0.0622	3.1500	0.0624	-0.0027	-0.1566
0.0483	3.2000	0.0625	3.1000	0.0622	3.1500	0.0624	-0.0027	-0.1565
0.5125	3.2000	0.0625	3.1000	0.0622	3.1500	0.0624	-0.0027	-0.1565
0.5464	3.2000	0.0625	3.1000	0.0623	3.1500	0.0624	-0.0023	-0.1291
0.5551	3.2000	0.0625	3.1000	0.0626	3.1500	0.0625	0.0017	0.0960
0.5714	3.2000	0.0626	3.1000	0.0623	3.1500	0.0625	-0.0023	-0.1344
0.5928	3.2000	0.0626	3.1000	0.0623	3.1500	0.0625	-0.0023	-0.1294
0.6235	3.2000	0.0625	3.1000	0.0623	3.1500	0.0624	-0.0022	-0.1244
0.6721	3.2000	0.0625	3.1000	0.0623	3.1500	0.0624	-0.0023	-0.1323
0.6943	3.2000	0.0625	3.1000	0.0623	3.1500	0.0624	-0.0023	-0.1324
0.7355	3.2000	0.0625	3.1000	0.0623	3.1500	0.0624	-0.0023	-0.1322
0.7691	3.2000	0.0625	3.1000	0.0623	3.1500	0.0624	-0.0023	-0.1321
0.7891	3.2001	0.0625	3.1001	0.0623	3.1501	0.0624	-0.0023	-0.1326
0.8143	3.2002	0.0624	3.1002	0.0622	3.1502	0.0623	-0.0024	-0.1392
0.8317	3.2002	0.0624	3.1002	0.0622	3.1502	0.0623	-0.0024	-0.1392
0.8514	3.2003	0.0624	3.1003	0.0622	3.1503	0.0623	-0.0024	-0.1391
0.8688	3.2004	0.0624	3.1004	0.0621	3.1504	0.0623	-0.0032	-0.1830
0.8882	3.2006	0.0624	3.1006	0.0621	3.1506	0.0623	-0.0037	-0.2119
0.8955	3.2007	0.0624	3.1007	0.0621	3.1507	0.0623	-0.0037	-0.2118
0.9033	3.2007	0.0624	3.1007	0.0621	3.1507	0.0623	-0.0037	-0.2117
0.9117	3.2009	0.0624	3.1009	0.0620	3.1509	0.0622	-0.0039	-0.2235
0.9196	3.2011	0.0624	3.1011	0.0620	3.1511	0.0622	-0.0039	-0.2223
0.9288	3.2014	0.0624	3.1014	0.0620	3.1514	0.0622	-0.0038	-0.2180
0.9365	3.2017	0.0624	3.1017	0.0620	3.1517	0.0622	-0.0041	-0.2331
0.9426	3.2020	0.0624	3.1020	0.0620	3.1520	0.0622	-0.0041	-0.2330
0.9485	3.2023	0.0624	3.1023	0.0620	3.1523	0.0622	-0.0041	-0.2326
0.9600	3.2031	0.0624	3.1031	0.0619	3.1531	0.0622	-0.0041	-0.2369
0.9676	3.2037	0.0624	3.1037	0.0619	3.1537	0.0621	-0.0044	-0.2547
0.9774	3.2045	0.0624	3.1045	0.0619	3.1545	0.0621	-0.0046	-0.2621
0.9843	3.2051	0.0623	3.1051	0.0619	3.1551	0.0621	-0.0045	-0.2606
0.9940	3.2060	0.0623	3.1060	0.0619	3.1560	0.0621	-0.0045	-0.2582
1.0015	3.2069	0.0623	3.1069	0.0619	3.1569	0.0621	-0.0046	-0.2649
1.0061	3.2074	0.0623	3.1075	0.0618	3.1574	0.0621	-0.0049	-0.2781

1.0163	3.2088	0.0623	3.1088	0.0618	3.1588	0.0621	-0.0049	-0.2793
1.0233	3.2099	0.0623	3.1100	0.0618	3.1599	0.0621	-0.0051	-0.2899
1.0306	3.2113	0.0623	3.1113	0.0618	3.1613	0.0621	-0.0054	-0.3098
1.0390	3.2129	0.0623	3.1130	0.0618	3.1630	0.0621	-0.0055	-0.3134
1.0472	3.2148	0.0623	3.1148	0.0618	3.1648	0.0621	-0.0057	-0.3293
1.0545	3.2165	0.0623	3.1165	0.0618	3.1665	0.0621	-0.0057	-0.3270
1.0643	3.2190	0.0623	3.1191	0.0618	3.1691	0.0620	-0.0054	-0.3081
1.0746	3.2220	0.0623	3.1221	0.0618	3.1721	0.0620	-0.0052	-0.2984
1.0817	3.2243	0.0622	3.1244	0.0618	3.1744	0.0620	-0.0041	-0.2369
1.0915	3.2277	0.0622	3.1279	0.0617	3.1778	0.0620	-0.0047	-0.2688
1.0985	3.2302	0.0622	3.1304	0.0617	3.1803	0.0619	-0.0043	-0.2489
1.1072	3.2335	0.0621	3.1336	0.0617	3.1835	0.0619	-0.0038	-0.2182
1.1175	3.2374	0.0620	3.1376	0.0618	3.1875	0.0619	-0.0012	-0.0698
1.1265	3.2410	0.0616	3.1412	0.0619	3.1911	0.0618	0.0032	0.1818
1.1327	3.2436	0.0614	3.1438	0.0620	3.1937	0.0617	0.0064	0.3669
1.1393	3.2464	0.0611	3.1466	0.0621	3.1965	0.0616	0.0097	0.5560
1.1468	3.2497	0.0607	3.1499	0.0622	3.1998	0.0614	0.0156	0.8944
1.1535	3.2525	0.0601	3.1528	0.0624	3.2027	0.0613	0.0231	1.3216
1.1610	3.2559	0.0594	3.1562	0.0626	3.2060	0.0610	0.0321	1.8396
1.1694	3.2597	0.0585	3.1601	0.0630	3.2099	0.0607	0.0448	2.5642
1.1769	3.2631	0.0574	3.1636	0.0633	3.2133	0.0604	0.0589	3.3767
1.1833	3.2661	0.0564	3.1667	0.0637	3.2164	0.0600	0.0729	4.1794
1.1914	3.2701	0.0548	3.1709	0.0641	3.2205	0.0594	0.0938	5.3744
1.1970	3.2729	0.0536	3.1738	0.0643	3.2234	0.0590	0.1076	6.1655
1.2047	3.2769	0.0519	3.1781	0.0646	3.2275	0.0582	0.1275	7.3037
1.2095	3.2795	0.0508	3.1810	0.0646	3.2303	0.0577	0.1392	7.9729
1.2230	3.2879	0.0506	3.1890	0.0619	3.2385	0.0563	0.1133	6.4890
1.2347	3.2950	0.0479	3.1964	0.0620	3.2457	0.0550	0.1413	8.0979
1.2436	3.3007	0.0458	3.2024	0.0619	3.2515	0.0538	0.1622	9.2925
1.2511	3.3057	0.0440	3.2077	0.0616	3.2567	0.0528	0.1763	10.0999
1.2606	3.3123	0.0418	3.2146	0.0609	3.2635	0.0514	0.1926	11.0373
1.2733	3.3218	0.0389	3.2244	0.0596	3.2731	0.0493	0.2083	11.9340
1.2821	3.3289	0.0372	3.2316	0.0584	3.2803	0.0478	0.2140	12.2641
1.2934	3.3385	0.0350	3.2414	0.0568	3.2899	0.0459	0.2200	12.6073
1.3027	3.3469	0.0333	3.2499	0.0555	3.2984	0.0444	0.2241	12.8400
1.3117	3.3553	0.0315	3.2584	0.0542	3.3069	0.0429	0.2289	13.1130
1.3213	3.3647	0.0298	3.2679	0.0528	3.3163	0.0413	0.2321	13.2988
1.3310	3.3746	0.0281	3.2779	0.0515	3.3262	0.0398	0.2365	13.5498
1.3403	3.3845	0.0265	3.2879	0.0503	3.3362	0.0384	0.2407	13.7901
1.3484	3.3935	0.0253	3.2969	0.0492	3.3452	0.0373	0.2415	13.8350
1.3575	3.4041	0.0241	3.3074	0.0480	3.3558	0.0360	0.2408	13.7955
1.3653	3.4134	0.0233	3.3167	0.0468	3.3651	0.0351	0.2379	13.6321
1.3733	3.4232	0.0226	3.3264	0.0456	3.3748	0.0341	0.2319	13.2857
1.3812	3.4333	0.0221	3.3362	0.0441	3.3848	0.0331	0.2227	12.7599
1.3886	3.4433	0.0239	3.3451	0.0408	3.3942	0.0324	0.1705	9.7695

1.3955	3.4516	0.0237	3.3533	0.0400	3.4025	0.0319	0.1640	9.3990
1.4047	3.4623	0.0237	3.3638	0.0395	3.4130	0.0316	0.1580	9.0552
1.4116	3.4701	0.0238	3.3716	0.0394	3.4208	0.0316	0.1561	8.9421
1.4215	3.4813	0.0240	3.3828	0.0389	3.4321	0.0315	0.1495	8.5638
1.4288	3.4897	0.0240	3.3911	0.0387	3.4404	0.0313	0.1476	8.4576
1.4382	3.5006	0.0237	3.4020	0.0384	3.4513	0.0310	0.1482	8.4914
1.4455	3.5090	0.0236	3.4104	0.0382	3.4597	0.0309	0.1460	8.3628
1.4542	3.5190	0.0235	3.4204	0.0378	3.4697	0.0307	0.1436	8.2251
1.4611	3.5271	0.0238	3.4283	0.0373	3.4777	0.0305	0.1353	7.7523
1.4702	3.5374	0.0232	3.4387	0.0373	3.4881	0.0302	0.1410	8.0797
1.4774	3.5456	0.0231	3.4470	0.0372	3.4963	0.0302	0.1416	8.1153
1.4869	3.5564	0.0231	3.4577	0.0370	3.5070	0.0301	0.1388	7.9499
1.4946	3.5651	0.0231	3.4664	0.0369	3.5157	0.0300	0.1379	7.9018
1.5037	3.5751	0.0231	3.4765	0.0370	3.5258	0.0300	0.1398	8.0098
1.5078	3.5795	0.0232	3.4809	0.0373	3.5302	0.0302	0.1415	8.1090
1.5096	3.5815	0.0233	3.4829	0.0373	3.5322	0.0303	0.1413	8.0972
1.5159	3.5883	0.0235	3.4897	0.0376	3.5390	0.0306	0.1406	8.0543
1.5237	3.5969	0.0239	3.4982	0.0379	3.5476	0.0309	0.1406	8.0536
1.5302	3.6037	0.0244	3.5050	0.0381	3.5544	0.0312	0.1373	7.8643
1.5380	3.6120	0.0247	3.5133	0.0385	3.5627	0.0316	0.1381	7.9104
1.5443	3.6186	0.0248	3.5199	0.0390	3.5692	0.0319	0.1424	8.1602
1.5519	3.6264	0.0246	3.5279	0.0398	3.5772	0.0322	0.1523	8.7248
1.5580	3.6328	0.0247	3.5343	0.0401	3.5835	0.0324	0.1545	8.8527
1.5648	3.6399	0.0249	3.5415	0.0405	3.5907	0.0327	0.1566	8.9702
1.5714	3.6468	0.0250	3.5484	0.0409	3.5976	0.0330	0.1596	9.1436
1.5799	3.6557	0.0251	3.5573	0.0412	3.6065	0.0331	0.1612	9.2358
1.5874	3.6633	0.0249	3.5650	0.0413	3.6141	0.0331	0.1640	9.3965
1.5960	3.6721	0.0246	3.5739	0.0413	3.6230	0.0330	0.1677	9.6067
1.6041	3.6805	0.0245	3.5823	0.0411	3.6314	0.0328	0.1663	9.5290
1.6127	3.6894	0.0244	3.5912	0.0414	3.6403	0.0329	0.1709	9.7946
1.6191	3.6961	0.0243	3.5979	0.0413	3.6470	0.0328	0.1706	9.7752
1.6282	3.7055	0.0243	3.6072	0.0411	3.6563	0.0327	0.1685	9.6571
1.6347	3.7122	0.0241	3.6140	0.0409	3.6631	0.0325	0.1683	9.6438
1.6433	3.7211	0.0241	3.6228	0.0406	3.6719	0.0323	0.1657	9.4967
1.6501	3.7281	0.0240	3.6297	0.0403	3.6789	0.0321	0.1642	9.4108
1.6589	3.7373	0.0239	3.6388	0.0399	3.6881	0.0319	0.1600	9.1698
1.6658	3.7444	0.0240	3.6459	0.0395	3.6951	0.0317	0.1557	8.9210
1.6741	3.7531	0.0241	3.6544	0.0391	3.7038	0.0316	0.1502	8.6072
1.6787	3.7578	0.0238	3.6592	0.0390	3.7085	0.0314	0.1524	8.7334

Table of coordinates of node 131643 and node 132437 and the calculation of the coordinates of the centroid of the girder for different time steps for the 8-mm mesh case.

	Node 131643		Node 132437					
Dt (seconds)	**x (m)**	**y (m)**	**x (m)**	**y (m)**	**Mean x (m)**	**Mean y (m)**	**Rot Angle (rad)**	**Rot Angle (deg)**
0.0002	3.2000	0.0578	3.1000	0.0634	3.1500	0.0606	0.0002	0.0113
0.1002	3.2000	0.0603	3.0999	0.0655	3.1499	0.0629	-0.0041	-0.2367
0.2006	3.2000	0.0603	3.0999	0.0655	3.1499	0.0629	-0.0041	-0.2360
0.3001	3.1999	0.0603	3.0999	0.0655	3.1499	0.0629	-0.0041	-0.2347
0.4008	3.1999	0.0603	3.0999	0.0655	3.1499	0.0629	-0.0041	-0.2337
0.5001	3.1999	0.0603	3.0999	0.0655	3.1499	0.0629	-0.0041	-0.2328
0.6006	3.1999	0.0602	3.0999	0.0655	3.1499	0.0629	-0.0031	-0.1772
0.7010	3.2000	0.0602	3.1000	0.0655	3.1500	0.0629	-0.0026	-0.1508
0.8007	3.2000	0.0601	3.1000	0.0655	3.1500	0.0628	-0.0016	-0.0933
0.9012	3.2003	0.0601	3.1003	0.0654	3.1503	0.0628	-0.0022	-0.1275
1.0011	3.2039	0.0600	3.1038	0.0654	3.1539	0.0627	-0.0019	-0.1068
1.1008	3.2247	0.0597	3.1248	0.0653	3.1747	0.0625	0.0003	0.0163
1.2003	3.2648	0.0550	3.1660	0.0672	3.2154	0.0611	0.0658	3.7684
1.3001	3.3359	0.0361	3.2399	0.0620	3.2879	0.0490	0.2067	11.8416
1.4013	3.4492	0.0199	3.3535	0.0472	3.4013	0.0335	0.2213	12.6773
1.5001	3.5644	0.0410	3.4673	0.0618	3.5159	0.0514	0.1534	8.7879
1.6002	3.6758	0.0419	3.5767	0.0501	3.6262	0.0460	0.0260	1.4896
1.7001	3.7937	0.0257	3.6958	0.0437	3.7447	0.0347	0.1244	7.1295
1.8006	3.9172	0.0241	3.8193	0.0424	3.8683	0.0333	0.1845	10.5716